Curvature Lines for Lesion Detection and Visualization in CT Colonography

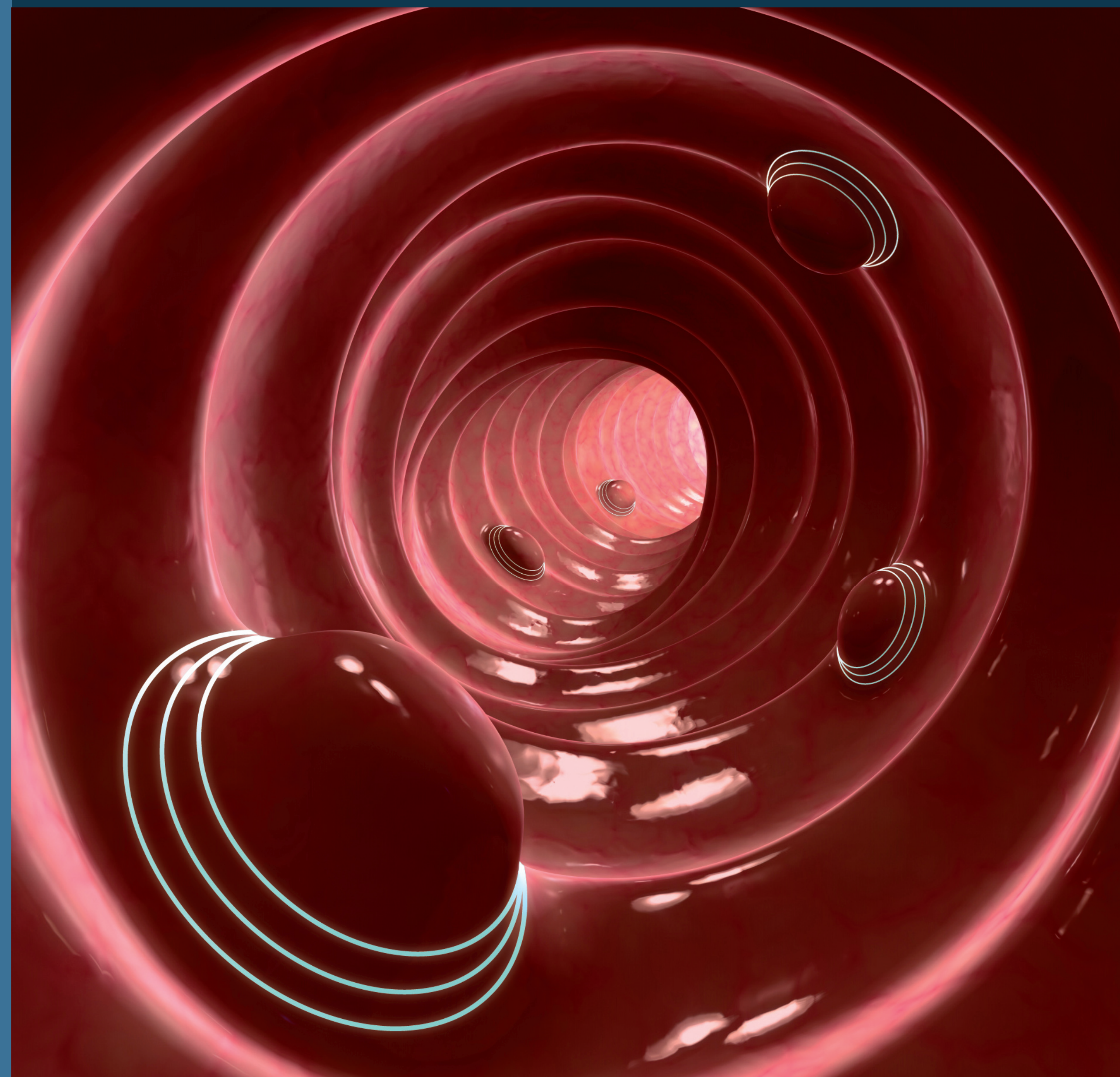

Lingxiao ZHAO

In this thesis, we present an automatic polyp detection approach that integrates knowledge from flow visualization techniques. Our primary goal was to compute additional characteristic polyp features that improve the CAD performance of existing polyp detection approaches by eliminating found false-positive polyp candidates. We found that surface principal curvature directions presented discriminating patterns on surface areas that belong to colonic polyps. These could be visualized using lines of curvatures. We developed novel approaches for generating lines of curvature on the colon wall. In order to provide sufficient shape information, lines of curvature were distributed using curvature-adaptive streamline seeding and spacing strategies. Geometric features of lines of curvature were used to differentiate between true polyp detections and false positives. The visualization of the colon wall was also enhanced by visualizing lines of curvature.

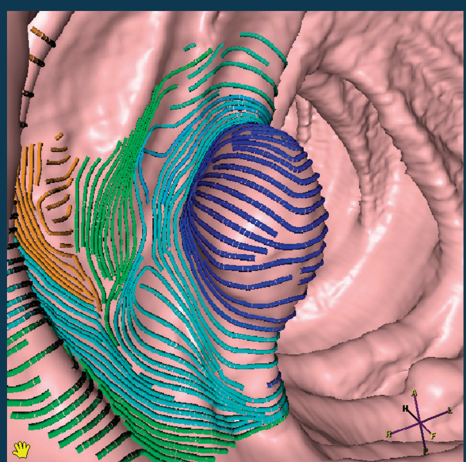

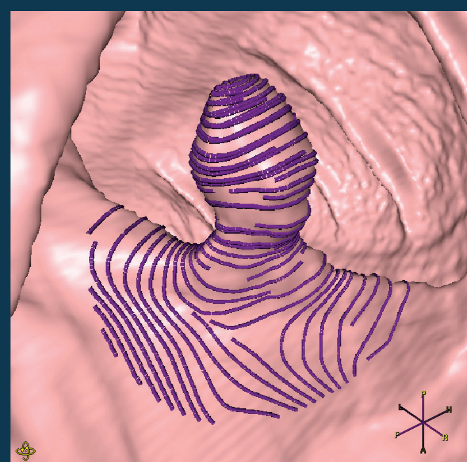

ISBN 978-94-6169-036-4

Curvature Lines for Lesion Detection and Visualization in CT Colonography
Lingxiao ZHAO

Curvature Lines for Lesion Detection and Visualization in CT Colonography

About the cover
The front cover illustrates the visualization of a colonic surface. Several colonic polyps are presented on the colon wall as spherical protrusions. These polyps are highlighted by rendering lines of curvature around their neck areas. The back cover shows two images from Chapter 6 of this thesis.

Curvature Lines for Lesion Detection and Visualization in CT Colonography

Proefschrift

ter verkrijging van de graad doctor
aan de Technische Universiteit Delft,
op gezag van de Rector Magnificus prof.ir. K.C.A.M. Luyben,
voorzitter van het College voor Promoties,
in het openbaar te verdedigen op woensdag 9 maart 2011 om 10:00 uur

door

Lingxiao ZHAO

Master of Science in Technical Informatics
Technische Universiteit Delft, Nederland
geboren te Zhengzhou, China.

Dit proefschrift is goedgekeurd door de promotor:
Prof. dr. ir. F.W. Jansen

Copromotor:
Dr. C.P. Botha

Samenstelling promotiecommissie:

Rector Magnificus, voorzitter
Prof. dr. ir. F.W. Jansen, Technische Universiteit Delft, promotor
Dr. C.P. Botha, Technische Universiteit Delft, copromotor
Ir. F.H. Post, Technische Universiteit Delft
Prof. dr. ir. L.J. van Vliet, Technische Universiteit Delft
Prof. dr. ir. J. Dankelman, Technische Universiteit Delft
Prof. dr. J. Stoker, Universiteit van Amsterdam
Prof. dr. B. Preim, Otto-von-Guericke-Universität Magdeburg

Advanced School for Computing and Imaging

This work was carried out in the ASCI graduate school.
ASCI dissertation series number 228.

ISBN 978-94-6169-036-4

To my dear grandpa and grandma.

Contents

CHAPTER 1

Introduction

This thesis documents research on techniques for the extraction of structures of interest from CT data for application in CT colonography-related computer-aided diagnosis. Our approach is unique in that it applies scientific visualization knowledge, namely advanced volume and surface geometry processing, to extract useful information from CT images for automatic polyp detection.

In this chapter, we will first introduce background knowledge of colorectal cancer, which is the target of computer-aided diagnosis in our research. Then we discuss colonography techniques, particularly the role of CT colonography and automatic polyp detection. Motivations and objectives of our research project are also presented and contributions of our work to related research fields are outlined. At the end of this chapter, an overview of the rest of this thesis is given.

1.1 Colon Cancer and Polyps

Cancer is a serious illness and currently the second major cause of death. For most types of cancer, there is no effective cure yet. In many cases, the disease mechanisms underlying cancer are not well-understood.

The colon (Figure 1.1) or large intestine (bowel) is an important segment of the human body alimentary canal, where waste materials are temporarily stored and water and some vitamins are absorbed. Cancerous growths can develop on the interior surface of colon. Colorectal cancer (also called colon cancer or large bowel cancer) has a high mortality rate. It accounts for approximately 639000 deaths worldwide per year [Org09] and is the third leading cause of cancer deaths in the western world [col09a].

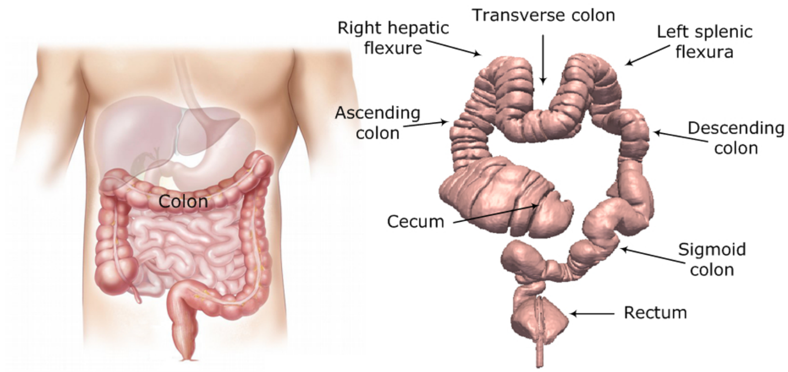

Figure 1.1: Structure of the human colon (Left image from [Cro]).

Colon cancer is a common type of the malignant tumor that is located on the colon wall. Like most other cancers, it occurs when some cells in the body begin to divide and multiply in an uncontrolled manner. Normally after a long period of development, the group of abnormal cells gets bigger and bigger. Finally, it forms a mass (also called a tumor) that invades into the colon wall, where normal cells are replaced and destroyed. Colon cancer can lead to a change of colon behavior, a feeling of incomplete defecation and a reduction of stool diameter. A large tumor can obstruct the colon and even cause bleeding inside. In some cases, cancer cells can also spread to other areas of the human body and damage organic functionalities there.

Factors that increase a person's risk of developing colon cancer include:

- Age: Older people are at a higher risk of developing colon cancer. More than 90% of people diagnosed with colon cancer are older than 50 [col09b]. Younger cases are uncommon.
- Heredity: Members of a family that has a history of colon cancer are at a higher risk of developing colon cancer [LdlC03].
- Diet and living habits: Studies show that diets high in red and processed meat and lacking in fresh fruits, vegetables, poultry and fishes increase the risk of colon cancer [CTC$^+$05]. Certain living habits, e.g. smoking, drinking alcohol and physical inactivity, also increase the colon cancer risk.
- Other factors are, for instance, viruses, having inflammatory bowel disease, environmental impacts and so on.

Colonic polyps have been studied as an important precursor of colon cancer. It is normally a benign growth of tissue projecting from the mucous membrane of the interior colonic surface. In terms of their shapes, colon polyps can be categorized into two types:

- The *pedunculated* polyp (Figure 1.2(a)) is attached to the colon wall by a narrow elongated stalk. It typically presents as a protrusion shaped like a mushroom.

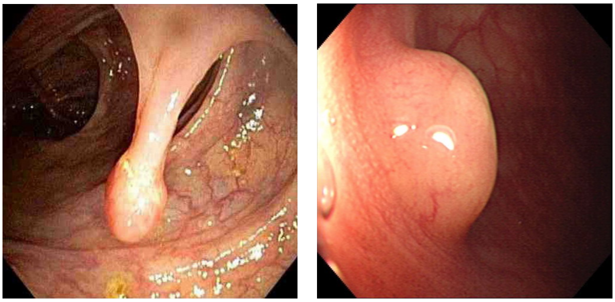

(a) (b)

Figure 1.2: (a) A pedunculated polyp (Image from [TA]), (b) a sessile polyp (Image from [KLL$^+$07]).

- The *sessile* polyp (Figure 1.2(b)) grows directly into the inner wall of the colon and is similar in appearance to a drop of spilled paint.

Depending on their severities, polyps can also be classified as:

- Hyperplastic polyps: small polyps (normally less than 5*mm* in diameter).

- Adenomatous polyps: bigger polyps (larger than 10*mm* in diameter).

Hyperplastic polyps are usually considered to be harmless and usually don't turn malignant. They are not always distinguishable from adenomatous polyps. Adenomatous polyps are really pre-cancerous and have a greater malignancy potential. They account for approximately two-thirds of all colonic polyps, although only a minority will develop into colon cancer over years. The risk of malignancy increases with both the size of the polyp and the degree of villous component.

Colonic polyps commonly occur in about 30% to 50% of adults. The development from an adenoma to colon cancer usually takes about 10 years. In the early stage of such a cancer development, pre-symptoms are detectable. Although not all polyps will become cancerous, almost all colon cancer incidences are developed from colonic polyps. Therefore, early detection of colonic polyps is important.

1.2 Diagnosis and Therapy of Colonic Polyps

Fortunately, colon cancer can be effectively prevented by early detection and removal of colonic polyps. Diagnostic techniques are applied to first find colonic polyps on the colon wall. Then the patient must undergo a surgical polyp removal treatment. This procedure can help to keep a survival rate after 5 years of 92% [KvCMS04].

1.2.1 Detection of Colonic Polyps

Currently, available polyp diagnosis techniques include fecal occult blood test, barium enema, sigmoidoscopy and colonoscopy. Screening options, e.g. colonoscopy, which enable visual examination inside the colon, are preferred.

There are currently two screening techniques for colon cancer diagnosis: traditional optical colonoscopy and CT colonography. Optical colonoscopy is suggested as the gold-standard screening approach for colon cancer diagnosis by some professionals. CT colonography is a modern and more advanced screening approach that allows the visual inspection of the interior colon wall using radiation technology.

1.2.2 Removal of Colonic Polyps

After polyps are found, the patient must undergo optical colonoscopy to remove them. Optical colonoscopy has the advantage that the detection and surgical removal of polyps can be accomplished in one single procedure. This is favorable for those patients who prefer to have everything done without having to go through another preparative regime and colonoscopic examination.

Since the mucous membrane of the interior colonic surface does not have nerve endings, the removal of a colonic polyp is a relatively painless surgical procedure. When a colonic polyp is found during the examination of optical colonoscopy, the doctor uses the colonoscope to hitch the target with a looped wire inserted through the tube. The polyp is then cut and removed out of the body. Such a procedure is called polypectomy. A 90% reduction of colon cancer development and 92% reduction of mortality has been claimed if the patient has optical colonoscopy and subsequent polyp removal.

1.3 Colonography and Automatic Polyp Detection

In this section we will discuss the two methods for colonoscopy (optical colonoscopy and CT colonography) in more detail.

1.3.1 Optical Colonoscopy

Traditional optical colonoscopy allows the complete and direct visual inspection through the entire colon. The procedure is accomplished by inserting a flexible probe (called the colonoscope) into the anus and then moving it slowly into the rectum and further through the colon (Figure 1.3). The colonoscope is as thick as a finger and has a bright light and a video camera on its tip. During the examination, video images are transmitted from the camera and displayed on a television monitor in realtime. In such a way, the examiner is allowed to evaluate the inside appearance of the colon.

Optical colonoscopy requires the patient's colon to be emptied in advance using laxatives. This preparation enlarges the exposed area of the colon wall and facilitates the visual inspection. Immediately prior to the examination, an intravenous infusion is started and sedation is administrated. Normally, adults over 50 years of age are recommended to have colonoscopy, particularly those with colon cancer risk factors or even with pre-symptoms.

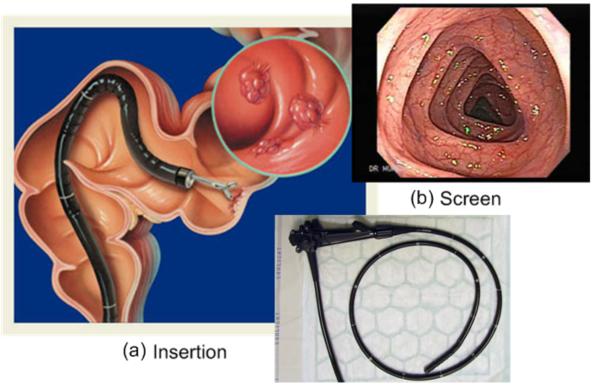

(a) Insertion (b) Screen (c) Colonoscope

Figure 1.3: Optical colonoscopy (Images: (a) from [cola], (b) from [colb] and (c) from [colc]).

One major disadvantage of optical colonoscopy is its potential harm and discomfort to the patient. The invasion and movement of the colonoscope often leads to a feeling of pressure, cramping and bloating. Currently, notable discomfort can only be minimized with the aid of medication. Optical colonoscopy generally is well tolerated by applying conscious sedation, which is safer than general anesthesia.

However, technical limitations arise in the application of optical colonoscopy. The colonoscope has a unidirectional nature. Due to the geometric complexity of the colon wall, a number of hidden areas are difficult to reach. For example, there are many folds that curtain deep valleys of the colon wall. Furthermore, the visual inspection can be time-consuming. Depending on the expertise of the examiner, the full inspection can take half an hour or so, and additional time has to be taken for the sedative medication. This makes optical colonoscopy inefficient for screening low incidence rates.

1.3.2 CT Colonography

The application of radiation technology in medicine has evolved significantly since the *computed (axial) tomography (CT)* device was first invented by a British engineer, Godfrey N. Hounsfield (1919-2004) [Hou73], who hereby earned the 1979 Nobel Prize in Medicine. CT screening allows inspection of the colon wall in an less-invasive way. Modern CT scans commonly have a slice resolution of 512×512 and include up to thousands slices, providing details within $0.5 - 1.0$ mm. The CT scanning process has also been accelerated to finish in seconds to favor the acquisition of time-dependent data.

CT colonography is a modern and effective screening approach that allows radiologists to inspect the interior surface of the colon for colonic polyp detection. It makes use of CT scans and computer imaging and visualization techniques and is minimally invasive without the need to insert any detection instrument into the colon. It allows to take cross-sectional views through the abdomen, and then reconstruct virtual images of the colon using specific computer software. The result provides a radiologist with essentially a similar view to that a gastroenterologist would have using an optical colonoscopy.

(a)

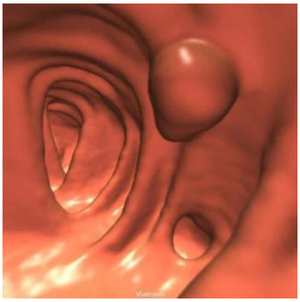

(b)

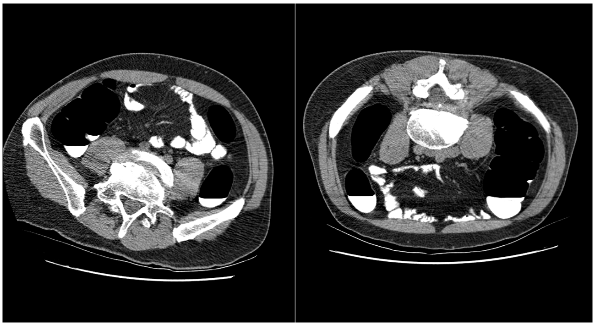

(c)

Figure 1.4: (a) A Philips MX8000 CT scanner, (b) the 3D view of CT colonography (Image from [Pic]), (c) left is a CT image of supine position, right is a CT image of prone position.

CT colonography normally consists of three steps:

1. Preparation: Similar to optical colonoscopy, the removal of stool or fecal residues using laxatives is required before the patient undergoes CT scanning.

2. CT data acquisition: In general, the patient's body is scanned by a multi-detector spiral CT scanner (Figure 1.4(a)) in both supine and prone direction (Figure 1.4(c)). During the scanning, the colon is inflated by inserting a thin tube into the rectum and then pumping carbon dioxide air into the colon for better viewing. The scanning result is a stack of 2D cross-sectional gray images.

3. Visual examination: Using the CT data of the colon, a radiologist can perform a direct examination based on the 2D axial viewing provided by 2D CT images. The stack of 2D CT images are also manipulated by computer software to reconstruct 3D virtual viewing (Figure 1.4(b)) of the colon, which is similar to the display of optical colonoscopy, however with more advantages for colon cancer diagnosis.

CT colonography alleviates the two major drawbacks of conventional optical colonoscopy. First, it has a lower invasiveness level and provides much less discomfort to the patient, although it still involves air infusion to the colon. No conscious sedation is required. Second, the virtual examination is less time-consuming than optical colonoscopy. It takes about 15 minutes for the radiologist to examine the colon data of a patient using CT colonography. Hidden areas of the colon can be inspected well and even better with the assistance of digital colon cleansing techniques.

CT colonography has been well researched and used for clinical applications. However, a significant question arises: Is CT colonography reliable enough or does it have a comparable performance for colonic polyp detection as the gold-standard optical colonoscopy? There have been several trials for evaluating CT colonography over recent years. Some of them showed that CT colonography had significant limitations, particularly in finding small polyps. However, Pickhardt et al. [PCH$^+$03] reported that CT colonography is an accurate screening method and compares favorably with optical colonoscopy in terms of the detection of clinically relevant polyps. This greatly encouraged research on CT colonography. Later, more evaluations have been conducted and concluded that CT colonography has a polyp detection rate equivalent to that of optical colonoscopy [PTK$^+$06, KPT$^+$07, BBJ$^+$07, DBK$^+$09, Dac09].

In general, Optical colonoscopy has better performance than CT colonography in detecting small polyps (less than 5mm in diameter), which are mostly benign. CT colonography provides a less-invasive screening technique than conventional optical colonoscopy. However, it is not likely that CT colonography will render optical colonoscopy obsolete, since the removal of polyps is conducted in optical colonoscopy.

Since the CT device was invented, there have been innovations of advanced radiology hardware and computer technology. Medical imaging and visualization techniques have been widely studied and applied in CT colonography. CT scanning provides detailed three-dimensional structural information on the internals of the human body. However, from the acquired visualization of the internal colon wall it is not easy to detect possible polyps among all protrusions and folds. It helps if some local shape properties such as curvature and size of the protrusion are first derived. These shape properties can be computed on the surface by 2D imaging and 3D geometry processing techniques. First, image features are computed from the original CT data and interpreted visually to unveil connotative and characteristic structures. In this way, clinicians can get more insight into the data and review the internal structures of the human body. Second, certain structures of interest can be located by analyzing related quantitative information. Visualization and automated detection techniques assist medical specialists to better understand the complex internal structures of their patients and hence to perform more precise diagnosis. Computer-aided diagnosis is one of the main reasons why CT colonography is getting more interest in medical research.

1.3.3 Computer-Aided Diagnosis (CAD)

There are currently several active research topics in CT colonography, e.g. fast realtime volume rendering, accurate colonic surface segmentation, automatic navigation path tracking, digital cleansing, automatic polyp detection and so on. Computer-aided diagnosis, i.e. automatic polyp detection, is among the most interesting of these topics.

Computer-aided diagnosis (CAD) is the technique that facilitates the visual inspection by the radiologist with potential polyp candidates, which are pre-detected by applying automatic polyp detection schemes (Section 2.5.2). On the basis of geometric feature calculation (e.g. curvature, shape, size, etc...), the CAD procedure roughly includes three steps: colonic surface segmentation, polyp candidate generation and selection of the most likely candidates on basis of pattern recognition. First, a preferable colonic surface representation is either computed as an explicit triangle mesh or rendered directly as an implicit iso-surface using volume ray casting. Second, characteristic surface or volumetric features are computed based on the surface representation. Then these features are used for the intermediate polyp candidate generation and subsequent false-positive reduction using pattern recognition techniques. Feature calculation and pattern recognition for polyp candidate selection (false-positive reduction) are two key steps that strongly determine the sensitivity and specificity of automatic polyp detection. Having potential polyp candidates, the remaining task for the radiologist is the confirmation or rejection of candidate detections.

It has been demonstrated that automated detection of colonic polyps is a feasible technique, especially for clinically important large polyps [SJP$^+$01]. Sensitivity and specificity are two criteria to evaluate the performance of polyp detection. Sensitivity measures the portion of correct polyp detections in all true polyps. Specificity measures the portion of polyps identified correctly in all detections. A high sensitivity of automatic polyp detection can be achieved with an acceptable specificity [YMM$^+$02].

1.4 The Project

The research project documented in this thesis focuses on improving current techniques for computer-aided diagnosis in CT colonography by integrating knowledge from scientific visualization. Among the key steps of the automatic polyp detection pipeline, we focus on polyp feature computation and pre-detected polyp candidate classification for false-positive reduction.

1.4.1 Motivation

In recent years, many attempts have been made for automatic polyp detection in CT colonography. A variety of polyp features have been defined and used in numerous existing automatic polyp detection schemes. These polyp features include surface and image, geometric or volumetric properties. Each of them covers a specific part of the information that can be used to describe polyp characteristics in terms of shapes or internal structures. For example, surface curvatures and derived measurements have been frequently used in early CAD research.

A good CAD scheme should be selective, i.e healthy tissue should not be wrongly identified as polyp. However, several problems stand in the way of applying automatic polyp detection schemes in CT colonography for clinical diagnosis. First of all, most features proposed in literature are too localized to outline the overall information of a large scale area and to be robust against image noise. This usually limits CAD performance with a large number of false-positive detections. Second, one single feature is seldom enough for successful detection, and a combination of different shape measures is needed.

In this project, we will explore additional polyp features that better characterize the surface area of a polyp, use several geometric shape characteristics in the classification, and are also less prone to image noise. Our primary motivation is to improve the performance of existing automatic polyp detection schemes. We will explore the use of surface and volume geometry processing. To evaluate the improvement associated with applying geometry processing techniques, we integrate our work into a prototype CAD system and incorporate our new polyp features with other useful information for polyp detection.

1.4.2 Research Objectives

The project presented in this thesis consists of the following research tasks:

Define and compute characteristic polyp features Features based on scalar curvature values used in existing CAD schemes do not supply sufficient shape information for polyp characterization. This is mainly because point-wise principal curvatures are incapable of describing shape characteristics of a large scale surface area. Our research focuses on the improvement of CAD performance by applying a proper polyp shape model based on surface principal curvature direction fields.

Improving feature computation Having a better polyp model and additional feature definitions is not always enough. The computation of polyp features should be able to deal with image noise. CT imaging may introduce noise that can badly affect feature computation and reduce polyp detection accuracy. We develop robust computation approaches that provide accurate features for the false-positive reduction step and help to improve polyp detection results.

Polyp surface partitioning The partitioning of a polyp surface has two benefits: (1) it supports the computation of overall shape features within each surface partition; (2) Each surface partition is geometrically homogeneous and can be used for the initial segmentation of polyp candidates.

Evaluation Visualization-based techniques for polyp feature computation are integrated into a prototype CAD system. Additional features are used in supervised pattern recognition approaches to reduce the number of false positives pre-detected in a pre-processing step. The performance in terms of sensitivity and specificity is evaluated using pattern recognition techniques. The evaluation results also suggest research directions for improvement.

1.4.3 Contributions

The work described in this thesis contributes to the research field of colonic polyp detection in CT colonography with the following:

1. We find that surface principal curvature direction fields show characteristic shape features that can be used to identify colonic polyps. We use such vector fields as a basis for calculating shape features in a large scale surface area, as opposed to point-wise features. A new polyp shape model is constructed for the feature calculation. Curvature streamlines are generated and used to describe characteristics of the two principal curvature direction fields. New features for polyp detection (mainly the false-positive reduction step) are calculated on curvature streamlines. In particular:

   (a) To generate curvature streamlines on the colonic surface, principal curvature directions need to be estimated first. Robust curvature estimation methods are applied to cover CT data noise.

   (b) We present algorithms that compute surface constrained curvature streamlines for both explicit triangle meshes and implicit iso-surfaces embedded in 3D volume data. In order to sufficiently describe polyp shapes, curvature streamlines are distributed over the polyp surface using novel curvature-controlled seeding and spacing strategies.

   (c) Our new polyp model models a polyp as two parts: (1) polyp cap and (2) polyp neck. The polyp neck is of great interest and typically a closed-ring and anticlastic surface. Approximately closed curvature streamlines are used to locate polyp neck areas. The Winding Angle of curvature lines and Mean Radius of closed curves are used as two new geometric features for colonic polyp detection.

2. In further work, we present two major improvements of the curvature streamline computation:

   (a) The streamline seeding strategy is adapted to the local surface curvatures so that the streamline generation becomes more efficient.

   (b) A streamline defragmentation approach is developed to generate sufficiently long curvature streamlines that better describe surface shapes.

3. A novel colonic surface partitioning method is used to aggregate shape features in large scale surface areas for automatic polyp detection.

4. Our features are incorporated with other existing techniques (i.e. protrusion based polyp detection method) in the false-positive reduction step of a complete automatic polyp detection pipeline (See Figure 1.5). The evaluation results showed that our curvature streamline based features are highly correlated with true-positive polyp detections.

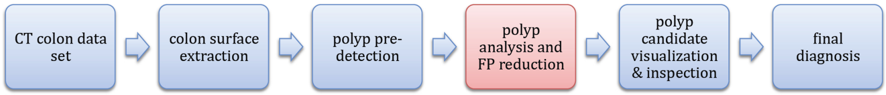

(a)

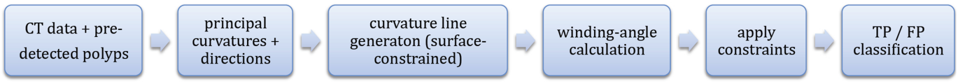

(b)

Figure 1.5: Our technique is integrated into a prototype CAD system: (a) shows the overall pipeline of our CAD system, (b) shows the procedure of our false-positive reduction scheme.

1.5 Thesis Structure

The remainder of this thesis is structured as follows:

- Background knowledge of CT colonography and computer-aided diagnosis techniques is given in chapter 2. Colonic surface rendering techniques, display modes, navigation and user interaction approaches, digital colon cleansing and existing automatic polyp detection schemes are discussed.

- Chapter 3 presents a survey of visualization techniques related to our automatic polyp detection method, including 3D surface principal curvature computation, curvature streamline generation and streamline seeding and spacing strategies.

- Chapter 4 describes our automatic polyp detection approach using 3D surface curvature streamlines. Curvature-controlled streamline generation and distribution algorithms are presented in detail. Features are computed on selected curvature streamlines and used for the classification of polyp candidates. Preliminary evaluation results indicate that these streamline features are highly correlated with true-positive polyp detections.

- Two important improvements are documented in chapter 5. A streamline defragmentation approach is used to generate sufficiently long curvature streamlines. A curvature-adapted streamline seeding strategy makes the streamline generation more efficient.

- Chapter 6 presents a colonic surface partitioning approach based on clustering of curvature streamlines. This approach is used to aggregate surface geometric information within each geometrically homogeneous surface partition for automatic polyp detection.

- A more in depth evaluation of the role of our curvature streamline features in the classification of pre-detected polyp candidates is given in chapter 7. Different data resources are included and our features are used with protrusion-based and volumetric polyp features in the supervised pattern recognition step. The results showed that our visualization-based techniques help improve the sensitivity and specificity in an existing CAD scheme.

- In chapter 8 we draw our conclusions and discuss potential avenues for future research.

CHAPTER 2

CT Colonography and Computer-Aided Diagnosis

This chapter provides a survey of existing techniques used in CT colonography and particularly for automatic polyp detection. It starts with a short introduction of important topics in current CT colonography research in Section 2.1. Then it discusses visualization techniques of colonic surfaces in Section 2.2. Navigation and interaction approaches are outlined in Section 2.3, followed by a brief description of electronic cleansing techniques in Section 2.4. Existing automatic polyp detection schemes, including feature extraction and pattern recognition, are outlined with the discussion of their performances from Section 2.5 to Section 2.8. In Section 2.9, we give a short summary and position our project within the whole research context.

2.1 Problems and Methods of CT Colonography

The pipeline of colon cancer diagnosis in CT colonography is described in Figure 2.1. Before the CT colonography examination, patients are required to clean their bowels by taking laxatives, e.g. pills or cathartic liquid, so that the screening of the colon wall can be sufficiently clear. Then they undergo CT scanning and 3D volume data of their body are acquired. Such a 3D volume is represented as a stack of 2D DICOM images. Voxels of the 3D volume that belong to the colon part are segmented. Voxels of remaining stool residues are removed by electronic cleansing, which obtains a clean colon volume. Radiologists can directly examine the patient data based on the 2D slice view of 3D DICOM images, or using 3D visualization as a review process for confirmation. Virtual navigation facilitates the inspection of the colon wall. Computer-aided detection techniques may be applied to provide potential polyp candidates and support the diagnosing.

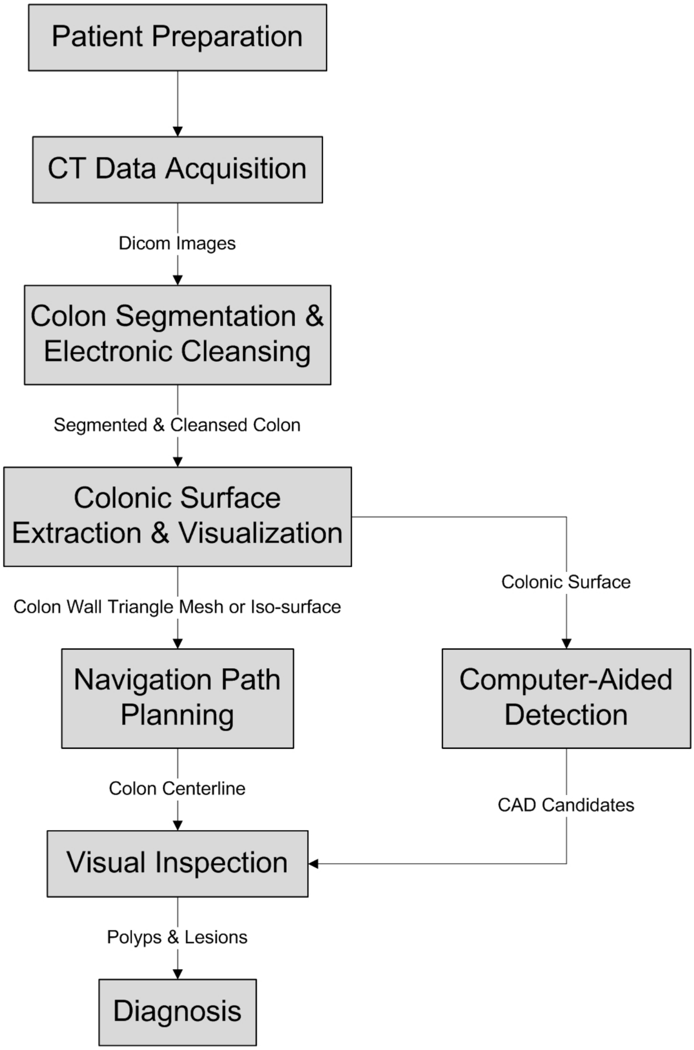

Figure 2.1: CT colonography pipeline.

In CT colonography, the following four topics are important:

- *Visualization of the colon wall*: To support the visual inspection of the colon wall using 3D scans, e.g CT volume data, the colonic surface is firstly segmented from the 3D volume and rendered using various 3D visualization techniques.

- *Navigation and Interaction*: The usability of a CT colonography system is determined by the navigation of a virtual camera through out the colon and the interaction approach. Algorithms have been developed for automatic generation of the navigation path and the "unfolding" of the colon surface.

- *Electronic cleansing*: In order to reduce the influence of remainder stool and fluid residue inside colon for the examination, electronic cleansing techniques are necessary to replace these non-tissue materials with air in 3D volume data.

- *Computer-aided diagnosis*: For the reduction of examination time and cost, automatic polyp detection schemes have been suggested as a helpful addition to the CT colonography pipeline. Automatic polyp detection has attracted significant research interests and efforts in recent years.

A recent State of the Art survey for techniques used in CT colonography is written by Blachar et al. [BGKS07]. In the following sections, we discuss existing work that deals with the four issues mentioned above.

2.2 Visualization of the Colonic Surface

CT volume data is usually represented on a regular 3D grid. A commonly used volume element is the 3D *voxel*. It has two slightly different definitions in the literature. One of the interpretations defines a voxel as a small volumetric block, centered at each grid point and associated with the data value at this point. The data value is constant everywhere inside. Another voxel definition considers a voxel as a cell in between eight grid points in the 3D volume space. Data values of the in-between space are obtained using trilinear or cubic interpolation schemes. The second interpretation offers more flexibility and is used in this thesis.

Two types of 3D rendering techniques are widely used in CT colonography:

- *Surface Rendering* based on triangle meshes generated using the *Marching Cubes* algorithm [LC87].

- *Volume Rendering* based on the *volume ray casting* technique for implicit iso-surfaces embedded in 3D volume [MJC02].

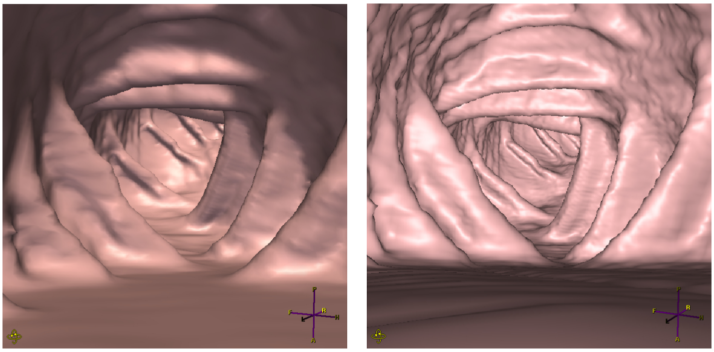

(a) (b)

Figure 2.2: (a) Surface rendering of the colon wall triangle mesh, extracted using the Marching Cubes algorithm, (b) volume rendering of the colon wall implicit iso-surface embedded in 3D volume data, using CPU-based ray-casting technique.

2.2.1 Surface Rendering

The surface rendering process starts with surface mesh construction. The Marching Cubes (MC) algorithm [LC87] segments volume voxels on the colon wall using a simple thresholding approach. Triangles are generated in each grid cell using linear interpolation to find exact vertices and building edges according to the inter-slice connectivity. Normals at triangle mesh vertices are also calculated by interpolating image gradients at neighboring voxels.

There are several advantages of the MC algorithm:

1. Memory costs for the implementation of MC mainly contribute to the storage of the resulting triangle mesh, not much memory is required by overhead of the algorithm itself.

2. Triangles of the surface mesh are calculated directly, no intermediate data structures are needed.

as well as some disadvantages:

1. The resulting mesh is an approximation of the original surface with loss of shape information.

2. Many mesh triangles with bad shapes can be generated.

3. A large number of triangles can be generated and this leads to difficulties for interactive rendering.

4. Topological ambiguities can occur.

The main problem of the MC algorithm is that the approximation accuracy is highly dependent on the grid resolution. A number of approaches have been developed to compensate for this drawback by applying surface remeshing [ACSD+03, AUGA05], mesh refinement [ACMS98, WDSB00, dBVP+00], and other methods that generate surface triangles with local decisions [BMR+99, KS01] and use a set of sampling conditions to bound errors [SSFS06, sSS06].

Irregularities of triangle sizes and shapes have a significant impact on the image quality and surface geometry processing step [AG01]. There are regularization techniques [Fre01, FF91, Boe94, dBvMV+02], decimation algorithms [KT96, SZL92] and re-tiling schemes [Tur92] to reprocess the resulting triangle mesh.

Normally millions of triangles are generated by MC in CT colonography. Such a large number of triangles leads to (1) high computational cost of MC and (2) an insufficient interactive frame rate. Problem (1) was addressed by [CMM+97, LSJ96, SHLJ96, WvG92] using span space or octrees, while problem (2) was solved by [MiHiT+96, HMK+97, BS99, KT96, SZL92, MSS94, MSS00, SFYC96] using occlusion culling, mesh simplification or mesh decimation techniques.

The original MC algorithm may introduce topological ambiguities, where multiple topologies could be interpreted for one configuration of cell-surface intersection [vGW94]. The *Asymptotic Decider* [NH91] is one of the earliest approaches to address this problem based upon bilinear interpolation of data values along faces of the grid cell. Trilinear interpolation based methods were also developed in [CGMS00, Nie03].

For the 3D view in CT colonography, triangle meshes extracted using the MC algorithm are directly rendered using the graphics hardware. Such a surface rendering technique offers relatively higher frame rate for the interaction. However it is usually applied with care to trade off between the image quality and rendering speed. Particularly the piece-wise linear representation of the colonic surface exposes diamond artifacts. Figure 2.2(a) shows a triangle mesh of the colonic surface extracted using the MC algorithm and rendered in CT colonography.

2.2.2 Volume Rendering

Direct volume rendering (DVR) technique may be used to directly render the implicit isosurface of the colon wall embedded in the 3D CT volume data. In contrast to surface rendering (discussed in Section 2.2.1), the volume rendering technique offers better image quality at the cost of lower frame rates. Its main advantage is the ability to render translucent structures and reveal internal structures. As high-quality visualization is more important than interactivity in CT colonography, volume rendering is the preferred rendering technique.

Volume rendering techniques can be classified as either image-order or object-order methods, in terms of the way that the 3D volume data is traversed. There are traditional CPU-based techniques and more up-to-date GPU-based approaches.

The most widely used object-order volume rendering techniques are projection-based techniques, such as shear-warp [LL94] and splatting [Wes91, HMSC00, MMC99, MSHC99]. *Volume ray casting* [Lev88] is an image-order technique that integrates data values along the viewing ray. It is the most important and popular volume rendering method for the visualization of the colon wall in CT colonography, which provides good image quality for the visual inspection. However, because of the expensive computation, its rendering speed is usually not high enough for realtime interaction in CT colonography using old hardwares. Some CPU-based methods tried to accelerate the volume rendering speed [Kni00, MJC02, GBKG04b, GBKG04a]. GPU-accelerated techniques have recently gained more attention [CN93, CCF94, WE98, MHS99, WS01, GWGS02, KW03, RGW+03]. GPU-accelerated volume ray-casting usually provides fast rendering speed when the volume data fits into graphics memory. However, once the data size exceeds the graphics memory, expensive data transfer has to be performed between system main memory and graphics memory, which may significantly slow down the rendering. Therefore there is some reluctance to adopt GPU-based volume rendering in CT colonography.

CPU-based approaches are still dominant in most of the CT colonography applications. Figure 2.2(b) shows the colon wall rendered using CPU-based volume ray-casting technique in the ViewForum system of Philips Healthcare.

2.2.3 Display Modes

One general requirement for CT colonography is the effectiveness, in terms of how much of the colonic surface area is actually displayed. An effective screening of the entire colon must display the surface area as complete as possible. This problem has been addressed in the literature.

Beaulieu et al. [BJK+99] outlined three widely used display modes for CT colonography (Figure 2.3):

- Axial CT is a 2D slice-based view, in which CT images are displayed in a cine or stack. In 2D axial CT view, the direction of the viewing plane can be interactively changed inside the volume and the displayed 2D images are obtained using interpolation. For each patient data set, all the CT slices have to be examined.

- Perspective 3D view displays 3D colon wall based on surface or volume rendering. In the evaluation of the 3D view mode by Dachille et al. [DKW+01], the single view performed in a single-direction fly-through can only review approximately 70% of the colonic surface, while a dual-direction fly-through can review up to 95%. Serlie et al. [SVvG+01] designed a novel visual representation of the surface 3D viewing based on image-based rendering using a cubic environment map. Vos et al. [VvGS+03] conducted an experimental comparison between the conventional single 3D view and the unfolded-cube display. On average, 93.8% of the colonic surface can be reviewed using conventional display mode and 99.5% for unfolded-cube display mode. Sensitivity and specificity for polyp detection were not significantly different between these two methods.

- Panoramic display is an alternative to the conventional 3D single view and unfolded-cube view. In such a method the 3D colonic surface is flattened and fitted into a 2D

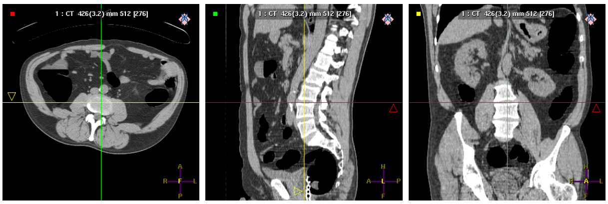

(a)

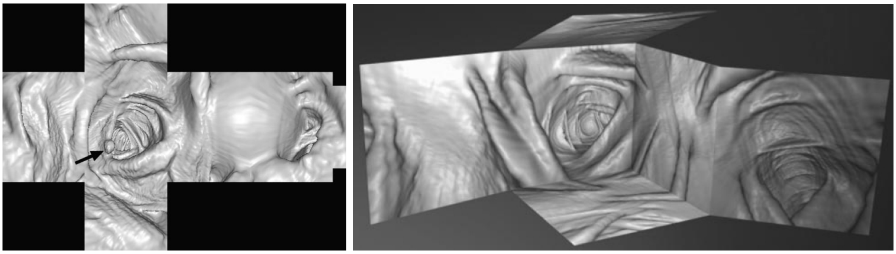

(b)

(c)

Figure 2.3: Three display modes in CT colonography: (a) shows axial CT mode, (b) shows unfolded cube mode and (c) shows flattened colon wall.

rectangular plane [WV95, WMBV98, BWK+01, BWKG01]. Some methods have been developed for angle preserving to minimize the distortion [HATK00, HGQ+06].

2.3 Navigation and Interaction

Visualization of the colon wall determines the effectiveness of a virtual colonoscopy system. Whereas, the employed interaction and navigation approaches determine its usability.

2.3.1 Automatic Navigation Path Computation

The first problem for navigating through the colon is the pre-computation of a navigation path. A navigation path is usually defined as the centerline of the colon, from a start point to an end point specified by the user. Automatic path tracking techniques have been proposed to facilitate the navigation and interaction in CT colonography [CK97, Set99, DC00, DC01, TDC01, WLK+02, LKS06, Hon08].

2.3.2 Navigation Paradigms

Various navigation approaches have been applied in current CT colonography systems. These schemes can be roughly classified into three classes as presented in [HMK+97]:

- *Automatic navigation*, also called planned navigation, generates an offline animation flying though the colon after the navigation path is specified. No flexibility is offered to the users. If important areas are not covered, the only way for improvements is to refine the pre-computed navigation path. Examples of such systems are [HKW+95, RBA+96]. Many other systems, e.g. [NHKG01, HH99], employ multi-mode navigation schemes to provide more options to the users.

- A *manual or free navigation* approach is a fully interactive method without any pre-specified assistance. It can be very difficult in such a way to navigate to the target structures. Most current commercial CT colonography systems use the surface-based rendering technique based on the triangle mesh representation (Section 2.2.1), for the manual navigation approach.

- *Guided navigation* provides full flexibility to the user. It assists the user to have a more effective and efficient examination of the colon wall by combining user guidance (i.e. specific constraints) and an efficient collision-avoidance scheme. Different techniques can be applied to add constraints to guided navigation in CT colonography [HMK+97, BKG99].

Using only one of the above mentioned navigation schemes is normally insufficient. Usually multiple interaction approaches are employed in each of the current CT colonography systems. The user can select a suitable one for a specific application.

2.3.3 Dealing With Interaction

Interactivity is an important issue for the visual examination of the colon in CT colonography. To facilitate a reasonably interactive screening of the colonic surface, both an interactive rendering technique and a flexible navigation scheme are required. It is necessary to find a tradeoff between image quality and rendering speed.

In CT colonography, the most important task is to identify colonic polyps. Sufficient shape information has to be demonstrated for the visual inspection by the radiologist. Therefore, the requirement of high image quality is considered to be more important than rendering speed. With the fast development of graphics hardware, GPU-accelerated volume rendering is gaining more interest.

However, for the comfort of users and optimizing the examination efficiency, interactivity of CT colonography systems still needs to be addressed. Many approaches have been implemented to improve the user interaction of volume rendering based CT colonography. The FreeFlight system [VSA$^+$97] reduces the resolution of the volume data set to adapt to the actual rendering capabilities of the graphics hardware. ViewForum by Philips Healthcare includes a first-hit ray-casting technique that renders the images at a lower resolution when the camera is moving through the colon, and at full resolution for still images. CT colonography on the Syngo platform of Siemens Healthcare applies a space leaping technique as its main acceleration technique for volume ray-casting. General Electric's system also employs an acceleration technique based on a reduction of rendering quality.

2.4 Electronic Cleansing

The volume data set of a clean colon is crucial for a good examination in CT colonography. Unfortunately, the patient preparation is never sufficient to get an ideally clean colon. Stool remains that have an equivalent data value as the tissue may make important parts of the colon wall invisible in 3D views of CT colonography. Sometimes their shapes are even polyp-like. Electronic cleansing techniques have been introduced to discriminate between soft tissue and remains.

Electronic cleansing addresses the problems of partial-volume effect, non-uniform distribution of materials and CT data noise [STF$^+$03]. Positions where air-fluid level interfaces with the colon wall can have segmentation artifacts [PC03]. Such surface areas covered by the three-material transitions have to be carefully processed.

Many approaches have been published for electronic cleansing in CT colonography. Normally the patient CT images are obtained using an oral contrast agent for tagging the intraluminal remains inside the colon. This helps to classify multi-material transitions. The technique presented by Laidlaw et al. [LFB98] is based on voxel intensity histograms. Lakare et al. [LWSK00] developed an approach based on the characteristics of two-material transition areas. In later work, the authors [LCL$^+$03] proposed an automatic tagged-residue detection technique using vector quantization based classification. Zalis et al. [ZPFH03] made use of a binary subtraction mask to classify the opacified residues. The approach of Serlie

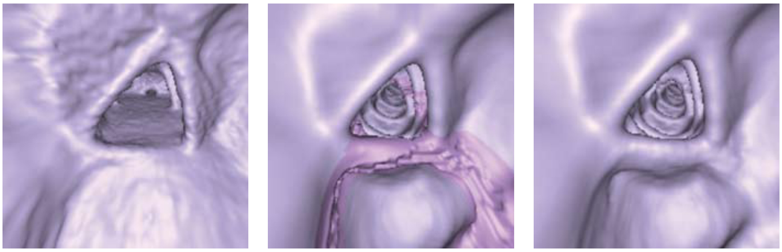

(a) (b) (c)

Figure 2.4: Electronic cleansing of the colon CT data: (a) shows volume rendering of the colon wall without electronic cleansing, (b) shows electronic cleansing was only applied to 2-material transitions, (c) shows electronic cleansing was applied to 3-material transitions.

et al. [STF$^+$03, SdVV$^+$08] specifically allowed the proper classification of transitions between three materials: air, tissue and tagged residues, using the $L-H$ histogram. Wang et al. [WLL$^+$06] presented an improved electronic cleansing method based on the well-established statistical expectation-maximization (EM) algorithm. Figure 2.4 demonstrates an example of the electronic cleansing result in CT colonography, based on the work in [STF$^+$03, SdVV$^+$08].

Electronic cleansing is an important technique in CT colonography. It digitally removes residues in the colon and a more completely visible colonic surface can be visualized. This increases the sensitivity and specificity of polyp detection, not only for visual inspection but also for automatic detection.

2.5 Introduction to Computer-Aided Diagnosis

Computer-aided diagnosis (CAD) techniques can facilitate the laborious visual examination for identifying colonic polyps. In this section, background knowledge and existing CAD techniques are discussed.

2.5.1 Motivation and Goals

CT colonography provides a visual mode for radiologists to virtually fly through the human colon and observe the inside surface. Several problems have been encountered in applications of CT colonography. First, current visual examination techniques are still time-consuming. Second, direct visual inspection has several factors that limit the polyp detection sensitivity:

- Insufficient patient preparation: the colon is not always well distended.
- Examiner performance: less experienced radiologists normally have longer interpretation time and high variability of diagnostic accuracy.

- Colon surface complexity: Hidden areas might be missed and some of them are important for diagnosing.

Since the colonic surface has a high geometry complexity, even with assistant navigation and interaction schemes, a thorough examination of all structures is complicated and time-consuming. The efficiency of diagnosing colon cancer only based on visual inspection is still low, particularly in mass screening of low-incidence populations. Furthermore, important structures may be missed during the inspection. This can be due to incompletely cleaned colon or limited skills of radiologists. The sensitivity of diagnosing colon cancer in this way is not guaranteed. These aspects make CT colonography unattractive for large scale population screening. Computer-aided diagnostic techniques have been suggested in order to reduce expenses of the visual examination, as well as ensure high sensitivity and efficiency of diagnosing.

In CT colonography, computer-aided diagnosis mainly refers to automatic colonic polyp detection schemes. These methods support the diagnosis of colon cancer by pre-detecting suspected areas on the colon wall. By first automatically detecting and visualizing polyp candidates, the procedure of visual inspection in CT colonography can then be more focused, while a high sensitivity and a high specificity are both maintained. It has been suggested that automatic polyp detection as a second reader has great potential in improving colon cancer diagnosis [BCD$^+$05].

2.5.2 Methods of Automatic Polyp Detection

Computer-aided diagnosis usually consists of five basic steps:

1. Colonic surface segmentation.
2. Pre-detection of polyp candidates with high sensitivity.
3. Candidate collection and feature extraction.
4. Reduction of false positive detections based on supervised pattern recognition.
5. Polyp segmentation and size measurements.

Steps 2, 3 and 4 form the process of an automatic polyp detection scheme. In general, good patient preparation and image data preprocessing (e.g. denoising) can improve the automatic detection results. Detected polyp candidates or calculated features can be visualized to help the final visual diagnosis.

Polyp candidate pre-detection step is usually based on filtering CT images by hysteresis thresholding of image features, e.g. curvatures. These image features normally should be calculated on the colon wall. Then image features are filtered to identify suspected positions that possibly belong to colonic polyps. Pre-detected candidates are obtained by fuzzy clustering of connected elements. Usually these pre-detections are represented as central locations of candidate areas. Due to discretization and limited accuracy of these preliminary features, the pre-detection step can produce a large number of candidates. All true polyps should be included. Among these pre-detections, the non-polyp candidates (i.e. false positives) need to be eliminated. The number of false positives is reduced in the following steps, by which polyps and non-polyps are differentiated.

Having pre-detected candidate locations, various features are further used to reduce false positives. These additional features are estimated per candidate, sometimes based on a pre-segmentation of the target object. They represent various properties of the candidate and are able to capture characteristics within large scale areas. For example, shape information of the candidate area can be quantified as a geometric feature. Underlying voxel intensities can be used as a volumetric feature. A collection of such features can have stronger discriminating power for the identification of true polyps than a single feature.

The final candidate classification step is performed based on supervised pattern recognition techniques. A classifier is trained using sufficient training data sets. These training data sets are prepared using real patient CT scans. Polyp candidate pre-detection and collecting additional features per candidate are first performed for each CT scan. Then true polyps are annotated among these candidates by experienced radiologists. Parameters of the classifier are configured according to additional features and true polyp annotations of the patient data sets for training. Then the classifier is applied to patient data sets for testing to differentiate true polyps and false positive pre-detections. In such a way, the performance of an automatic polyp detection approach can be evaluated in the pattern recognition step, in terms of:

- *Sensitivity*: the proportion of candidates that are correctly identified as polyps against the total set of pre-selected candidates that are true polyps.
- *Specificity*: the proportion of candidates that are correctly identified as non-polyps against the total set of pre-selected candidates that are actually non-polyps.

These two criteria can be described mathematically as follows:

$$Sensitivity = \frac{TP}{TP+FN} \times 100\% \tag{2.1}$$

$$Specificity = \frac{TN}{TN+FP} \times 100\% \tag{2.2}$$

where TP is the number of true positives, FP is the number of false positives, TN is the number of true negatives and FN is the number of false negatives. A high performance of automatic polyp detection means both a high sensitivity and a high specificity.

The receiver operating characteristic (ROC) curve is remarkably useful for assessment of the performance of a feature or classifier. It is a widely-used tool for the evaluation of automatic polyp detection. The ROC curve is a 2D graphical plot of sensitivity against specificity. Normally the vertical axis denotes sensitivity and the horizontal axis denotes specificity. For automatic polyp detection, the ROC curve is often represented as a plot of true positive rate against false positive rate (or just the number of false positives). A higher sensitivity is usually accompanied by a higher false positive rate (or a large number of false positives), which means a lower specificity. The shape of the ROC curve indicates the tradeoff between sensitivity and specificity. The closer the ROC curve bends towards the upper left corner of the ROC space, the more accurate an automatic polyp detection approach is.

As described above, the accuracy of automatic polyp detection depends on two factors:

- The discriminating power of the extracted features.
- How sensitive the classification scheme (or the classifier) is.

Therefore, current research on automatic polyp detection in CT colonography has been divided into two directions:

- *Feature extraction*: methods for the computation of characteristic image features.
- *Pattern recognition*: classification approaches for the discrimination of polyp candidates.

Extraction of image features is crucial for automatic polyp detection. Definitions of features that are more discriminating are the basis of a more accurate polyp detection result. Robustness and efficiency are two major concerns of the image feature computation. Robustness deals with the feature computation accuracy, which can be influenced by CT image noise and the computation algorithm itself. Data noise manifests itself as distorted geometry in CT images. A robust feature computation method should be resistant to data noise since noise cannot be completely eliminated. With regard to the scale of CT image noise, point-wise image features are more susceptible. Features that take larger scale areas into account are more characteristic and robust. Furthermore, due to the nature of CT scanning, CT images are discrete representations of physical objects in terms of a volume of samples. In order to support an accurate feature estimation result, higher order interpolation schemes are normally employed to provide a continuous representation of the image structure. However, either feature computation within larger scale areas or higher order interpolation requires more computational expenses. A tradeoff between robustness and efficiency should be carefully considered for feature extraction. This helps to accelerate the detection procedure with loss of effectiveness as less as possible.

To classify candidates as true or false polyps we can apply supervised pattern recognition techniques. This procedure makes use of a collection of additional image features and takes pre-detected polyp candidates as the input. An important task of supervised pattern recognition is feature selection. The selection of useful features depends on the configuration of the classifier. For a good classification a set of well-chosen parameters is needed. To derive better estimates for some measures such as the largest diameter of the polyp, we apply a surface segmentation to the polyp region. As will be shown later, a proper surface segmentation is a crucial step towards a more reliable feature computation and polyp classification.

Following automatic polyp detection is the step of polyp segmentation and size measurements. Polyp segmentation offers the possibility for a further analysis of the polyp candidate. For example, based on the segmented part, the largest diameter of a detected polyp can be computed as a size measurement of it. Polyp size measurement is important for diagnosis and decision making. A proper polyp segmentation approach is crucial to perform reliable feature computations for the polyp candidate classification.

A state-of-the-art survey of existing computer-aided polyp detection techniques was given by Bielen and Kiss [BK07]. The remainder of this chapter mainly focuses on feature extraction techniques. Pattern recognition techniques used for the analysis of image features and the evaluation of a CAD system will be discussed in Section 2.7.

2.6 Feature Extraction for Automatic Polyp Detection

Most of the features used in automatic polyp detection methods are derived from the CT image properties, in 2D or 3D. The majority of these features explicitly or implicitly model polyps as spherical protrusions. Feature definitions proposed in the literature can be roughly classified into four classes:

- Surface features describe characteristics represented by the polyp surface geometry.
- Volumetric features describe characteristics inside the image volume of the polyp.
- Model-based features describe correlations with predefined polyp models.
- Other features refer to features that do not fill into any of the categories above.

In following subsections, methods based on these feature types will be discussed in the order as outlined above.

2.6.1 Surface Features

In 3D perspective view of CT colonography, visual identification of polyps greatly depends on perceiving surface shape information by the radiologist. Surface features can be used to quantitatively describe local surface shapes. These features have been widely used in existing automatic polyp detection schemes to characterize polyp shapes.

Surface features are normally computed based on the surface representation. Therefore, an accurate colonic surface extraction is important. To reduce the effects by stool and residues and enable a full review of the complete colon wall, cleansing techniques (see Section 2.4) are applied to get the correct segmentation of a cleaned colon. In addition, surface improvement techniques are necessary preprocessing steps for surface feature estimation. For triangle meshes, mesh smoothing and regularization methods are normally employed to enhance the mesh quality. For implicit iso-surfaces, denoising and blurring approaches are normally applied.

Surface features are normally calculated at discrete positions on the colon wall. The computation of surface features throughout the complete colonic surface is relatively inexpensive, compared to going through the whole volume. Many surface features were derived from mathematical concepts of differential geometry. Among these concepts, surface curvature is a most popular one.

An early attempt to use surface curvature for polyp detection is made by Summers et al. [SSM+98]. In their method, the colonic surface mesh was first smoothed using Taubin's approach [Tau95a]. Then principal curvature values (discussed in Section 3.1) were calculated at vertices of the colonic surface mesh. These mesh vertices were classified based on the signs of principal curvatures. Hyperbolic and parabolic (see Section 3.1) vertices were discarded and elliptic (see Section 3.1) vertices were retained. A polyp candidate was detected as a cluster of connected vertices that shared the desired classification and together covered an area larger than a preset threshold. However, such an approach can result in a large number of false positives. In their later work [SBP+00], the curvature estimation method was updated applying a faster convolution-based kernel method. More restrictive criteria were used to discriminate false positives, including the *mean curvature*, the *sphericity* and the *polyp size*. An assessment was performed by Summers et al. [SJP+01], using real CT data sets from twenty patients. Nine shape criteria and three iso-surface threshold were examined. They achieved 71% sensitivity with a mean of six false positives per patient for polyps of 10*mm* or larger. However for smaller polyps, the performance significantly decreased.

Volumetric shape index (SI) and *curvedness* (CV) are two well-known surface features for automatic polyp detection, first used by Yoshida et al. [YN01, YNM+02, YMM+02]. They were defined as:

$$SI = \frac{1}{2} - \frac{1}{\pi}\arctan\frac{k_{min}+k_{max}}{k_{min}-k_{max}} \tag{2.3}$$

and

$$CV = \sqrt{\frac{k_{min}^2+k_{max}^2}{2}} \tag{2.4}$$

where K_{min} and K_{max} are principal curvature values. The volumetric shape index characterizes the shape in the vicinity at a point on the surface. Particular values of SI describe unique surface shapes, e.g. the cap, ridge and cup, which correspond to polyps, folds and normal colonic walls. The volumetric curvedness represents the magnitude of how the surface is curved. Suspicious regions were found by hysteresis thresholding of SI and CV and polyp candidates were generated by fuzzy clustering of connected components. The authors claimed that they got a 95% (100%) sensitivity with 1.2% FPs/data set (2.0% FPs/case). SI is often used to first find candidate regions. Unfortunately the method can result in a large number of false-positives.

There are other surface features used for automatic polyp detection in the literature. Paik et al. [PBR+04] developed a surface normal overlap method that detected concentrations of neighboring surface normal vectors as indicators of polyps. This method was applied to colonic polyp detection and lung nodule detection in helical CT images. The performance was evaluated using 8 colon CT data sets and the authors were able to achieve a 100% sensitivity for polyps of 10*mm* and larger with an average of 7.0 FPs/dataset. In the work of Huang et al. [HSH05], kernel-based and surface patch based methods for principal curvature estimation were compared. The authors proposed a two-stage curvature estimation method to estimate surface curvatures at vertices on the triangle mesh. Mesh vertices were filtered by their mean curvature values. The passed vertices were aggregated to form regions of interest

(ROI). Finally, suspicious areas were found by screening ROI using the *sphericity index*:

$$SPi = 2\times \mid \frac{K_{min} - K_{max}}{K_{min} + K_{max}} \mid \tag{2.5}$$

where K_{min} and K_{max} are principal curvature values. An experimental study based on 29 patients (58 data sets) demonstrated 88.7% sensitivity with an average of 18.6 Fps/dataset.

Surface evolution is another CAD approach that indirectly measures surface shapes. Van Wijk et al. [vWvRV+06] used a shape and size invariant surface feature for robust polyp detection. Surface evolution was performed on triangle meshes at those regions where the minimum curvature value was larger than zero implying a convex surface shape. This surface area was flattened until the minimum curvature was smaller or equal to zero. The amount of deformation was computed and used as a protrusion measure for finding polyp candidates. This method achieved a result of 95% sensitivity at 10 FPs/dataset. Konukoglu et al. [KAP+07] developed an approach that was applied directly to implicit iso-surfaces embedded in 3D volume data. This method was based on a use of level set theory. The basic idea was not flattening the surface but evolving polyps towards ideally spherical protrusions. Thus the characteristic features defined in existing CAD schemes were enhanced to be more discriminating for colonic polyps. It was claimed that this approach increased the sensitivity of an arbitrarily chosen CAD method by 8.1% for small polyps of sizes ranging from 5.0 to 9.0 mm in diameter.

The above mentioned automatic polyp detection methods are mostly based on scalar surface curvature values. Our work in [ZBB+06, ZBT+08] explored the potential of principal curvature direction fields. Polyp surface shapes were characterized using curvature directions and patterns in circular curvature lines. Details of our approach are presented in Chapters 4, 5, 6 and 7.

As a summary, most of the proposed surface features are directly or indirectly surface curvature based. Surface normal overlaps and protrusion measure are indirectly curvature-based. If a voxel within the tissue has a high concentration of intersecting surface normals, this means its neighboring surface area has an approximately uniform distribution of convex surface curvatures, i.e. spherical shape. Protrusion measures are highly correlated with surface curvatures. Typically, elliptic surface areas have larger protrusion measures with surface evolution. These elliptic areas are also characterized by principal curvatures. Lines of curvature deal with principal curvature directions. Such curves always follow the direction of maximum or minimum curvature. For CAD methods based on surface features, surface curvature estimation is crucial for the detection accuracy. Robust 3D surface curvature estimation will be discussed in Chapter 4.

2.6.2 Volumetric Features

Volumetric features can be computed directly using intensity values of CT images, in the subvolume of interest. They are mainly used to characterize the organic structures of polyps. The computation of volumetric features is usually more expensive than that of surface features for the complete colonic surface. Therefore, volumetric features are normally calculated at pre-detected candidate positions and used in the polyp candidate selection step for false positive reduction (see Section 2.5.2).

Several volumetric features have been proposed to characterize internal structures of polyps for automatic polyp detection. Summers et al. used a shape-based approach based on elliptic curvature [SSM+98] to pre-detect polyp candidates and improved the specificity of automatic polyp detection using CT attenuation [SJP+01]. Their results showed that 39% false positives could be discarded by sampling CT attenuation at the candidate position, without losing the sensitivity.

Göktürk et al. proposed that computing volumetric image features on triples of planes, rather than on individual planes, captured 3D shape aspects more completely [GTA+01a, GTA+01b]. Polyp candidate subvolumes were generated using an existing polyp detector, e.g. [PBR+04, YN01]. For each candidate subvolume, several geometric features were calculated from many triples of perpendicular random images. Histograms of these geometric features were used as a feature vector for the classification of true polyps and false positives. The authors achieved a reduction of 80% false positives at a sensitivity of 80%.

Acar et al. [ANP+01, ABG+02] developed an automatic polyp detection method that attempted to model the way that a radiologist recognizes a polyp in 2D axial slice viewing using the optical flow field (OFF). In their method, polyp candidates were pre-detected using a Hough Transform-based polyp detector (HTD) [PBR+04]. The optical flow field, which is a vector field embedded in a candidate subvolume, was computed and used to characterize the change of intensity at the air-tissue boundary in the diagnosing direction of the image plane. A 3D vector feature was computed in OFF and used for the classification of true polyps and false positives. They tested their method on 8 real patient data sets. The pre-detection step generated 220 polyp candidates and 20 of them were true polyps. A preliminary 10-fold cross validation study resulted in an average of 75% specificity at 100% sensitivity.

Volumetric texture analysis is another automatic polyp detection approach using volumetric features. Näppi and Yoshida [NY02, NY03] made use of CT texture features for the reduction of false-positive detections returned by their polyp candidate generation step [YN01]. In their evaluation, a combination of mean shape index and directional gradient concentration (DGC) and the variance of CT values yielded 100% (95%) sensitivity with 2.4 (1.7) false positives per patient (per data set), using a quadratic classifier.

Kiss et al. [KvCSM03] presented a two-pass method based on a volumetric feature. Volume voxels of colonic polyps and folds were first segmented. Then a slope density function (SDF) was used to differentiate between colonic polyps and folds. The SDF can be seen as the statistical histogram of gradients at voxels. Since polyps were modeled as circular or elliptic objects, SDF of polyps usually presented smooth patterns while SDF of folds presented peaks. Finally colonic polyps were identified and segmented using fuzzy clustering and the mean position of clustered voxels was returned as a polyp candidate. They claimed to have above 85% sensitivity for polyps larger than 6*mm* as initial results.

Yao et al. [YMFS04] proposed an automatic polyp segmentation method and based on the segmentation of each pre-detected candidate, several features were computed for the reduction of false positives. These features included average density and standard deviation of density inside the model, volume of the polyp segmentation and three-dimensional aspect ratio of the polyp. The resulting FROC curve demonstrated a 100% sensitivity with 11.5 false positives (reduced 30% pre-detected FPs) per data set, and further a 80% sensitivity with 5.5 false positives (reduced 50% pre-detected FPs).

In the work of Wang et al. [WLL+05b], three types of internal volumetric features were used to reduce the number of false positives. For each pre-detected candidate subvolume, CT image density distribution was analyzed. Geometrical features, textural features and morphological features were directly calculated in the subvolume. *Volume* and *Axis_Ratio* were two geometrical features providing shape information of the candidate. *Growth_Ratio* was a textural feature that reflected the whole image density distribution pattern within the subvolume. Another textural feature was the *CT density mean value*, which could be used to differentiate some false positives caused by stool or residues. There were two morphological features as well, *Coverage_Ratio* and *Radiation_Ratio*. These six internal volumetric features were used in their final pattern recognition step to eliminate false positives. 93.1% of the false positives were discriminated from the pre-detected polyp candidates. Their approach achieved 100% sensitivity with on average 2.0 false positives per data set for polyps of $10-30mm$, and 100% sensitivity with 3.44 false positives per data set for polyps of $4-10mm$.

Volumetric features are normally derived from the underlying data values of the colon wall. Some of them are based on a pre-segmentation of the polyp candidate. For methods using these volumetric features, the accuracy of the polyp pre-segmentation plays an important role.

2.6.3 Model-Based Features

Several model-based features are also presented in the literature. The basic idea of model-based features is to match local surface or image shapes to some pre-defined polyp models. Usually, the correlation between shapes and models is quantified and this information is used to detect polyp candidates or differentiate between polyps and non-polyps. Model matching approaches can be applied on the colonic surface or on 3D volume images.

Colonic polyps are often modeled as spherical objects. Kiss et al. [KCT+02] developed an approach taking advantages of both surface normal overlap [PBR+04] method and sphere fitting method. The scheme was tested using data sets of 18 patients. The results showed 100% sensitivity with approximately 8 false positives per patient for polyps of $10mm$ or larger. The method proposed by Kiss et al. [KvCD+05] was applied to solve CAD problems in CT colonography using low-dose data sets. This method modeled colonic polyps using gray level intensity profiles and extended Gaussian images. A sphere fitting method was used to find initial polyp candidates. To separate false positives, intensity profiles sampled along a sphere (the spherical harmonics) and mapping gradient information onto the unit sphere (extended Gaussian images) were chosen to characterize the shape of a polyp. A polypoid model database was built on previously acquired cases. Those features allowed an easy comparison between a polyp candidate and pre-built polyp models in the database.

Chowdhury et al. [CWG06] made use of morphological characteristics of colonic polyps in their CAD method. Initial polyp candidates were detected using the surface normal intersection values. Polyps were modeled as either spherical or ellipsoidal in this method. Additional model-based features for false positive reduction were sphere fitting error and radius, three axes of the fitted ellipsoid and ellipsoid fitting error. The proposed method was tested to have 100% sensitivity for polyps larger than $10mm$ and 91.67% for polyps of $5mm - 10mm$ with 4.5 false positives per data set.

Bhotika et al. [BMS$^+$01] presented a model-based technique for polyp detection in CT colonography that used analytical shape models to map the local shape at individual voxels to anatomical labels. Analytical shape models were introduced for haustral folds and for pedunculate and sessile polyps. Surface principal curvatures were estimated on implicit iso-surfaces embedded in CT volume data to characterize these primitive shape models. Parameters were computed for these models of relevant anatomical colon structures, resulting in a simple voxel labeling scheme. They were used as features to map local principal curvatures at volume voxels to anatomical labels, which correspond to polyps or folds or neither. Their FROC curve analysis indicated a sensitivity of 81.6% at 10.4FPs (76.3% at 6.2FPs) per data set for polyps of $6mm$ or larger. For polyps of $4mm$ or larger, the method achieved a sensitivity of 77.2% at 12.9FP or 75.4% at 10.4FP per data set.

In general, the CAD performance of model-based features and corresponding techniques is highly dependent on the quality of pre-defined models and the modeling method. Current used models are usually built based on the abstraction of known shape characteristics of colonic polyps. Therefore, the applicability of model-based CAD schemes is limited by the variability of polyp shapes in practice. Large colonic polyps can be very complex in their shapes. They often have many concave or cylindrical regions on their caps. These are not polypoid shapes as addressed in most of existing CAD methods and their combinations result in significant irregularities. Sometimes even small polyps can have irregular shapes. The problem of flat lesions is actually due to the lack of a generalized characterization. Therefore, model-based features and techniques often suffer from low sensitivities and low specificities. Human vision and perceiving abilities can handle these problems by training and experience. However this is currently a difficult issue for computer systems. As a summary, a good generalization of colonic polyp shapes is crucial for a robust polyp detection approach.

2.6.4 Other Features

Besides surface, volumetric and model-based features, several features of other types have been investigated. In this section, we briefly discuss two techniques that convert the 3D detection problem into a 2D one.

In the automatic polyp detection pipeline developed by Hong et al. [HQK06], the colonic surface extracted from the CT data set as a triangle mesh was first mapped to a 2D rectangle image using conformal mapping. Thus geometric features and texture features were computed in 3D and mapped to 2D. Polyp candidates were detected using a 2D clustering method on the 2D electronic biopsy image. The RGB values of a given pixel and its neighbors formed a 39-dimensional local feature vector for finding polyp candidate. False positives were further reduced using a gradient concentration feature that was only calculated at candidate positions in the volume. The authors achieved 100% sensitivity with a very low FP rate as their priliminary result.

Wang et al. [WLL05a] developed a different technique that used a volume-based algorithm to flatten the colonic surface. Different rendering schemes were used to transfer the 3D flattened colon volume into a 2D image. This 2D image displayed the intensity variations behind the colon wall. It was used for polyp detection, according to different intensity variation patterns of polyps and other structures.

2.6.5 Discussion of Features

There are varieties of features computed in different ways using CT data sets for automatic polyp detection. Each feature has certain advantages as well as limitations. Proposed features can have discriminating power for polyp candidate pre-detection and false positive reduction, however usually only under specific circumstances. A collection of features can retain all advantages while their limitations are mutually compensated. Hence, many existing prototype CAD systems employ a combination of features for detection and classification. In this case, a feature selection procedure has to be conducted. This is an important issue for the pattern recognition step, which will be discussed below.

2.7 Pattern Recognition for Polyp Candidate Classification

After candidate pre-detection and feature extraction, a supervised pattern recognition (PR) step is performed to identify whether a polyp candidate is a true polyp or a false positive. There are two essentials of the PR step: feature selection and classifier design. The main task is to devise an optimized combination of features and classifiers that provides high automatic polyp detection accuracy. As a result, a decision boundary is computed in the selected feature space and used to separate polyps and non-polyps.

In early stages of CAD research, simple linear classifiers were widely used. Features were simply thresholded to detect polyp candidates. In the methods by Summers et al. [SSM+98, SJP+01], a linear classifier was applied on curvature-based features. Polyp detections were identified by hysteresis thresholding of Gaussian and mean curvatures and the size of connected structures. Van Wijk et al. [vWvRV+06] and Acar et al. [ANP+01] used linear classifiers to evaluate their polyp detection methods. Huang et al. [HSH05] applied a linear filtering of surface curvatures, sphericity indices and size of potential clusters. A Mahalanobis distance based linear classifier was used in [ABG+02]. This classifier provided linear and non-linear decision surfaces in feature space. A significant drawback of linear classifiers is the resulting low sensitivity and specificity.

Non-linear classifiers can generate more correct boundaries in feature space. An effective classifier introduced in [Fuk90] is based on quadratic discriminant analysis (QDA). This classifier was used in [YN01]. It is a statistical classifier that uses a hyper-quadratic surface for the decision boundary. It can optimally partition the feature space into a polyp class and a false positive class. For each pre-detected polyp candidate, the distance from the decision boundary was computed as the polyp likelihood. This value provided the ranked ordering of the likelihood that a candidate is a polyp. A thresholding of the polyp likelihood determined the final detected polyps.

The support vector machine (SVM) classifier is another non-linear classifier used for differentiating between polyps and false positives [GTA$^+$01a]. It generates a hypersurface boundary between the two classes [Vap95]. This boundary not only correctly classifies the data, but also maximizes the margin of the closest data points to the hypersurface. SVM implicitly maps the given feature vector onto new vectors in a higher-dimensional space. The hypersurface boundary becomes a plane in higher dimensional space. Thus, the linearly inseparable data in the original feature space can be separated in higher dimensional space.

Classifiers are designed by setting up their parameters. There are also non-parametric classifiers, such as neural networks. To apply the neural network for the classification of polyp candidates, it must be first efficiently trained using training data sets. Jerebko et al. [JSM$^+$03] compared the classification results of two approaches: neural networks and binary trees. They designed a backpropagation neural network with one hidden layer and trained it with Levenberg-Marquardt algorithm. The neural network performed better with a sensitivity of 90% and 16 false positives per study. They proposed a revised classification method using a collection of multiple neural networks [JMFS03]. The final decision for each polyp candidate was based on the majority vote across the neural network committee and reflected the weighted votes of all networks. This multiple neural network approach reduced 36% false positives and improved the sensitivity by 6.9% compared to the method using a single neural network. A new scheme assembling SVMs for classification, a smoothed leave-one-out cross-validation method for obtaining error estimates and a bootstrap aggregation for training and model selection was introduced by their later work [JMFS05].

2.8 Automatic Polyp Segmentation and Size Measurement

Automatic polyp detection can support visual inspection by indicating suspect locations for colon cancer diagnosis in CT colonography. The size of a detected polyp is important for diagnosis and decision making. In clinical experiences, polyps with diameter $\geq 5mm$ require removal via optical colonoscopy, whereas smaller polyps are not significant. Usually the largest polyp diameter is taken as the size of a polyp. Manual measurement has significant inter- and intra-observer variability. Automatic methods enable more accurate measurements of polyps. Robust polyp measurement is usually based on a proper segmentation of the polyp. Such a procedure is also useful in CAD schemes, to provide more accurate and complete information for the detection.

Early methods for automatic colonic polyp segmentation directly worked on CT images. Jerebko et al. [JTFS03] developed a method employing the Canny edge detector and Radon transformation to segment 2D subvolume images of polyp candidates. Näppi and Yoshida [NY03] made use of feature-guided analysis in the segmentation and feature extraction of polyp candidates.

Yao et al. [YMFS04] proposed an automatic polyp segmentation method based on a combination of fuzzy clustering and deformable models. The segmentation step first took the candidate position as input and computed a subvolume centered at the candidate seed. Then a fuzzy c-mean (FCM) clustering is applied to compute the membership values of “lumen air”, “polyp tissue” and “non-polyp tissue” classes for each voxel of the subvolume. This resulted in an approximated polyp region on a 2 slice. An initial deformable model was fitted to this potential polyp region. Once one slice was processed, this procedure was propagated to neighboring slices until no segmentation could be found. Finally, the 3D segmentation was reconstructed by stacking up all 2D segmentations.

Dijkers et al. [DvWV$^+$05] applied an iterative method on triangle mesh surfaces for polyp segmentation and size measurement. The method started at the candidate position and propagated to its neighborhood if local surface normals did not deflect too much from the center point. In such a way, the edge of the polyp was defined as the boundary of the segmentation. Based on the segmentation, the polyp size was automatically derived by projecting the edges of the segmentation along the polyp axis onto a plane and then taking the largest diameter of a fitted ellipse.

2.9 Value and Positioning of the Thesis

This chapter outlined CT colonography and related techniques. These topics include visualization schemes for displaying the colonic surface, navigation and interaction approaches for supporting the visual inspection, electronic cleansing methods for virtually removing stool and residues, and computer-aided diagnosis techniques for automatic polyp detection. For each of these topics, background knowledge and current existing techniques in literature were discussed.

We mainly focus on the research of automatic polyp detection in this thesis. The survey of existing CAD schemes covers two research directions: extraction of discriminating features and the subsequent pattern recognition step for polyp candidate classification. A taxonomy of derived features used in current automatic polyp detection methods is presented. These features are classified as: 3D surface features, volumetric image features, model-based features and other features. Proposed methods using combinations of features and classifiers are discussed, as well as approaches for automatic polyp segmentation and size measurement. One important problem that still remains for automatic polyp detection is that existing techniques based on point-wise features generate many false-positive polyp candidates. This is because polyp shape and size vary greatly in practice.

The subject of this thesis is novel feature extraction techniques for the classification of polyp candidates to improve detection sensitivity and specificity. In the following chapters, we will introduce techniques for calculating new additional features for the reduction of false positive detections in a prototyping automatic polyp detection system. These features are derived from surface principal curvature direction fields and curvature line geometries, instead of point-wise features based on scalar principal curvatures and other image features used in existing methods presented in this section. Geometric information of a whole surface area is taken into account, so that our features better describe the overall shape of a surface area than those features that only take point locations into account. To compute such new features, techniques for generating curvature lines on 3D surfaces will be presented. Our feature extraction methods for polyp detection integrate flow visualization techniques for surface and volume geometry processing and form part of the CAD functionality of a CT colonography pipeline. The evaluation shows that our curvature line based features can significantly help to reduce the number of false-positive detections of an existing polyp detection approach.

Our features based on curvature lines are derived using 3D surface curvature estimation and streamline generation techniques, which will be discussed in the next chapter.

CHAPTER 3

3D Surface Curvature and Lines of Curvature

Our automatic polyp detection method uses features derived from surface principal curvature directions and streamline geometry. In this chapter, we discuss 3D surface curvature estimation and streamline techniques in specific applications. These are two research topics most related to the work presented in this thesis. In the first section (Section 3.1), mathematical concepts of surface curvatures are given. Existing curvature estimation algorithms are surveyed in Section 3.2. There are two types of surface curvature estimation methods applied on different surface representations: explicit triangle meshes and implicit iso-surfaces. Curvature lines are introduced in Section 3.3 and existing generation methods on 3D surfaces are discussed in Section 3.4. An overview of streamline placement techniques, particularly in flow visualization, is given at the end of this chapter in Section 3.5.

3.1 3D Surface Curvature

Curvature is an important quantity for describing shapes of 2D curves and 3D surfaces in differential geometry [DS96]. It measures how much a 2D curve bends or a 3D surface is curved. 3D surface curvature is widely used in computer graphics applications. The CAD scheme presented in this thesis is based on the use of principal curvature directions. In this section, mathematical definitions of curvature are described.

3.1.1 Definitions in Differential Geometry

Basically, curvature is defined as the magnitude of the rate of rotation of the tangent vector along a plane curve in 2D. In differential geometry, the concept is defined as a quantity of

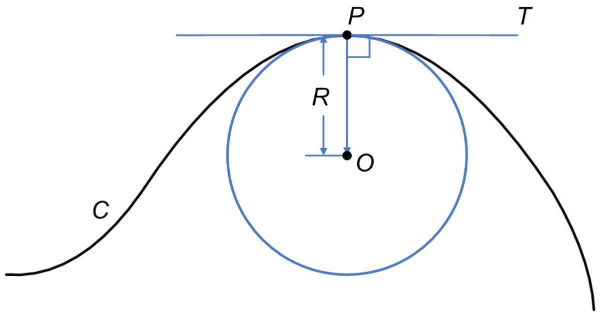

Figure 3.1: The curvature of a plane curve is equal to the inverse of the local osculating circle radius: P is a point on a plane curve C, where the tangent direction is T and local osculating circle is O with radius R.

second order derivatives. This concept is extended for 3D surfaces, which is considered as an integral of infinite curves. There are several definitions of 3D surface curvatures.

Normal Curvature and Principal Curvatures

On 3D surfaces, the normal curvature k_n is defined as the curvature of the normal curve. At a point P of surface S, the normal curve is the intersection curve of the surface and the normal plane, which is defined by the surface normal N and an arbitrary tangent direction T (Figure 3.2). The rotation of T around P results in a continuous change of k_n. Thus the value of k_n can be considered as a continuous function with its minimum and maximum values: k_{min} and k_{max}. k_{min} and k_{max} are defined as principal curvature values at P. Their corresponding tangent directions: T_{min} and T_{max}, are called principal curvature directions, which are orthogonal. Principal curvature values do not directly represent surface shapes. To provide quantified descriptions of surface shapes, Gaussian curvature and Mean curvature are derived.

Gaussian Curvature and Mean Curvature

Gaussian curvature is defined as the product of principal curvature values:

$$K = k_{min} \cdot k_{max} \tag{3.1}$$

Based on the signs of principal curvatures, Gaussian curvature can be used to classify three characteristic shapes of the 3D surface (Figure 3.3).

Gaussian curvature is not able to clearly describe how much a 3D surface is curved, while *Mean curvature* is introduced for this purpose. It is defined as the average of principal curvature values:

$$H = \frac{k_{min} + k_{max}}{2} \tag{3.2}$$

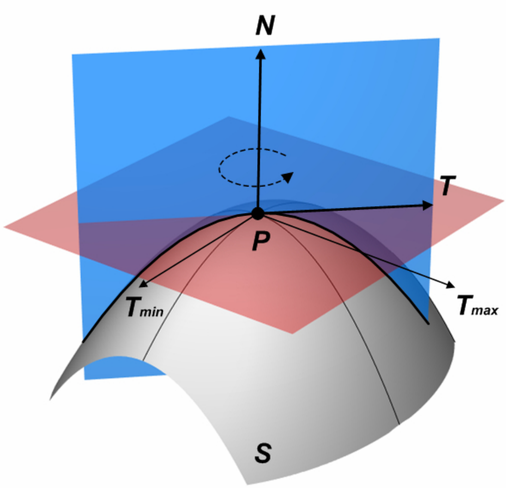

Figure 3.2: Definition of the normal curvature and principal curvatures: the red plane is the tangent plane of surface S at a point P. The blue plane is a normal plane defined by the surface normal N and an arbitrary tangent vector T. The corresponding normal curve is presented as a thick black curve. T_{min} and T_{max} are principal curvature directions at P with their corresponding normal curves presented as thin black curves.

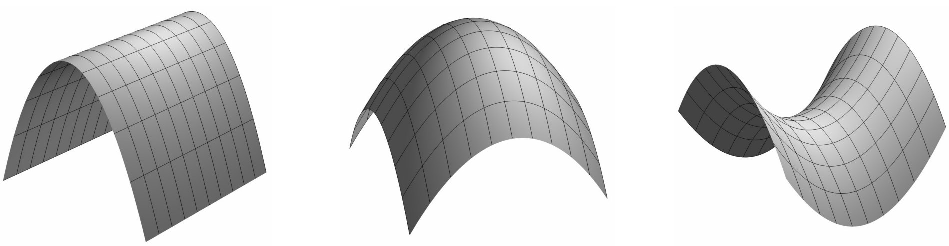

(a) (b) (c)

Figure 3.3: Three surface shapes characterized using Gaussian curvature: (a) parabolic surface has $K = 0$, (b) elliptic surface has $K > 0$ and (c) hyperbolic surface has $K < 0$.

Principal curvatures, Gaussian curvature and Mean curvature are important geometric properties of 3D surfaces. In computer graphics and visualization applications, representations of objects are normally not analytical models but composed of discrete surfaces. As discussed in Chapter 2 Section 2.2, explicit triangle meshes are used in surface rendering and implicit iso-surfaces are used in volume rendering. In such cases, it is not viable to use analytical methods for curvature estimation. Therefore discrete curvature techniques have been developed and applied for surface geometry processing in visualization applications.

3.1.2 Applications of Surface Curvatures

There are a variety of applications for surface geometry processing using curvatures. Curvature measures can be used in segmentation, shape detection, geometric modeling, surface remeshing, mesh simplification, surface smoothing, image noise diffusion and so on.

Scalar curvatures are popular mesh features used in mesh segmentation methods [Sha04, LDB05, BJ88, MW99]. Curvature-driven geometric partial differential equations were used to solve several surface modeling problems [XPB06]. Alliez et al. [ACSD+03, AUGA05] made use of lines of curvature for triangulated surface remeshing. In mesh simplification, surface curvatures were used as the most important information for the decision of mesh vertex removal and to get edges of reasonable lengths for optimal triangulations [YCL02]. Desbrun et al. [DMSB99] developed an algorithm for 3D data noise removal by using mean curvature flow to smooth surface meshes. Kindlmann et al. [KWTM03] used curvature-based transfer functions to enhance volume rendering effects in three different applications: non-photo realistic rendering, surface smoothing via anisotropic diffusion and visualization of iso-surface uncertainty.

Curvature-based surface geometry processing techniques have been extensively applied to automatic polyp detection in CT colonography. Features derived from surface curvatures are used to identify characteristic polyp shapes [SSM+98, YN01, HSH05, ZBB+06]. In this thesis, we present a prototype automatic polyp detection system based on the use of surface curvature lines to characterize shape features of colonic polyps. As the first step in our CAD scheme, robust and accurate curvature estimation is crucial to the detection result.

3.2 Curvature Estimation on 3D Surfaces

In this section, existing curvature estimation approaches are surveyed. The performance of each method will be discussed, in terms of speed, robustness and accuracy.

Corresponding to the triangle mesh and implicit iso-surface representations, there are in general two classes of surface curvature estimation methods:

- Kernel methods work directly on voxel gray-values of 3D volume images.
- Mesh methods calculate curvatures at vertices of triangle meshes generated by the Marching Cubes algorithm.

Due to the discrete nature of 3D surfaces in computer graphics, both of these estimation methods are discrete curvature techniques. This means that analytical surface functions are not directly known and original curvatures are actually approximated based on discrete samplings of the surface. Analytical theories and concepts in differential geometry can still be used yet need to be transfered and adapted in discrete cases.

3.2.1 Curvature Estimation on Implicit Iso-surfaces Embedded in 3D Volumes

Kernel-based curvature estimation methods are applied to the implicit representation of the surface in 3D volume data. They calculate curvature values and directions based on the partial derivatives of 3D images. Partial derivatives of the implicit iso-surface can be directly computed using gray values of 3D image voxels, without extracting the surface first. Such methods are known as kernel-based, because the partial derivatives are normally calculated by convolution with Gaussian derivative kernels.

Before the development of kernel-based methods for 3D surface curvature estimation, traditional methods were based on surface fitting [MAS91]. These methods fitted a parametric surface to the 3D image and iso-surface curvatures were then approximated using the analytical function of the fitted surface. A major problem of such methods is the significant fitting error.

Monga et al. [MBF92] developed a fundamentally new approach whereby they first defined a local coordinate system using the gradient vector and two arbitrary orthogonal vectors in the tangent plane. Principal curvature values and directions were computed using the Hessian matrix. All entries of the Hessian matrix are second order partial derivatives of the 3D image and can be calculated using recursive filters or Gaussian convolution masks. Similar to the method in [MBF92], van Vliet and Verbeek developed a method also based on the Hessian matrix for isophote curvature estimation in 3D [vVV93]. The authors later developed a new strategy to design recursive Gaussian derivative filters, which yielded a high accuracy and excellent isotropy in n-D space [vVYV98]. This method were used to improve their kernel-based isophote curvature estimation.

Thirion and Gourdon proposed a classical kernel-based curvature estimation method in [TG95a]. In their method, implicit iso-surface curvatures and directions were represented using only the first and second partial derivatives of the 3D image in the three axial directions. This helped to avoid the problems of parameterizing the iso-surface.

Kindlmann et al. [KWTM03] developed a method using the Hessian matrix to calculate iso-surface curvatures. Curvatures were described as the change of image gradients within the tangent plane of the iso-surface. They derived a simple matrix, called the *Geometry Tensor*, to estimate principal curvature values.

As pointed out by Campbell and Summers [CS04], and van de Weijer et al. [vdWvVVvG01], kernel-based methods might lead to tremendous errors when applied to curved plates, hollow objects and concentric shells. This is due to zero gradients at such thin structures. To solve these problems, van de Weijer et al. [vdWvVVvG01] proposed to use parametric curvilinear models that were fitted to the local gradient vector fields. Also based on the use of local gradient vector fields, Rieger et al. [RTvVV04] proposed to incorporate the kernel-based approach with the gradient structure tensor and Knutsson mapping for thin shells and hollow objects. Van Wijk et al. [vWTvG+04] used normalized convolution to measure curvature features on the implicit iso-surface of the colon wall for detecting colonic polyps. Their method optimized the trade-off between noise reduction and mixing of adjacent image structures.

In summary, kernel-based curvature estimation methods for implicit iso-surfaces embedded in 3D volume are significantly dependent on the kernel design. The partial derivatives of 3D images computed by convolving with Gaussian derivative kernels are crucial to the curvature estimation accuracy. Concerning the nature of 3D volume, which is normally a rectangular grid in CT colonography, these partial derivatives have to be computed as isotropic quantities, in order to preserve balanced image characteristics. Therefore the directional sampling for the convolution and the kernel size of the Gaussian filter should be isotropic. This can significantly help to guarantee the curvature estimation accuracy. In general, due to the nature of Gaussian convolution theories and the implicit surface representation, kernel-based methods can provide more accurate curvature estimation results and therefore are usually favored for iso-surface geometry processing in CT colonography.

3.2.2 Curvature Estimation on Triangle Meshes Extracted from 3D Volumes

A lot of efforts have been done for the development of curvature estimation methods on polygonal meshes. These methods take a certain neighborhood of the mesh vertex of interest and estimate curvatures based on connections of the central vertex and its neighbors. Only positions of mesh vertices and edges are used, without any convolution and Gaussian filtering involved. This is the major difference between mesh-based methods and kernel-based methods.

Several surveys have been published in the literature [GS03, SMS+03a, TT05, MSR07]. Various taxonomies of curvature estimation methods on triangle meshes were proposed in these surveys. Following these taxonomies, current methods in this section are classified into five classes:

- Parametric Surface Fitting (or Paraboloid Fitting): This method approximates a small neighborhood of a vertex on the triangle mesh using a parametric surface. Principal curvature values and directions are approximated using second order derivatives of the fitted analytical surface function.

- Circular Fitting: This method makes use of directional normal curvatures of the triangle mesh. Each neighboring vertex corresponds with a directional curvature value. Principal curvature values and directions are computed by merging these directional curvatures based on Euler and Meusnier theorems [Car76].

- Discrete Differential Geometry Approach: This method derives discrete approximation forms of the original differential geometry formulas and computes surface curvatures by directly solving these discrete equations based on the central mesh vertex and its neighbors.

- Curvature Tensor Voting: This method computes mesh surface curvatures by estimating the curvature tensor and the eigen analysis of it. Different voting mechanisms are employed to improve the accuracy of curvature tensor computation.

- Approach based on Multiscaling and Smoothing: This method obtains a more robust curvature estimation by means of surface mesh smoothing in advance or using a multiscale local surface description.

Parametric Surface Fitting

By fitting an analytically smooth mesh to surface mesh patches, surface mesh noise and irregularities were expected to be covered. The principal curvatures that need to be estimated are considered to be identical to the principal curvatures of the fitted parametric surface. Second order partial derivatives can be calculated analytically using the fitted surface function. In these methods, the local mesh surface is normally assumed to be planar, biquadratic, bicubic or biquartic. An important problem here is to find a proper parametric surface fitted to the local mesh.

Paraboloid fitting [SW92, KLM98] is an often used approach for parametric surface fitting. Alternative fitted functions are cubic B-spline [Die93] and quadratic polynomials [Ham93]. A comparison of these surface fitting methods was performed by Huang et al. [HSH05]. They found that cubic B-spline fitting performed the best regardless of large orientation variances. Cubic B-spline fitting and quadratic polynomial fitting performed equally well for large samples while the latter performed better for small ones. The authors proposed a two-stage curvature estimation approach, in which the cubic B-spline fitting was performed first for its insensitivity to orientation and then a small data sample was fitted by a quadratic function if the spline fitting errors was too large.

Circular Fitting

By definition (Section 3.1.1), principal curvatures are maxima of directional curvatures of normal curves passing through a surface point. The two methods developed by Chen and Schmitt [CS92], and by Martin [Mar98], made use of directional normal curvatures to compute principal curvatures. A circle is fitted to the central mesh vertex and two of its immediate neighbors. Then the curvature of this fitted circle is considered as the corresponding directional normal curvature. For the central vertex and its all neighbors, corresponding normal curvatures are then merged to compute principal curvatures.

The circular fitting method proposed by Watanabe and Belyaev [WB01] produced higher quality estimates. They derived integral formulas for calculating Gaussian and Mean curvatures. Then these equations were approximated using the trapezoid approximation for the discrete neighborhood of the central mesh vertex. These approximated equations were solved using the central vertex and its immediate neighbors to get Gaussian and Mean curvatures.

Discrete Differential Geometry Approach

In discrete differential geometry, analytical equations are reformulated to piecewise representation. Original quantities and concepts are redefined or approximated using the 3D shape information represented by mesh vertices and edges. This means that deduced discrete formulas only consist of variables of mesh vertices and directly express how to compute principal curvatures using these vertices. The deduction of discrete forms is based on finite element theories. These discrete formulas are usually short and have small computational complexity at the cost of some accuracy loss. For example, the average of the dihedral angles between all faces surrounding a mesh vertex can be used.

Several works using discrete differential geometry were outlined by Krsek et al. [KLM98]. The Gauss-Bonnet theorem [Car76] was widely used in these methods. The discrete approximation of the Gauss-Bonnet theorem applied on triangle meshes is based on the angle deficit computation. It was used to calculate the Gaussian curvature using immediate neighboring triangles of the central vertex [DHKL01, MDSB02, KKL02]. The meaning of angle deficit is that, for a flat surface with zero curvature, the sum of angles of neighboring triangle outer edges at a central vertex is 2π, while for nonzero-curvature surfaces, this sum is smaller than 2π. Particularly in the work by Meyer et al. [MDSB02], a set of differential geometry operators were defined as well as their discrete approximations. Principal curvatures were calculated in a straightforward way using these simple formulas.

Curvature Tensor Voting

The curvature tensor associates the normal curvatures to each tangent direction at a point on the surface [Car76]. The principal curvature values and directions can be computed by first restricting the curvature tensor matrix (a 3×3 symmetric matrix in 2D manifolds) to the tangent plane at a surface point, and then performing eigenanalysis of the resulting 2×2 matrix. Its eigenvectors are equivalent to principal curvature directions and principal curvature magnitudes can be computed by applying a fixed homogeneous linear transformation to the eigen values.

Taubin's method [Tau95b] is considered as the basis for triangle mesh curvature estimation using curvature tensor. This method works on the 1-ring neighborhood, which is composed of the immediate neighbors of the central mesh vertex. The curvature tensor was approximated using directional normal curvatures corresponding to a finite set of neighboring edges. The normal of the central vertex was computed as the average of its 1-ring neighboring triangle plane normals. The resulting eigenvalues were used to compute principal curvature values. Corresponding eigenvectors were principal curvature directions.

Various approaches for improving the computation of curvature tensor on triangle meshes followed Taubin's work. These approaches either used extended neighboring regions to cover noise impacts [GKS00] or applied reasonable voting mechanisms to better approximate the overall shapes [TT05]. Page et al. [PKS$^+$01, PSK$^+$02] improved Taubin's method by employing a more accurate directional normal curvature approximation and an enlarged neighborhood bounded by the geodesic distance.

Multiscaling and Smoothing Schemes

Researchers have noticed that curvature estimation results are highly sensitive to noise. This problem has been handled in three ways:

1. Some methods were proposed to have more robust curvature estimation by means of smoothing or using a multiscale local surface description.

2. Some methods tried to smooth the surface mesh first and then computed principal curvatures using an existing estimation approach on the smoothed mesh.

3. Others modified the surface mesh parameterization for the curvature computation, while actually smoothing was performed within their formulation.

The advantage of multiscale techniques is that they improve multiple computation problems, e.g. interpolation, smoothing and segmentation.

A representative approach of them was developed by Mokhtarian et al. [MKY02]. This method first smoothed the surface mesh by iteratively convolving local parameterization of the surface with 2D Gaussian filters. Semigeodesic coordinates were constructed at each mesh vertex. Then Gaussian and Mean curvatures were computed on the smoothed surface mesh at multiple scales. Their results showed that curvature estimation became more robust after surface smoothing. Also in [DT97], a multiscale curvature technique was presented for more stable shape representation and recognition.

3.2.3 Discussions on Accuracy and Robustness

There are three essential factors that influence the quality of iso-surfaces in CT colonography:

- CT data noise lead to distorted shapes.

- Triangle mesh resolution determines how much details are presented.

- Triangle mesh irregularity results in unbalanced sampling for curvature estimation.

CT data noise is inevitable in practical applications, in spite of the use of denoising and smoothing techniques during preprocessing. For the accuracy of later stages in the analysis pipeline, having curvature estimation methods that are robust to varying surface quality is important. The problem is how to cover image data noise and surface mesh irregularities. Since a preprocessing step is not always the best solution, some approaches tried to make the estimation procedure relatively invariant to the surface quality.

In order to cover image noise and preserve details of small but important structures, a proper kernel size has to be carefully selected for kernel-based methods applied on implicit iso-surfaces. In order to reduce the influence of image noise, a larger kernel is normally desired, while a smaller kernel is used to preserve more detailed information of the iso-surface. The trade-off between implicitly smoothing the surface and the sensitivity to surface details needs to be carefully considered.

For explicit triangle meshes, many approaches [Tau95b, DHKL01, MDSB02, KKL02] performed their computations at a mesh vertex within the immediate 1-ring neighborhood, which is usually a small surface area. The 1-ring neighborhood by definition is very sensitive to data noise and mesh irregularities, since the data noise normally has a similar scale. Consequently, it is very difficult to have an accurate curvature estimation against mesh artifacts only based on the 1-ring neighborhood, unless an ideally smoothed and regular mesh is given. Researchers have proposed extended regions on neighbors for the improved computation [GKS00, PKS$^+$01, PSK$^+$02]. The enlarged surface area couples more global shape information around so that the local surface is implicitly smoothed. In principal surface fitting approaches [KLM98, Mar98], a large sampling area is employed to obtain a better parameterization of local surface.

An important issue for extending the sampling neighborhood is how to configure the boundary of this area. This problem determines whether surface shape information can be captured isotropically in all directions. It is necessary to have a balanced description of local surface shapes by collecting neighboring contributions. This is very significant for accurate curvature estimation results. A simple definition is to bound the neighborhood using the Euclidean distance. This leads to a coarsely approximated balanced sampling. The *Normal Vector Voting* approach by Page et al. [PKS$^+$01, PSK$^+$02] made use of geodesic distance, which is a more reasonable definition and better supports the balanced directional sampling. Due to the high complexity of ideal geodesic distance computation, the authors proposed a linear approximation which still performed with robust results.

A robust curvature estimation approach should be able to overcome bad iso-surface qualities, i.e. image data noise and mesh artifacts and irregularities. The computation can be improved by a larger sampling scale and more balanced sampling. This can be achieved by enlarging the computation area and employing a reasonable area boundary. These improvements are particularly useful for approaches based on curvature tensor voting.

3.3 Lines of Curvature

The automatic polyp detection method presented in this thesis is based on the use of lines of curvature on the 3D colonic surface. These surface curves are used to visualize principal curvature direction vector fields. In this section, the definition and applications of lines of curvature are outlined.

3.3.1 The Definition and Properties

A line of curvature or curvature line is a curve on the 3D surface that is everywhere tangent to one of the two principal curvature directions. A more formal mathematical definition is given in [Gal00].

There are two lines of curvature passing through a point on the surface. By the definition of principal curvature directions (Section 3.1.1), these two curves are perpendicular to each other at this surface point. Figure 3.4 shows the two lines of curvature passing through the

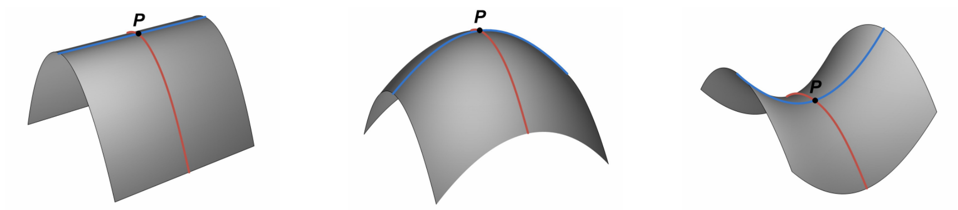

(a) (b) (c)

Figure 3.4: Two perpendicular lines of curvature passing through surface points with three different characteristic shapes: (a) passing through a parabolic surface point, (b) passing through an elliptic surface point and (c) passing through a hyperbolic surface point. Red curves indicate curvature lines of maximum curvature, while blue curves indicate curvature lines of minimum curvature.

parabolic, elliptic and hyperbolic points on the surface. Lines of minimum and maximum curvatures indicate respectively the slowest and steepest variation of the surface normal.

On isotropic surface areas around umbilical points, principal curvature values are equal and principal curvature directions are indeterminable. The orthogonal net of lines of curvature becomes singular at an umbilical point. Typical examples of such isotropic surface shapes are spheres and planes. Lines of curvature through umbilicus typically form one of the three configurations: star, lemon and monstar, while other configurations are possible for transitional cases. In computer graphics applications, these umbilicus regions need to be processed with particular operations.

3.3.2 Applications in Computer Graphics and Visualization

Line drawings are often used to facilitate the visual perception of shape features. A well known application is artistic drawings. For example, hatched line strokes are used to exhibit cascaded objects in charcoal drawings and a caricaturist only uses a few featured strokes to convey strong geometric information. In engineering design and manufacturing, reflection lines projected onto surfaces help automobile designers to improve the quality of their products [PM02]. In the scientific community of computer graphics and visualization, surfaces curves, including lines of curvature, have been increasingly used in the fields of *computer-aided geometric design (CAGD)*, *non-photorealistic rendering (NPR)*, *surface remeshing* and so on.

There are a number of papers dealing with lines of curvature in the field of computer-aided geometric design. Principal patches were introduced by Martin [Mar83] as a surface area bounded by lines of curvature. Among the principal patches, Dupin's cyclide patches of which lines of curvature are all circular arcs were used for surface blending [DMP93]. Lines of curvature obtained considerable attentions for plate-metal-based manufacturing [Mun87]. The computation of lines of curvature around umbilical points on implicit surfaces were analyzed in [MWP96, CPZ07].

Surface curves have been widely used to enhance the displaying of 3D surfaces in non-photorealistic rendering. Many techniques of using ridge and valley lines for shape recognition, coding and quality evaluation were developed by [KWTM03, IFP95, OBS04]. Lines of curvature were used in hatching techniques that generated perceptually convincing displays of complicated surfaces [RK00, GIHL00, HZ00].

Alliez et al. [ACSD+03] presented a surface remeshing algorithm that used anisotropic information represented in geometries of lines of curvature. To the best knowledge of the author of this thesis, lines of curvature have not been used for computer-aided detection of colonic polyps yet. In this thesis, we will present a novel technique using these curves to characterize polyp surface shapes (in Chapter 4).

3.4 Curvature Line Generation on 3D Surfaces

The generation of lines of curvature on 3D surfaces is a nontrivial issue in computer graphics and visualization applications. This may demand complex computations for iso-surfaces extracted from real data sets. A number of generation approaches have been developed for different applications.

3.4.1 Problems of Curvature Line Generation

Lines of curvature are special streamlines tangent to surface principal curvature direction fields. As streamlines, the generation of lines of curvature is normally based on the stepwise linear integration. There are three well known problems of streamline integration:

1. The order of the integration scheme.

2. The integration step length.

3. The interpolation of the vector fields.

There are first order, second order and even higher order streamline integration schemes. First order integration has the smallest computational complexity, while higher order integration leads to a more accurate result that better couples with features of the vector field. In the sense of efficiency and quality, there is a trade-off between computation cost and accuracy.

Fixed and non-fixed (or adaptive) step length for the streamline integration has been used in visualization techniques. The choice of step length is crucial for an accuracy streamline integration. Normally a small step length is desired to trace a more accurate streamline in the vector field. However, this needs more computation costs with regard to the resolution of the field. Smaller step length is necessary in the regions where the vector direction changes rapidly, while in gentle regions they introduce unnecessary costs. Therefore, adaptive step length has been proposed in order to optimize the computation efficiency while presenting the vector field features.

In real data sets, the vector field is usually piecewise linear and discrete. The original continuous vector field has to be reconstructed using interpolation schemes. There are linear and higher order interpolation approaches. As discussed above, higher order schemes normally indicate higher computational complexities.

Computation efficiency and accuracy should be taken into account to achieve a good streamline generation method. Therefore, streamline integration and interpolation schemes have to be carefully selected. Normally, adaptive integration and higher order interpolation perform better. However, they require more computational expenses.

3.4.2 Methods for the Calculation of Lines of Curvature

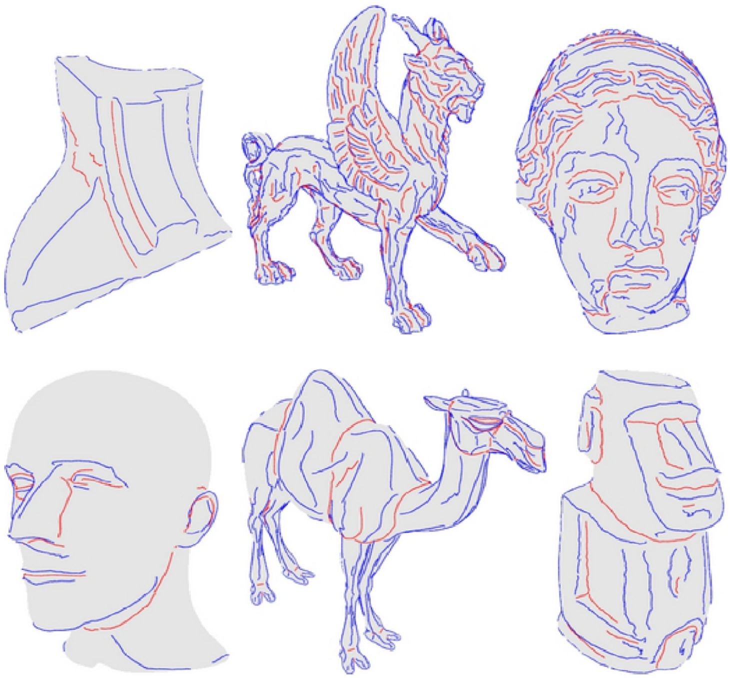

Figure 3.5: Crest lines are detected and rendered on 3D surface meshes.

Since lines of curvature are surface-constrained 3D curves, algorithms for generating surface curves can be used for generating lines of curvature. The adaption is to trace surface curves in one principal curvature direction vector field, instead of other vector fields on the surface.

There are a few existing algorithms developed for the generation of surface curves on triangle meshes. Ridge and valley lines and crest lines are two similar types of surface curves as lines of curvature. They are often used for the enhanced illustration of surface shapes. A ridge point on the surface is a point where curvature magnitude in the maximum curvature direction is a local maximum. A valley point is a point where the curvature magnitude is a local minimum in the maximum curvature direction. Monga et al. [MBF92] introduced

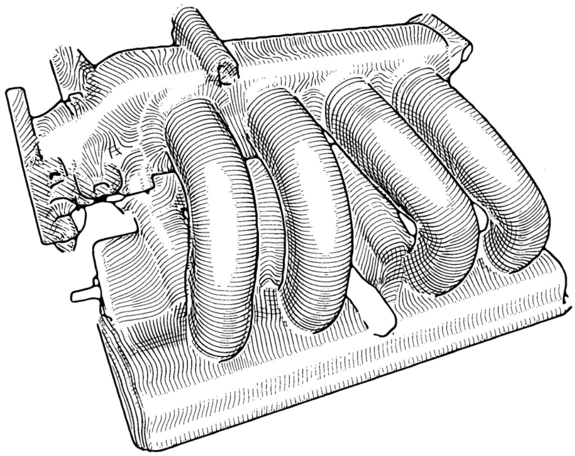

Figure 3.6: The line art of an technical part rendered by Rössl and Kobbelt.

a method that connected ridge and valley points on the surface to form feature lines for the enhanced visualization. Interrante et al. [IFP95] assigned additional opacity functions of principal curvatures to ridge and valley points and then used ridge and valley lines for rendering transparent skin surfaces.

Stylianou and Farin [SF03] developed an automatic crest line extraction method on triangle meshes. The authors presented a method using crest lines for surface segmentation and flattening in [SF04]. Hildebrandt et al. [HPW05] proposed two novel concepts for a more stable algorithm producing visually more pleasing feature lines. Yoshizawa et al. [YBS05] presented a fast and robust crest line integration method on triangle meshes (Figure 3.5). Curvature tensor and extremity coefficients were firstly estimated at mesh vertices. Each edge was examined to determine whether it contained curvature extrema. Crest lines were then detected and connected using the procedure presented in [OBS04]. These crest lines were used for adaptive mesh simplification.

Most of the techniques developed for curvature line calculation on triangle meshes were used in non-photorealistic rendering applications. A majority of them was used in applications of non-photorealistic rendering. Interrante et al. [IFP96] introduced a technique for texturing a transparent surface with uniformly distributed opaque short strokes. Interrante also described how principal curvatures and directions were used to control the placement of lines of curvature over a stroke texture on 3D surfaces [Int97]. Principal direction vector field on the surface was used to generate a single scan-converted solid stroke texture. This surface texture illustrated the essential shape information of any level iso-surface in the volume data.

Elber [Elb99] produced an interactive line art rendering method for freeform polynomial and rational surfaces. Line strokes following principal curvature directions were constructed on the parametric surface using the sketching scheme in [Elb98]. Rössl and Kobbelt [RK00] designed an interactive system for computer-aided generation of line art drawings to illustrate 3D models represented as triangle meshes. Curvature lines were traced in a 2D view of the

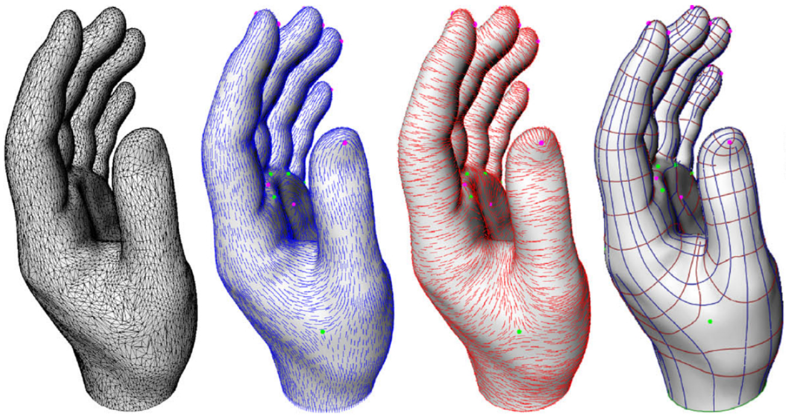

Figure 3.7: Lines of curvature were applied for anisotropic remeshing: from left to right, images are input mesh, minimum curvature direction field, maximum curvature direction field and the network of curvature lines generated.

scene and used for defining line strokes. An intuitive and simple tone mapping technique was derived to generate the final rendering shown in Figure 3.6, by exploring the special structure of the line strokes. A set of algorithms for line art rendering of smooth surfaces was presented in [HZ00].

Girshick et al. [GIHL00] developed a technique for generating lines of curvature on either implicit iso-surfaces or triangle meshes in non-photorealistic rendering. The stepwise line integration was constrained within the mesh triangle plane. The distribution of curvature lines followed the evenly-spaced scheme proposed by Jobard and Lefer [JL97]. Lines of curvature were also applied for anisotropic polygonal remeshing [ACSD+03]. The network of curvature lines was traced on a flattened triangle mesh, using fourth-order Runge-Kutta integration and an adaptive step length [PFTV92]. The distribution of curvature lines were guided by the local curvature magnitudes (Figure 3.7). This surface constrained curvature line distribution scheme is used as the basis of curvature line generation in this thesis.

As far as the author of this thesis knows, no explicitly surface-constrained curvature line generation approach has been developed for the implicit iso-surface embedded in 3D volume data, and for automatic polyp detection in CT colonography. However, the implicit iso-surface rendered using volume ray-casting is usually the preferred surface representation for the visualization of colonic surfaces in CT colonography. In later chapters of this thesis, a novel technique for generating surface constrained curvature lines with curvature controlled seeding and spacing is presented for automatic polyp detection in CT colonography.

3.5 Streamline Seeding and Spacing Strategies

For visualization techniques of flow fields, normally a collection of streamlines are used to interpret topological or geometrical features of the vector field. For the same purpose, lines of curvature need to be well distributed to describe shapes of 3D surfaces.

3.5.1 Essentials of Streamline Placement in Visualization Techniques

An optimal distribution of streamlines is crucial to make these lines better correlate with overall or local features in the domain space. Two pivotal problems are the seeding and spacing schemes in streamline generation. Streamline seeding and spacing address the questions of where to trace streamlines and how many streamlines should be generated.

There are two competing objectives of visualization techniques using streamlines [CCK07]:

- Features of interest should be represented as completely as possible.
- Illustration should cause as little as possible cluttering.

Ideally, no information of the vector field is missed when using a dense enough streamline distribution. However, this may lead to severe cluttering effects. Also redundant and expensive computations can be generated in the implementation. Particularly in 3D cases, cluttering effects can be severe. A balance between the streamline density and represented field features should be carefully selected. That is: Generate streamlines as sparsely as possible while still representing features as completely as possible.

A collection of streamlines forms a sparse representation of a vector field. Its ability for presenting features is highly dependent on three factors:

- Seed location: the starting position for each streamline tracing.
- Spacing distance: how close two streamlines can be.
- Streamline length: the length of each streamline.

The seed position is the most important factor controlling streamline distribution. It controls the overall appearance of the generated streamlines. The spacing distance between streamlines is a criterion for the termination of each streamline tracing. It significantly influences the density of streamline placement. With regard to the variations of vector fields, the spacing distance also determines lengths of generated streamlines. For a better characterization of the vector field, longer streamlines are usually preferable to represent features of large scale areas.

There are feature-guided methods and density-guided methods for streamline placement. In specific applications, if features of interest are known and well-modeled, the feature-guided method can manage the streamline distribution to emphasize these features, which are of interest for certain research or engineering problems. Otherwise, a density-guided method is typically applied when features of interest are not certain. In this case, the distribution of streamlines is independent to the underlying vector flow function. These methods employ a user-specified density function over the vector field. However, such a function is usually not related to the vector flow.

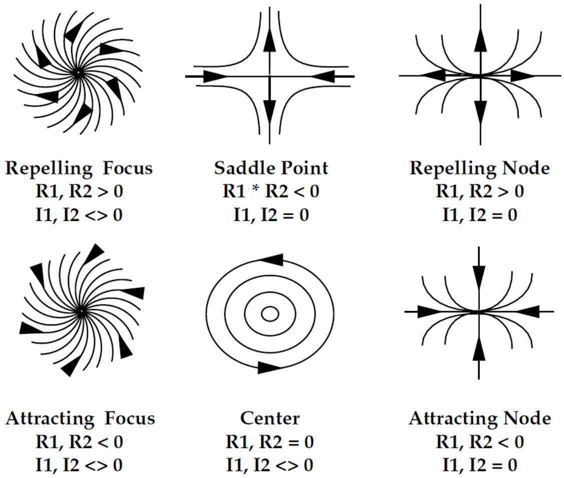

Figure 3.8: Classification of critical points based on the eigenvalues of the local Jacobian: R1 and R2 are eigenvalues, I1 and I2 are eigenvectors (Image source is the article [PVH+03]).

3.5.2 Existing Streamline Seeding and Spacing Algorithms

Streamline techniques are widely used in flow visualization [PVH+03, LHD+04]. As outlined in the previous section (Section 3.5.1), streamline placement strategies are classified into two classes: feature-guided methods and density-guided methods [CCK07].

Feature-Guided Streamline Placement

Feature-guided streamline placement starts with the identification of specific features in the vector field. Example features are boundary layers, separation lines and bubbles, critical points and so on. Critical points have gained particular attention for their specific attributes in flow vector fields. Critical points are defined as positions in the vector field with all zero magnitudes of local vectors. In a velocity field, a critical point has zero velocity so that no streamlines pass through it. Critical points can be classified into different types by the eigenvalues of the local Jacobian [PVH+03] (Figure 3.8). According to the topology in the vicinity of different critical points, different streamline seeding and spacing strategies are applied in order to more specifically characterize these features with different topologies.

Verma et al. [VKP00] first introduced a feature-guided streamline seeding method to capture flow patterns around critical points in 2D vector field. Streamlines were also distributed to obtain sufficient coverage in non-critical regions and guarantee that the overall presentation is aesthetically pleasing. Ye et al. [YKP05] extended the method of Verma et al. to 3D vector fields. They proposed a continuous $\alpha - \beta$ map of 3D critical points such that the seeding templates applied to critical points of different types could change shape depending on how far the critical point is from transitioning into another type of critical point.

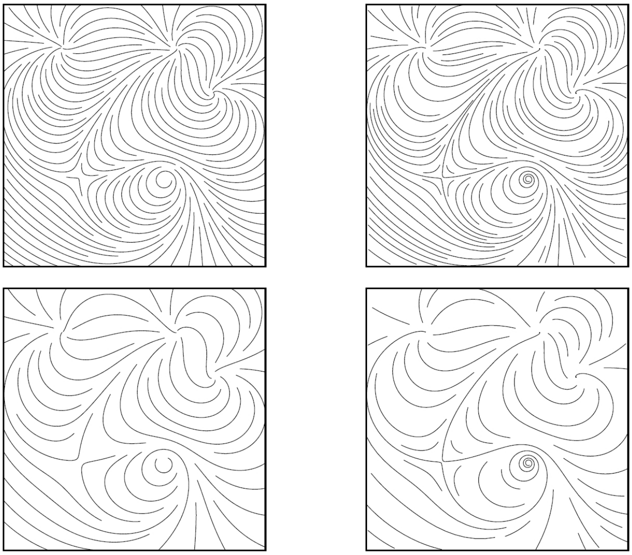

Figure 3.9: Comparison of density-guided approach and feature-guided approach: left images are generated using Turk and Banks' image-guided method, right images are generated using feature-guided approach of Verma et al. . Streamline spacing distance is set as 1.67% of image width for the upper row and 3% for the lower row.

There are two drawbacks of feature-guided streamline placement. First the identification of critical points is not always available and may introduce tremendous computation costs. Second, cluttering problems maybe very significant with a large number of critical points. In this case, a sparse and visually pleasing streamline representation won't be necessarily produced.

Density-Guided Streamline Placement

Density-guided streamline placement approaches are normally based on user-specified density or distance metrics. A function for bounding the distance between streamlines is predefined over the vector field and used to terminate the tracing procedure of each streamline. As the result, the distribution of generated streamlines is independent to the vector field itself and actually controlled by the appearance of these streamlines.

Turk and Banks [TB96] proposed an image-guided streamline placement method in 2D. An energy function was defined as the gray level of the low-pass filtered version of the image and used to guide streamline placement. Compared with the flow feature-guided streamline placement by Verma et al. [VKP00], this method might miss topological importance (Figure 3.9).

The evenly-spaced streamline seeding and spacing technique was developed by Jobard and Lefer [JL97]. The separating distance between adjacent streamlines was controlled by a fixed threshold, in terms of Euclidean distance and according to the overall density of the

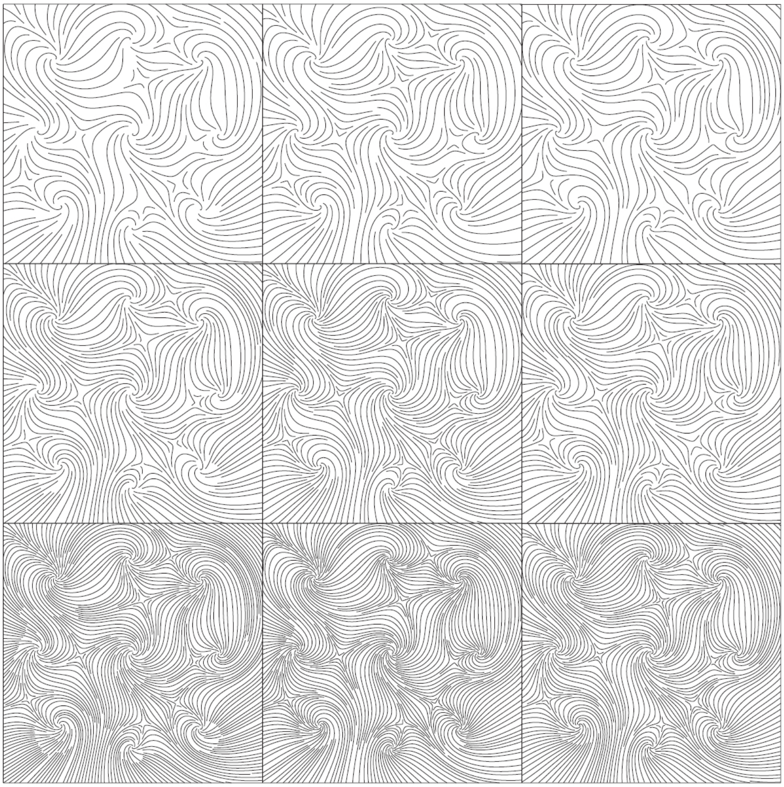

Figure 3.10: Comparison of three density-guided streamline placement: results are generated using the methods in [JL97] (Left), [LMG06] (middle) and [MAD05] (right).

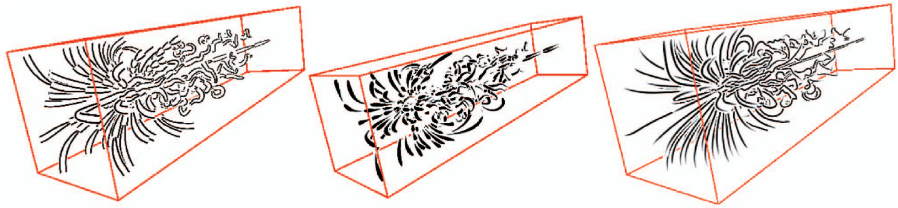

Figure 3.11: Streamlines generated using the viewing plane based method of Li and Shen in a 3D flow field.

image. In order to make a better global appearance of the streamline representation, the threshold (spacing distance) for the streamline termination was tuned as half of the seeding distance. Liu et al. [LMG06] improved the computation efficiency and quality of streamline generation in 2D flow fields for the evenly-spaced strategy. Mebarki et al. [MAD05] presented a farthest point seeding strategy to favor the generation of long streamlines. Figure 3.10 shows a comparison of above three methods presented by Liu et al. [LMG06].

Mattausch et al. [MTHG03] extended the 2D evenly-spaced streamline placement to 3D flow fields. The seeding and spacing distances between adjacent streamlines were thresholded using a 3D Euclidean distance metric. Li and Shen [LS07] argued that streamlines generated in 3D flow fields without considering their projections on the screen plane produced visually cluttered rendering results. They proposed a streamline seeding and spacing strategy in image space to avoid visual cluttering and allow a more flexible exploration of the flow field. The quality of streamline placement was highly dependent on the pre-computed depth image (Figure 3.11).

Schlemmer et al. [SHH$^+$07] proposed a "*Priority Streamlines*" method based on a definition of the streamline density as the ratio between the number of occupied pixels by streamlines and the total number of pixels of the region. Streamlines were placed with increased density in interesting regions, while sparsely in less interesting regions. Allieze et al. [ACSD$^+$03] controlled the distribution of curvature lines on 3D surfaces using the principal curvature magnitudes. Considering the fact that more streamlines were required to preserve sufficient shape information on highly curved surface areas, principal curvature values were used to define a density function adaptive to the surface curvedness for curvature line placement.

Density-based streamline placement methods generally include many redundant streamlines. This significantly increase the computation expense and cluttering effect. To address such problems, Chen et al. [CCK07] introduced an adaptive streamline placement algorithm based on a robust and effective streamline similarity metric. It not only considered the Euclidean distance between streamlines, but also statistically measured the similarities of their shapes and directions. This method implicitly enhanced the representation of flow features by providing streamlines that naturally accentuate regions of geometric interest (Figure 3.12).

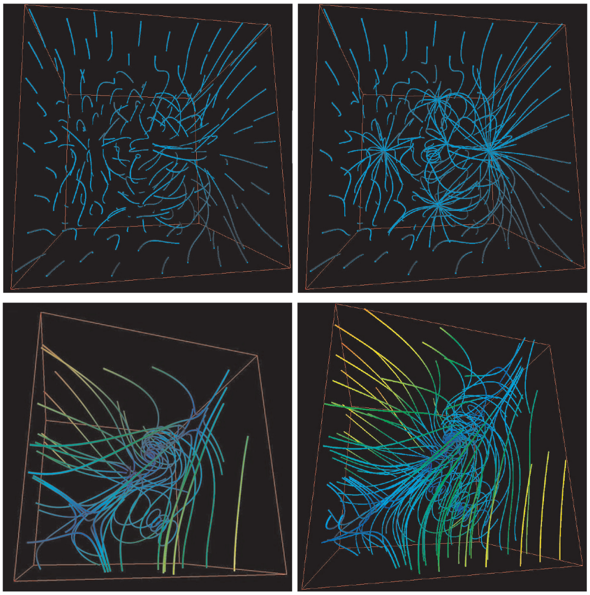

Figure 3.12: The method by Chen et al. (right column) is compared with the density-based method (upper left) using Euclidean distance and the feature-based method (lower left) based on critical points pre-identified.

3.6 Summary

This thesis presents research on automatic polyp detection using visualization techniques in CT colonography. More specifically, the use of surface principal curvature direction vector fields is explored and integrated in our CAD system. Lines of curvature following along principal curvature directions on the colonic surface are used to visualize this vector field and perspectively characterize surface shapes of colonic polyps.

In order to provide context for the use of lines of curvature for surface shape visualization and recognition, this chapter outlined curvature and curvature line computation techniques and visualization techniques using streamlines. Essentials of curvature estimation with regard to robustness and accuracy are also discussed. Streamlines are an important and widely used visualization technique for feature extraction and tracking. Since lines of curvature are considered as a special form of streamlines constrained on 3D surfaces, streamline-based techniques are of significant interest and valuable in our automatic polyp detection scheme.

We expect that there is a promising relation between surface shapes and surface principal curvature directions. Therefore, as a sparse representation of principal direction fields, lines of curvature can be used to extract features of these two vector fields. These features have high correlations with characteristic surface shapes, e.g. colonic polyps that are typically spherical protrusions. On the other hand, lines of curvature are also used to enhance the visualization of the colon wall as a valuable addition to the traditional shaded colonic surface.

In the following chapters of this thesis, techniques of generating lines of curvature are presented. Existing methods for curvature line seeding and spacing are adapted to our application and a novel approach applied on implicit iso-surfaces embedded in 3D volume data is introduced. These curves are used in our prototyping automatic polyp detection pipeline. An evaluation using a large number of real patient data sets demonstrates the discriminating power of curvature line features for polyp detection in CT colonography.

CHAPTER 4

Lines of Curvature for Polyp Detection in CT Colonography

This chapter is based on our paper published in IEEE Transactions on Visualization and Computer Graphics, volume 12, number 5, Sep-Oct 2006 [ZBB+06].

Abstract

Computer-aided diagnosis (CAD) is a helpful addition to laborious visual inspection for preselection of suspected colonic polyps in virtual colonoscopy. Most of the previous work on automatic polyp detection makes use of indicators based on the scalar curvature of the colon wall and can result in many false-positive detections. Our work tries to reduce the number of false-positive detections in the preselection of polyp candidates.

Polyp surface shape can be characterized and visualized using lines of curvature. In this paper, we describe techniques for generating and rendering lines of curvature on surfaces and we show that these lines can be used as part of a polyp detection approach. We have adapted existing approaches on explicit triangular surface meshes, and developed a new algorithm on implicit surfaces embedded in 3D volume data. The visualization of shaded colonic surfaces can be enhanced by rendering the derived lines of curvature on these surfaces.

Features strongly correlated with true-positive detections were calculated on lines of curvature and used for the polyp candidate selection. We studied the performance of these features on 5 data sets that included 331 pre-detected candidates, of which 50 sites were true polyps. The winding angle had a significant discriminating power for true-positive detections, which was demonstrated by a Wilcoxon rank sum test with $p < 0.001$. The median winding angle and inter-quartile range (IQR) for true polyps were 7.817 and $6.770 - 9.288$ compared to 2.954 and $1.995 - 3.749$ for false-positive detections.

4.1 Introduction

Colonic polyps are an important precursor of colon cancer, which is among the leading causes of cancer deaths in the western world [PSBG93]. A polyp is a benign growth of the colon lining. It typically presents as a sphere protruding from the colon wall. Early detection and removal of polyps significantly decrease the incidence of colon cancer. For this purpose, virtual colonoscopy has been developed as a procedure to inspect the interior wall of the human colon by using CT or MRI-scans.

Virtual colonoscopy is a minimally-invasive technique, which causes much less discomfort to the patient than traditional optical colonoscopy [Bar05, PCH+03]. The CT or MRI-scans are processed by iso-surface extraction or by direct volume rendering (DVR) to allow for visual inspection by a radiologist. However, a thorough, visual examination of the complete colon wall is rather time-consuming, which makes the method unattractive for large scale population screening. Therefore, computer-aided techniques have been proposed to pre-detect and highlight colonic polyps in order to reduce the examination time and cost, especially in mass screening of low-incidence populations [SYP+05].

A considerable amount of work has been done for automatic polyp detection; many schemes make use of curvature. Curvature is an important quantity from differential geometry [Car76], which is widely used in computer vision and visualization applications to characterize 3D surface shapes. It can be represented by a scalar (e.g. mean or Gaussian curvature), and by two vectors, indicating the directions of principal curvatures at a given point.

Indicators based on scalar curvature values have been frequently used in previous work for computer-aided diagnosis (CAD) of colonic polyps. Yoshida et al. [YNM+02] made use of 3D geometric features called the volumetric shape index and curvedness to develop a CAD scheme for polyp detection. Näppi and Yoshida [NY03] proposed to use feature-guided analysis for achieving high sensitivity and a low false positive rate in their CAD scheme. Huang et al. [HSH05] developed a two-stage curvature estimation method on triangular surface meshes and performed a filtering based on the sphericity index to identify potential polyps. Van Wijk et al. [vWTvG+04] introduced the technique of normalized convolution to measure curvature features in 3D volume data for automatic polyp detection. Accurate and noise-insensitive curvature calculation is essential for any such scheme. Representations based on point-sampling will in general be more sensitive to noise, whereas aggregation within a region of interest will enhance the robustness at the cost of some sensitivity. Using scalar curvature by itself for polyp detection can result in a large number of false-positive detections.

The potential of principal curvature direction fields has not yet been explored in current polyp detection techniques. On a surface, the two principal curvature directions define two orthogonal vector fields, and these can be visualized by *lines of curvature*, which are lines everywhere tangent to one of these vector fields. We will call these curves *streamlines of curvature*. They have also been used for surface shape analysis in engineering design [BFH86]. However, to the best of our knowledge, no attempt has been made to apply streamlines of curvature for colonic polyp characterization in medical visualization. We hypothesize that the patterns in streamlines of curvature are a good indicator of specific features to detect polyps, both visually and automatically.

In our work, the proposed CAD process proceeds in three steps: pre-detection of polyp candidates, candidate selection, and finally enhanced visualization. Polyp candidates are pre-detected using an existing polyp detection scheme. These polyp candidates include many false-positive detections. The main contribution of our work is to propose a new additional polyp candidate selection approach based on the use of streamlines of curvature, which helps to reduce the number of false-positive detections. We will present methods to generate streamlines of curvature on the colon wall. We have improved existing algorithms for explicit triangle mesh surfaces, and developed a new method for implicit surfaces embedded in 3D volume data. The basis of our work is a robust technique for the computation of principal curvature directions so that the streamlines are as smooth as the surface itself. Subsequently, we ensure that a streamline accurately traces the true principal curvature directions of the surface. Note that constraining the streamlines to the surface will require extra operations compared to unconstrained streamline generation in a 3D vector field. For a good view of the local surface shape, a set of streamlines with controlled spacing must be generated, to reveal the important shape features, and to cover all important details. Therefore, the seeding and spacing of the streamlines is governed by local surface curvature. We extract features strongly correlated with true-positive detections from the generated streamlines. These new features provide a new basis for an automatic polyp detection algorithm. The streamlines of curvature support the perception of surface morphology in addition to the traditional shading. The shape is summarized using the streamlines that have specific patterns at polyp positions.

The rest of the paper is organized as follows. A brief survey of relevant research is given in section 4.2. In section 4.3, a relation between principal curvature directions and polyp surface characteristics is established. In section 4.4, our approach to generate surface-constrained streamlines of curvature and the seeding strategy is described. We start with an improvement of the existing algorithm on triangle meshes and then we describe a new scheme based on implicit iso-surfaces. The performance and applicability of these two methods are compared. In section 4.5, new features are defined on streamlines of curvature and used to select true-positive polyp detections. An experimental study of our polyp selection scheme and enhanced visualization of the colon wall are given in section 4.6. At the end of the paper, we draw some conclusions and suggest items for future work.

4.2 Related Research

Our work is related to many other research fields. The main purpose is to generate and render streamlines of curvature on the colonic surface and use them for improving automatic pre-detection of polyps.

Drawing from computer vision and visualization, surface curvature estimation is the basis of our curvature streamline generation. Triangle meshes are problematic for surface curvature estimation. We often do not have an analytical function describing the continuous surface approximated by the mesh. Concepts in differential geometry are no longer applicable in this discrete case. Approaches have been developed to approximate original surface curvature

[SMS+03b]. Mesh quality significantly influences the estimation results. Current triangle mesh extraction techniques often introduce strong artifacts. Most estimation methods suffer from mesh irregularities and data noise. Computing curvature directly from 3D volume data is based on derivatives of 3D images. These derivatives are usually estimated using kernel methods [vVYV98]. Parameters of the kernel must be properly set to achieve accurate and reliable results [CS04].

For triangle meshes, some methods [KPH97] fit an analytic surface to a neighborhood of a mesh vertex and calculate curvature from the fitted function. Other methods estimate curvature for a surface region using total curvature defined in [O'N97]. Lin and Perry [LP82] used the angle deficit to measure the Gaussian curvature. Meyer et al. [MDSB02] defined discrete differential geometry operators on triangle meshes. Taubin's method [Tau95b] is unique among other methods. It calculated curvatures at mesh vertices using the curvature tensor. For implicit iso-surfaces in 3D volume data, Thirion and Gourdon's method [TG95b] was based on the implicit surface representations defined in differential geometry. The Hessian matrix of 3D volume data was introduced as another tool in [MBF92].

Lines are often used to express shape features. Reflection lines on surfaces give designers crucial feedback on the quality of their product [PM02]. Interrante et al. [IFP95] made use of line textures to enhance the perception of surface shape. In [ANP+01], streamlines in 2D optical flow were used to examine interesting features for polyp detection.

Streamlines of curvature can be traced on the surface and should be well distributed for efficient shape characterization. Nagy et al. [NSW02] presented an interactive technique based on streamlines of curvature in 3D volume. Girshick et al. [GIHL00] introduced a simple scheme to trace streamlines of curvature on triangle meshes. In their work, streamlines were evenly spaced by using a special seeding method [JL97]. Mebarki et al. [MAD05] proposed a fast farthest point seeding algorithm that can trace longer streamlines in 2D vector fields. Other work made use of local surface features to control the streamline density. Verma et al. [VKP00] discussed characteristics of a good seeding strategy and presented a method using local flow topology. Alliez et al. [ACSD+03] applied streamlines of curvature for surface remeshing. They traced streamlines in the parameter space of a surface after the original surface was flattened. Curvatures were employed to optimize the streamline density in order to preserve surface information after remeshing. However their work did not apply to implicit iso-surfaces.

4.3 Polyp Characterization Using Lines of Curvature

The idea of using streamlines of curvature for polyp candidate selection is inspired by visualizing the two vector fields of surface principal curvature directions. Our work starts with curvature estimation on triangular surface meshes, both for scalar curvature and for principal curvature directions.

A robust curvature estimation approach, named the Normal Vector Voting (NVV) method [PSK+02], is applied on triangular colonic surfaces extracted from real CT scans using Marching Cubes. We will discuss the NVV method later in Section 4.4.1. Visual inspec-

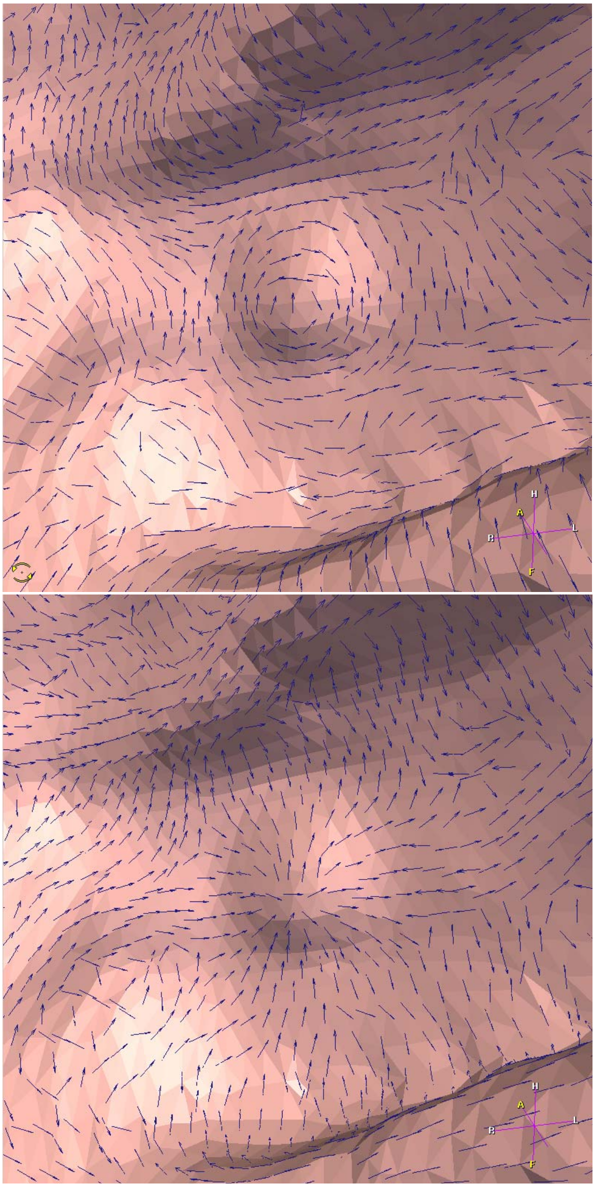

Figure 4.1: Distinctive patterns on polyp surfaces. Upper: Circular pattern in maximum curvature directions. Lower: Focusing pattern in minimum curvature directions.

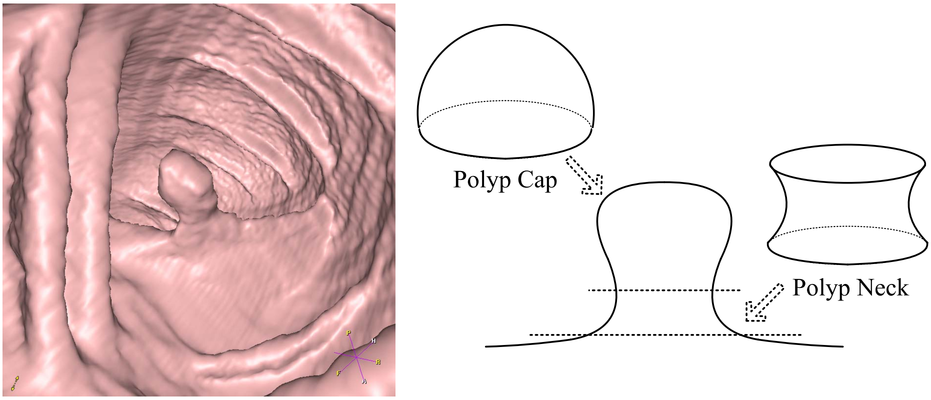

Figure 4.2: A polyp surface has two parts: ideally, the cap is spherical and convex, the neck is a closed-ring and anticlastic surface.

tion of principal curvature directions shows patterns on polyp surfaces that may discriminate polyps from healthy tissue (Figure 4.1). In the case that mesh surface normals point towards the interior of the colon, the maximum curvature directions around the polyp present a circular pattern while the minimum curvature directions present a focusing pattern. This relation can be explained with a generalization of the polyp surface.

A polyp surface consists of two parts, the top part and the bottom part (Figure 4.2). We call the top part the polyp cap and the bottom part the polyp neck. The polyp cap is the most protruding area on a polyp surface. It is ideally represented as a spherical or ellipsoidal surface. The polyp neck is the transition area from the background to the polyp cap. It is typically a closed-ring and anticlastic surface, i.e. all points on the polyp neck are hyperbolic. Considering the local geometric properties, surface principal curvature directions on the polyp cap do not always show characteristic patterns. Sometimes, a polyp can not be easily identified only according to its cap. Most existing polyp detection methods use indicators based on scalar curvatures, e.g. the volumetric shape index [YNM$^+$02] and the sphericity index [HSH05]. Such indicators only work on the polyp cap. Therefore, they sometimes can introduce many false-positive detections. The polyp neck is a distinctive part of the polyp. Every polyp has a neck as long as it protrudes from the colon wall. Around such an anticlastic area, principal curvature directions present particular patterns of polyps, i.e. circular or focusing patterns.

Streamlines of curvature can be used to visualize principal curvature directions on the colonic surface. Therefore, specific patterns in streamlines of curvature can help to discriminate polyps from background. The circular pattern in maximum curvature directions around the polyp neck suggests potential. Since the polyp neck is typically a closed-ring area, approximately closed streamlines are expected to locally represent the polyp narrow part or neck. For this reason, we propose to supplement existing polyp detection methods with an analysis on the polyp neck.

4.4 Generating and Rendering Lines of Curvature on Colonic Surfaces

Streamlines of curvature support polyp candidate selection and enhance polyp visualization when they are superimposed on the colon wall. This section describes techniques to generate these curves on explicit triangle meshes as well as on implicit iso-surfaces.

4.4.1 Lines of Curvature on Explicit Triangle Mesh Surfaces

The first step to generate streamlines of curvature on triangle meshes is curvature estimation. Smooth and regular principal curvature directions are desired to correspond with surface shape. The NVV method developed by Page et al. [PSK$^+$02] is a robust curvature estimation approach on general triangle meshes even with low quality. It uses the geodesic neighborhood as an improvement of other types of neighborhoods, e.g. the k-ring ($k = 1, 2, 3, \ldots$) neighborhood. It is defined to be a surface region bounded by a user-specified geodesic distance from the central mesh vertex. A k-geodesic neighborhood not only enlarges the computation area but also supports balanced directional sampling around a mesh vertex. This is very useful to reduce the effects of mesh irregularity and noise.

The NVV method provides robust curvature estimation on triangle meshes, for both scalar curvature values and principal curvature directions. We extended and improved the streamline tracing technique described in [GIHL00] on triangular colonic surfaces, by integrating the NVV method and a simplified computation. This algorithm traces the streamline on the mesh by projecting each integration onto the local mesh triangle. When the streamline reaches a mesh edge, the intersection point with that edge is added and the local mesh triangle is updated. We found calculating intersection points of mesh-constrained streamlines and edges to be complicated by the limited floating point precision. The inaccuracy caused by this accumulates as an error during streamline integration. To alleviate this problem and simplify the computation of intersection points, we transform the problem to 2D. We define a local 2D coordinate system for each triangle plane. A triangle vertex is set to be the origin. One axis coincides with a triangle edge. Intersections with edges can be easily computed in this 2D coordinate system and then transformed to 3D.

We characterize the local surface shape using collections of streamlines. Therefore it is important that streamlines of curvature are distributed regularly over the triangle mesh using a seeding strategy. The evenly distributed streamlines in [GIHL00] may lose details of surface shape. An adaptive and efficient way was presented in [ACSD$^+$03]. Although the application is different, curvature controlled seeding contributes much to polyp surface characterization. Streamlines of curvature on a colonic surface mesh are shown in Figure 4.3. In this case, the appearance and accuracy of streamlines are significantly affected by the mesh quality and estimated principal curvature directions.

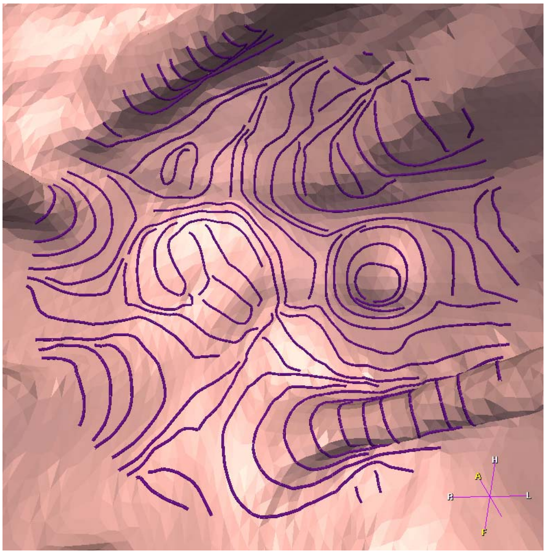

Figure 4.3: Streamlines of maximum curvature are generated and rendered on the triangular colonic surface.

4.4.2 Lines of Curvature on Implicit Iso-surfaces

Implicit surfaces are widely used in Virtual Colonoscopy. Compared to an explicit triangle mesh, an implicit surface provides a smoother and clearer visualization of the colon wall.

An implicit surface is embedded in a 3D volume as an iso-surface. It is usually visualized using volume ray casting techniques. In this section, we describe a new approach to generate streamlines of curvature on implicit iso-surfaces. We first discuss iso-surface curvature estimation. Then we describe our curvature streamline tracing on implicit iso-surfaces. We have adapted the strategy of curvature controlled seeding and spacing for this case.

Curvature Estimation on Iso-surfaces

We use the method proposed by Van Vliet and Verbeek [vVYV98] to estimate principal curvatures on an iso-surface in 3D volume data. There are three steps in this algorithm.

First, we calculate the gradient vector **g** and the Hessian matrix **H** at a position **P** on the iso-surface in 3D volume based on the following definitions:

$$\mathbf{g} = (f_x, f_y, f_z) \qquad \mathbf{H} = \begin{pmatrix} f_{xx} & f_{xy} & f_{xz} \\ f_{xy} & f_{yy} & f_{yz} \\ f_{xz} & f_{yz} & f_{zz} \end{pmatrix}$$

Entries in these definitions are partial derivatives of the 3D image:

$$f_x = \frac{\partial f}{\partial x} \qquad \text{and} \qquad f_{xx} = \frac{\partial^2 f}{\partial x^2}$$

These derivatives can be estimated in a 3D volume by convolution with the derivative of a Gaussian function with a specific kernel width σ.

Second, the Hessian matrix **H** is rotated to align one axis with the local gradient direction **g**. The rotated Hessian matrix can be written as:

$$\mathbf{H_r} = \begin{pmatrix} f_{gg} & \cdots & \cdots \\ \vdots & f_{uu} & f_{uv} \\ \vdots & f_{uv} & f_{vv} \end{pmatrix} = \begin{pmatrix} f_{gg} & \cdots \\ \vdots & \mathbf{H_t} \end{pmatrix}$$

where f_{gg} is the second order derivative along the gradient direction, u and v are the other two axes in the local coordinate system and $\mathbf{H_t}$ is a 2D Hessian matrix in the plane uv.

Finally we perform eigen analysis on the 2D $\mathbf{H_t}$. Local principal curvature values at **P** can be computed based on the local gradient magnitude and two eigenvalues λ_1 and λ_2:

$$k_1 = \frac{-\lambda_1}{\|\mathbf{g}\|} \qquad \text{and} \qquad k_2 = \frac{-\lambda_2}{\|\mathbf{g}\|}$$

The two eigenvectors correspond to principal directions in the tangent plane uv at **P**. They must be transformed to the original 3D coordinate system.

Since most 3D CT images involve noise, we must choose a proper Gaussian convolution kernel width σ. In our implementation, σ is set to be 2.0 millimeters and kernel size is 11 voxels with regard to covering noise and computational efficiency.

Tracing Lines of Curvature on Implicit Iso-surfaces

Tracing a streamline of curvature on an implicit iso-surface is different from a triangle mesh. The position of the surface is not explicitly known. The work in [GIHL00, NSW02] also included approaches tracing streamlines of curvature in 3D volume. But such streamlines are not constrained to iso-surfaces. In our approach, we restrict streamline points to the iso-surface in an implicit way when tracing through the 3D volume.

A streamline is traced using stepwise integration from a seed point in forward and reverse directions. For each integration step, first we calculate principal curvature directions at the current streamline point on the iso-surface using the method in Section 4.4.2. Currently we use linear interpolation to estimate the gradient, the Hessian and the data value at an arbitrary position in the 3D volume. Higher order interpolation, e.g. cubic interpolation, may give a better result. Then the streamline is propagated one step further following the local principal curvature direction. This is a first order integration and higher order schemes, e.g. second and fourth order Runge-Kutta methods, are other improvements. Higher order interpolation will work better only with higher order integration. Since the principal curvature directions are tangents to the iso-surface at the current point, the next point initially integrated in first order generally is not on the iso-surface (See Figure 4.4). Therefore, we project it back onto the iso-surface. First, the gradient vector **g** and data value i are calculated at the initial point **P**. If i is smaller than the isovalue I of the implicit iso-surface, the projection direction $\vec{D}$ is **g**. Otherwise, $\vec{D}$ is $-\mathbf{g}$. Then we iteratively move **P** along $\vec{D}$ for a step length d and compute

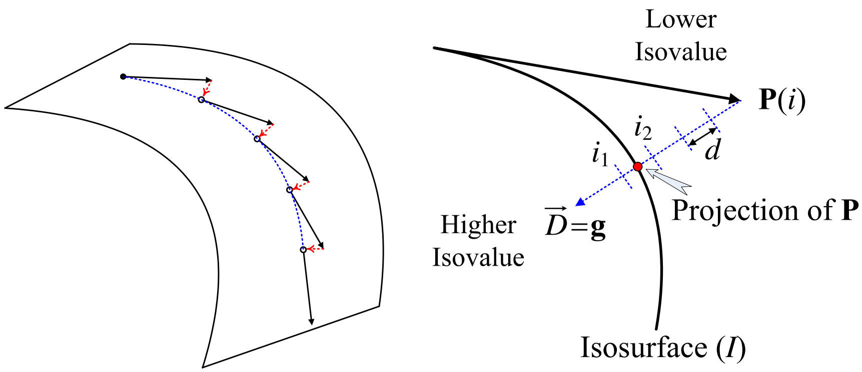

Figure 4.4: Left: Streamline tracing on iso-surfaces. Right: Projection of initially integrated point on iso-surfaces.

i at **P** after each step. i_1 and i_2 are defined to be two consecutive values of i. If one of them is smaller than I and the other is larger, we stop this procedure and compute $\mathbf{P}'$ as the projection of **P** on the implicit iso-surface using:

$$\mathbf{P}' = \mathbf{P} - (\tfrac{i_1 - I}{i_1 - i_2} \cdot d) \cdot \vec{D}$$

Streamline tracing and projection on implicit iso-surfaces are explained in Figure 4.4. A reasonable value for the projection step length d is $\frac{1}{20} \times VoxelLongestDiagonal$, where *VoxelLongestDiagonal* is the longest diagonal of a volume voxel. If we use a very small step length in first order integration or use the fourth order Runge-Kutta method to trace a streamline in 3D volume, this projection technique may not be necessary.

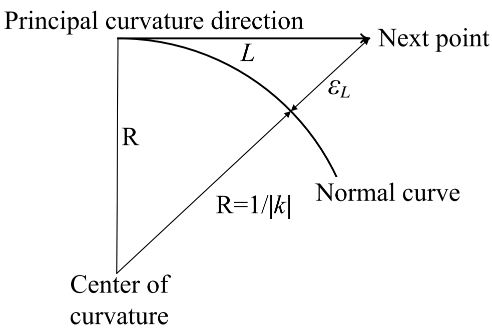

Figure 4.5: Use curvatures to adapt streamline integration step length on iso-surfaces.

On a highly curved surface area, a long streamline integration step may miss important surface information. This can be improved by using the surface curvature to adapt the step length. We developed the approach shown in Figure 4.5. The osculating circle is used to

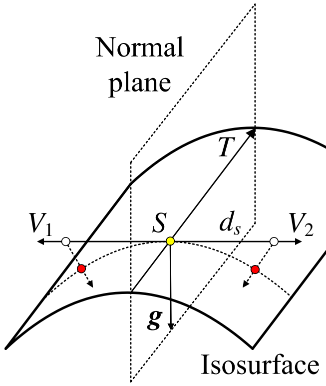

Figure 4.6: A pair of seeds is initially placed perpendicularly to each streamline segment. Then they are projected onto the iso-surface.

approximate the relative local iso-surface normal curve. When tracing in a principal curvature direction, the integration step length L is dependent on the corresponding curvature value k:

$$L = \sqrt{\varepsilon_L \left(\frac{2}{|k|} + \varepsilon_L \right)}$$

where ε_L is specified by the user to bound the distance how far the point is allowed to move away from the iso-surface. Our implementation sets $\varepsilon_L = \frac{1}{10} \times VoxelLongestDiagonal$. We also specify a longest step length $L_{max} = 0.3mm$ when tracing on a flat surface area.

Curvature Controlled Seeding on Implicit Iso-surfaces

We modified the curvature-adapted seeding strategy in [ACSD$^+$03] to distribute streamlines on implicit iso-surfaces. The basic idea of using curvatures to control streamline density on surfaces is to use minimum curvature value to determine the spacing distance between streamlines following maximum curvature direction, and vice versa. We follow a procedure similar to the evenly spaced seeding [JL97]. We first start a streamline from a chosen point on the surface. For each integration step of tracing, a pair of new seeds placed perpendicularly to the integration segment at the local curvature controlled spacing distance (Figure 4.6) is put into a seed queue. Then we iteratively pick another seed in the seed queue and start another new streamline. Except for the first streamline, every time a new streamline is generated, we must remove invalid seeds from the queue before new valid seeds are added. This seeding procedure stops when there is no valid seed. A seed is valid if the distance between it and any streamline point is not less than its local curvature controlled spacing distance. A streamline stops when it is too close to other streamlines or reaches a certain maximum number of integrations.

We developed a method to place the seed on the implicit iso-surface. For each streamline integration (Figure 4.6), we initially place a pair of seeds perpendicular to the current streamline segment on the local tangent plane. At every streamline point S, we construct a normal plane containing the streamline integration direction T and the local gradient vector $\mathbf{g}$. We then compute two vectors V_1 and V_2, orthogonal to and pointing outwards from the normal plane:

$$V_1 = T \times G \qquad \text{and} \qquad V_2 = G \times T$$

The next problem is to decide the spacing distance d_s to place the initial seeds along V_1 and V_2. In the case shown in Figure 4.7, the distance from the initial seed point to the iso-surface is bounded by ε_1. Then the spacing distance d_s will be specified based on the controlling curvature k:

$$d_s = \sqrt{\varepsilon_1 \left(\frac{2}{|k|} + \varepsilon_1 \right)}$$

These two initial seeds generally are not exactly on the iso-surface. Therefore they are projected using the projection technique described in Section 4.4.2.

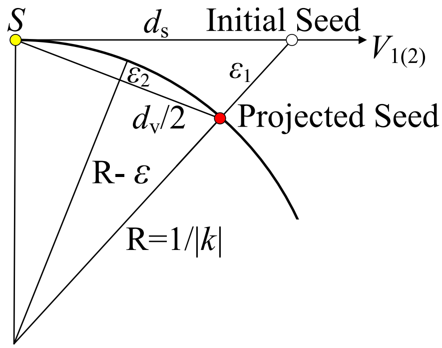

Figure 4.7: Use curvatures to control streamline spacing distance and seed validating distance.

Invalid seeds in the potential seeds queue are removed after a new streamline is traced. To validate a seed, we specify another error boundary ε_2. In Figure 4.7, an osculating circle approximates the intersection arc of the iso-surface between the local streamline point S and a seed on the iso-surface. The optimal spacing distance between these two points is the arc length. The Euclidean distance is used as an approximation to simplify the computation. Its path is offset from the circle arc by a small distance. This distance is bounded by ε_2. Thus the local curvature controlled spacing distance is dependent on the controlling curvature k:

$$d_v = 2 \times \sqrt{\varepsilon_2 \left(\frac{2}{|k|} - \varepsilon_2 \right)}$$

d_v can also be used to validate when to stop the tracing of a streamline. As ε_2 can be computed based on ε_1, we only need to specify one error boundary ε_1:

$$\varepsilon_2 = \frac{1}{|k|}\left(1 - \sqrt{\frac{2+|k|\times\varepsilon_1}{2\times(1+|k|\times\varepsilon_1)}}\right)$$

In our experiments, $\varepsilon_1 = \frac{1}{10} \times VoxelLongestDiagonal$ yielded the best result.

When tracing in one principal curvature direction, the controlling curvature k corresponds to the other principal curvature direction. Figure 4.8 shows the results of our algorithm on an artificial 3D volume data. On both triangle meshes and implicit iso-surfaces, a streamline of curvature is rendered as a ploy line. In order to make a streamline more visible, a thin tube is rendered around it.

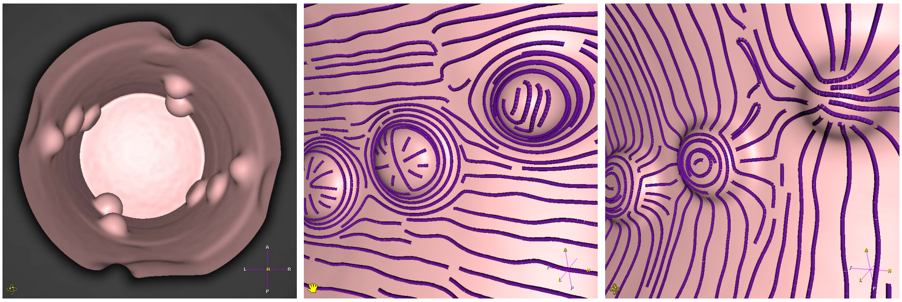

Figure 4.8: Streamlines of curvature on the implicit iso-surface embedded in an artificial 3D volume. Left: A synthetic colon model with many polyp-like bumps. Central: streamlines of maximum curvature. Right: streamlines of minimum curvature.

4.4.3 Comparison

We compared our two techniques described to generate streamlines of curvature on triangle meshes and implicit iso-surfaces. We only focused on the streamline tracing and spacing. Surface curvature estimation was performed as part of the preprocessing stage and we assumed comparable and robust curvature estimations in both cases. Linear interpolation and first order integration were used. We tested on both synthetic data sets and real data sets. Our workstation had a 2.60GHz Pentium 4 CPU with 1GB of memory. The graphics card was NVIDIA GeForce4 MX440 with 64MB.

Table 4.1: Comparison of Computation Time: Streamlines are generated per detection patch.

	triangle meshes	Iso-surfaces
Average Number of Streamlines	43.3	41.2
Average Number of Points	1781	1072
Average Computation Time (sec.)	6.60	3.78

We first recorded computation time in each implementation. Nine synthetic data sets and five real data sets were used. Streamlines were generated for each detection patch with a radius of 16 millimeters. Spacing distance between streamlines was less than 2 millimeters. Table 4.1 gives a first result for both techniques. It indicates that our technique applied to implicit iso-surfaces offers a faster computation for streamline tracing and spacing on a certain part of a surface. The main reason is that mesh-constrained streamlines have more integrations including many intersections with mesh edges.

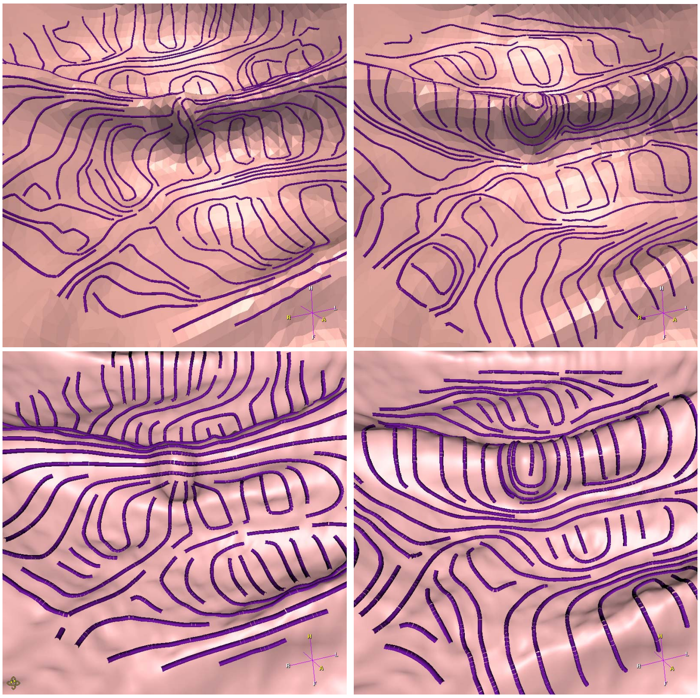

Figure 4.9: Comparison of curvature streamline appearance on the triangle mesh and the iso-surface of a medical 3D volume data: Left two show streamlines of minimum curvature, right two show streamlines of maximum curvature.

Another comparison criterion was the appearance of the streamlines. Since we want to use streamlines of curvature as a tool to characterize specific features of polyps, the shape of the streamline is most important. In Figure 4.9, streamlines of curvature are generated on a triangle mesh and an iso-surface in a real medical data. This 3D volume data is $512 \times 512 \times 255$. Judged by visual inspection, our technique for implicit iso-surfaces gives better results. Streamlines in this case appear to be smoother, longer and more characteristic.

Both triangle meshes and implicit iso-surfaces offer relative advantages in different visualization applications. These two different techniques should be employed on corresponding surface representations. If both of them are applicable, the technique for implicit surfaces is preferred. It favors our improved CAD process in virtual colonoscopy.

4.5 Feature Calculation on Lines of Curvature

Streamlines of curvature with specific patterns, i.e. (almost) closed streamlines, are inspected around the polyp neck. The polyp neck can be identified by detecting such characteristic curves on the colonic surface. To do this, we generate streamlines of curvature for each pre-detected polyp candidate area and select streamlines on each polyp neck. Then we calculate features on the selected streamlines to detect specific patterns.

4.5.1 Selecting Lines of Curvature on the Polyp Neck

We generate collections of streamlines on the colonic surface. Only those streamlines presenting distinctive patterns characteristic of the polyp neck are used for the diagnosis, others may even confuse the result.

We present a method to automatically select important streamlines. In our case, we are most interested in streamlines on the polyp neck area. We combined the use of curvature magnitudes with streamline selection. Considering the fact that the polyp neck area is an anticlastic surface (Section 4.3), the two principal curvature values everywhere on such a surface have opposite signs. In other words a streamline generated around the polyp neck should have many hyperbolic points. We define a quantity, named hyperbolic percentage HP, as a feature to select streamlines on the polyp neck:

$$HP = \frac{n_h}{N} \times 100\%$$

where n_h is the number of hyperbolic points and N is the total number of points on a streamline. A hyperbolic point on the surface has principal curvature values with opposite signs.

The HP is computed for each streamline generated. Then we select the first **N** streamlines with the largest n_h. Each selected streamline must have a $HP \geq 50\%$. Our experience shows that $\mathbf{N} = 3$ or 5 offers simplified computation and guarantees that streamlines on the polyp neck are always selected.

4.5.2 Calculating Streamline Features for Polyp Characterization

We want to find (almost) closed streamlines of maximum curvature in the region of the polyp neck. Therefore, our problem seems to be the topic of detecting (almost) closed streamlines on 3D surfaces.

The detection of specific patterns of streamlines, e.g. closed streamlines and swirling streamlines, is a topic in flow visualization techniques. Our polyp candidate selection scheme is similar to the detection of flow vortices using streamlines. In 2D flow fields, Portela [Por97] introduced the winding angle of streamlines to detect vortices. Sadarjoen et al. [SP99] proposed to use the sum of signed angles along a streamline as a simplification. In 3D cases, winding angles are no longer meaningful. Portela [Por97] suggested reducing the problem from 3D to 2D by projecting local vectors onto the swirl plane. Jiang et al. [JMT02] presented an algorithm to detect swirling features based on the geometry of streamlines.

Swirling streamline patterns used to detect vortices in fluid flow are different from the curvature line patterns to detect polyps. We want to find (almost) closed streamlines, but we can use similar techniques such as the winding-angle technique [SP99]. In 2D flow fields, the winding angle is defined as the cumulative change of direction of the streamline segments. It measures the rotation of a streamline. A swirling streamline must have a winding angle of at least 2π. This feature is used to detect swirling patterns of vortices in 2D flow fields. However the winding angle is inherently limited to 2D.

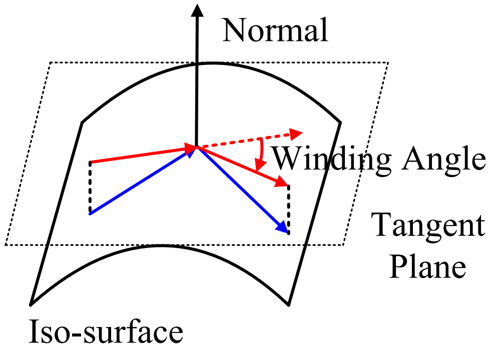

Figure 4.10: Adapt the winding angle method: the changing angle of streamline direction is projected onto the local tangent plane.

We generalized the winding angle concept to space curves. Since streamlines of curvature are traced on 3D colonic surfaces, surface normals could be obtained at streamline points. For each streamline point, the changing angle of streamline direction is projected onto the local tangent plane (Figure 4.10). This projected angle is signed according to the right-hand rule. The sum of such signed angles along a closed streamline may be less than 2π. Therefore, a streamline is considered to be closed if it has two points within a certain very small distance from each other, however the arc length of the streamline in between should be above a certain threshold. The winding angle is computed for each selected streamline, and then the largest winding angle is used as an important feature per pre-detected polyp candidate.

Only polyps larger than $5mm$ in diameter are significant for clinical diagnosis. There are also small bumps on the colon wall, which are not real polyps. Our streamline generation algorithm also generates (almost) closed streamlines around them. To separate them from true polyp detections, we also measure the size of the area enclosed by the (almost) closed streamline in terms of the mean radius. The mean radius of a closed streamline is defined as the average distance from the mean center of the streamline to its points. The mean radius of the selected streamline that has the largest winding angle is used as an additional feature per candidate area in our polyp candidate selection.

4.6 Experimental Study and Results

In this section we document the results of a study that we performed on 5 patient data sets to demonstrate the utility of our streamline selection and streamline-based feature calculation for polyp detection strategies. We also show renderings which illustrate how our surface-constrained curvature streamlines enhance the visual perception of colonic surface shape in virtual colonoscopy.

4.6.1 Polyp Candidate Selection Study

We are planning to integrate our streamline selection and streamline-based feature calculation in a complete polyp detection protocol. The first stage of the protocol is a polyp pre-detection phase [YNM$^+$02] that yields all true-positive detections (as confirmed by medical diagnosis), and also a large number of false-positive detections. Suspect locations are first detected on the colonic surface based on the volumetric shape index. During the second stage, the number of false-positive detections will be reduced using various classification techniques.

We assessed the value of our streamline selection and the winding angle calculation to discriminate between true- and false-positive polyp detections in a large number of candidate areas, with the goal of integrating these techniques in the second stage of polyp detection and classification. CT scans were performed on five patients with a Philips Mx8000 multislice scanner. The average voxel size of the 3D volume image is $0.77mm \times 0.77mm \times 1.60mm$. The preprocessing algorithm [YNM$^+$02] detected 331 polyp candidate areas in total. An expert opinion of an experienced radiologist was used to classify these candidate areas into true- and false-positive detections, where true-positive detection indicates a definite polyp and false-positive detection a non-polyp. Of the 331 candidate areas, 50 sites (15.1%) were classified as true-positive detections. True-positive detections were found in all 5 patients.

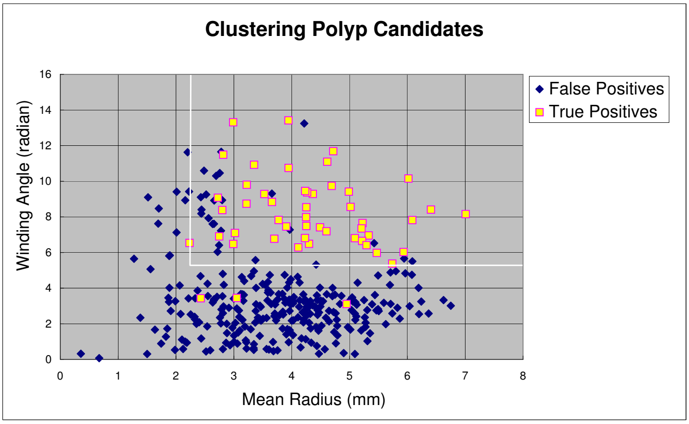

Figure 4.11: Features of Streamlines: Mean Radius and Alternative Winding Angles. True- and false-positive detections are visually clustered.

We applied our streamline selection and winding angle calculation method on all 331 candidate areas. The winding angle was significantly higher for true-positive detections than for false-positive detections (Wilcoxon rank sum test, $p < 0.001$). The median winding angle and inter-quartile range (IQR) for the true-positive detections was 7.817 and 6.770–9.288 compared to 2.954 and 1.995–3.749 for the false-positive detections. Figure 4.11 shows clustering of the true- and false-positive detections. These results indicate that streamline selection and winding angle measurements in candidate areas could make a valuable contribution to an approach for discriminating between true- and false-positive polyp candidate areas as detected by the preprocessing algorithm.

4.6.2 Enhanced Visualization

The visualization of the shaded colon wall can also benefit from streamlines of curvature (images on the left of Figure 4.12). This can greatly enhance the perception of colonic surface features, e.g. polyps. We also show the results of our automatic streamline selection method in the images on the right of Figure 4.12. As can be seen in these images, one or more of the selected streamlines are situated on the polyp neck.

4.7 Conclusions and Future Work

Our work explored the potential of surface principal curvature directions to characterize specific surface shape features, e.g. colonic polyps in virtual colonoscopy. Streamlines of curvature were used to visualize such vector fields. The most important elements are robust methods for curvature calculation, surface-constrained streamline integration, and the use of adaptive seeding and spacing of the streamlines. We developed a new scheme for curvature controlled spacing of streamlines on implicit iso-surfaces. Both the implicit and explicit surface implementations showed good results for surface curvature streamlines. In particular, our approach is useful for implicit surface characterization based on 3D volume data.

(Almost) closed streamlines can be generated on the polyp neck area. Therefore we expect that such characteristic patterns are a good indicator of colonic polyps in virtual colonoscopy. Streamlines are selected based on the local surface geometry and new features are calculated on selected streamlines. A statistical analysis indicated that such streamline features are highly correlated with true-positive detections of a preprocessing polyp detection method. The polyp neck area is considered as an addition to the polyp cap, which is often the main focus of current polyp detection techniques. Our newly defined features on curvature streamlines are expected to reduce the number of false-positive polyp candidates in a pre-detection. We proposed a new polyp candidate selection scheme that can be easily combined with other techniques to improve current computer-aided detection. An enhanced visualization of the colon wall by curvature line patterns can also improve the perception of colonic surface shape for radiologists.

There are a number of promising avenues for future research towards a robust polyp detection technique. For the techniques described, the use of higher order integration and interpolation methods can possibly lead to more accurate results. The streamline-enhanced visualization must be compared with the standard visualization in a clinical environment. Our polyp candidate selection scheme will also be tested with a large number of clinical CT scans to obtain a generalized specification of its performance.

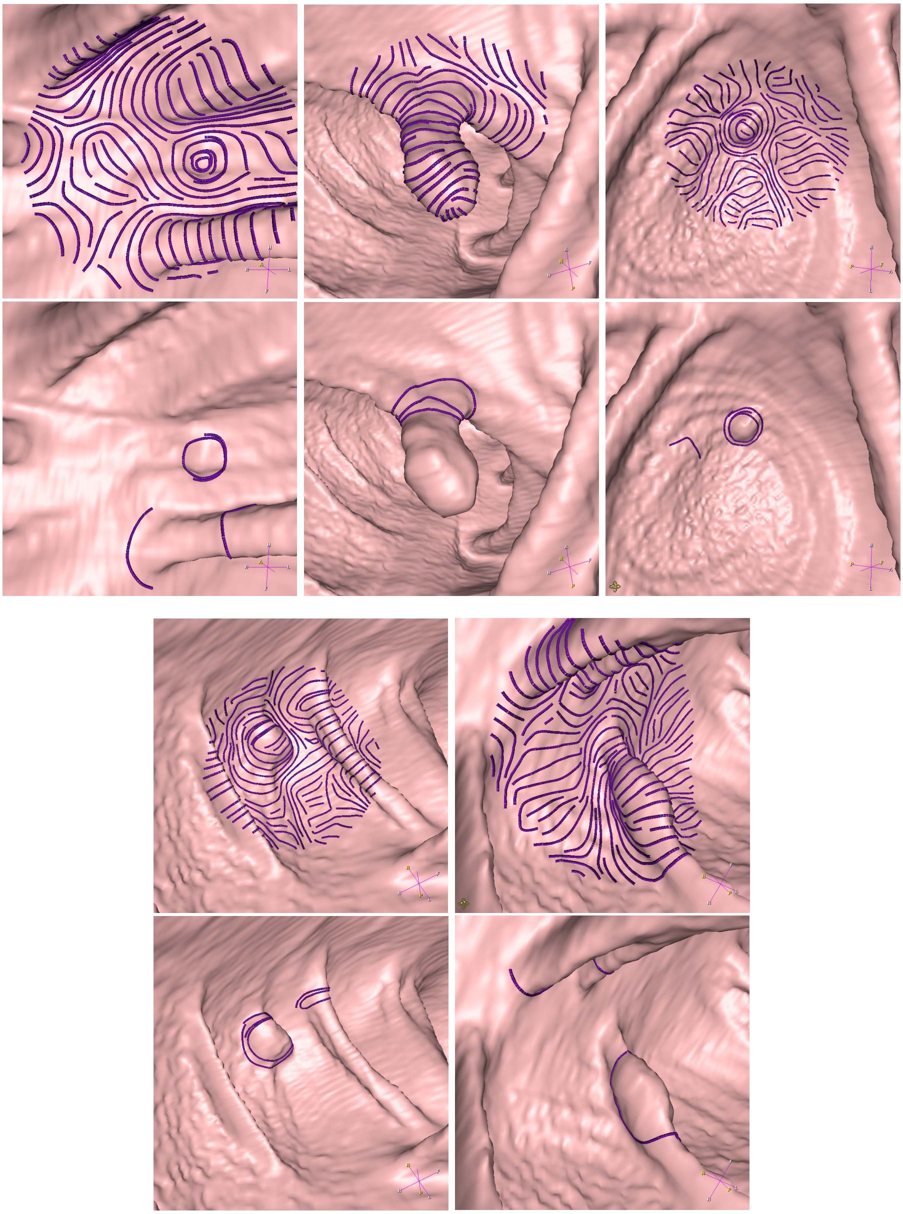

Figure 4.12: Five pairs of images for enhance visualization using streamlines of curvature and selected streamlines around the polyp neck area. Images in the upper row: The perception of colonic surface shape is enhanced using streamlines of curvature; Images in the lower row: Streamlines are automatically selected using the algorithm described in Section 4.5.1, one or more of the selected streamlines are situated on the polyp neck area.

CHAPTER 5

Efficient Seeding and Defragmentation of Curvature Lines for Colonic Polyp Detection

This chapter is based on our paper for the SPIE Conference on Medical Imaging, 2008 [ZBT$^+$08].

Abstract

Many computer-aided diagnosis (CAD) schemes have been developed for colon cancer detection using Virtual Colonoscopy (VC). In earlier work, we developed an automatic polyp detection method integrating flow visualization techniques, that forms part of the CAD functionality of an existing Virtual Colonoscopy pipeline. Curvature streamlines were used to characterize polyp surface shape. Features derived from curvature streamlines correlated highly with true polyp detections. During testing with a large number of patient data sets, we found that the correlation between streamline features and true polyps could be affected by noise and our streamline generation technique. The seeding and spacing constraints and CT noise could lead to streamline fragmentation, which reduced the discriminating power of our streamline features.

In this paper, we present two major improvements of our curvature streamline generation. First, we adapted our streamline seeding strategy to the local surface properties and made the streamline generation faster. It generates a significantly smaller number of seeds but still results in a comparable and suitable streamline distribution. Second, based on our observation that longer streamlines are better surface shape descriptors, we improved our streamline tracing algorithm to produce longer streamlines. Our improved techniques are more efficient

and also guide the streamline geometry to correspond better to colonic surface shape. These two adaptations support a robust and high correlation between our streamline features and true positive detections and lead to better polyp detection results.

5.1 Introduction

In recent years, significant progress has been made for using computer technology in clinical examinations. Computer imaging and visualization techniques are now widely used in visual diagnosis. Virtual colonoscopy is a patient-friendly technique that enables effective screening of the large intestines for colorectal polyps, which are well-known precursors of colon cancer [Bar05, Pic04]. The interior colon wall is extracted from the patient data set, usually CT scans, and then rendered to allow for visual inspection by a radiologist. Due to the complexity of the colon wall, a thorough examination of the entire colon is very time consuming. In order to achieve high efficiency and effectiveness in virtual colonoscopy, computer-aided techniques are developed to pre-detect and visualize polyp candidates.

A large number of automatic polyp detection schemes have been developed as helpful additions to the virtual colonoscopy pipeline [LFP+06, YN01, SYP+05, HSH05, KvCD+05, vWvRV+06, HQK06, ZBB+06]. Many of them are based on 3D surface curvature measures, i.e. scalar principal curvature values. An early example of the use of curvature concepts from differential geometry is due to Summers et al. [SSM+98]. Yoshida et al. [YN01] derived two geometric features, namely the shape index and volumetric curvedness, to characterize polyps, folds and colonic walls at voxels and indicate polyp candidates by a hysteresis thresholding. Huang et al. [HSH05] developed a two-stage curvature estimation method and derived the sphericity index as a shape-based discriminator to find polyp candidates. Accurate and noise-insensitive curvature estimation is essential for any such scheme. Only using scalar curvature measures can result in many false-positive detections.

Other work has been done trying to find complementary solutions instead of only relying on curvature and corresponding derivatives. Hong et al. [HQK06] presented a CAD polyp detection pipeline based on an integration of texture and shape analysis with volume rendering and conformal 3D colonic surface flattening. Kiss et al. [KvCD+05] fitted a spherical model to the colonic surface normals and considered convex regions as suspected polyps. Van Wijk et al. [vWvRV+06] considered that polyp shape and size vary greatly and are often far from the widely-used ellipsoidal polyp model, showing many irregularities. They proposed a shape and size invariant approach, in which the local colonic surface is deformed until the minimum curvature is close to zero. The amount of deformation is computed as a "protrusion" measure and used for detecting polyp candidates.

Our previous work [ZBB+06] explored the potential of surface principal curvature directions, which are represented as two orthogonal vector fields on the surface. We integrated flow visualization techniques in a complete polyp detection protocol. Useful features were calculated on curvature streamlines and used to reduce the number of false-positive detections, which are the result of a pre-detection stage. However, during further testing with a larger number of patient data sets, we found that the correlation between our curvature streamline features and true polyp detections could be affected by CT noise and the characteristics of our streamline generation scheme. In this paper, we present two major improvements of our curvature streamline generation to strengthen the discriminating power of curvature streamline features. We adapt our streamline seeding strategy to the local surface geometry so that the integration of curvature streamlines becomes more efficient. Our experiments also suggested that longer curvature streamlines are more suitable for feature calculation. We improved our streamline tracing algorithm to produce longer streamlines that better correspond to colonic surface shape. These two adaptations support a better polyp detection result using curvature streamline features.

The rest of the paper is organized as follows: a more detailed discussion of our previous work is given in section 5.2. We present our surface-adaptive streamline seeding strategy and improved longer streamline tracing algorithm in section 5.3. In section 5.4, we give an analysis for using improved streamline features in automatic polyp detection. Finally, we summarize our work with some conclusions and propose for future work in section 5.5.

5.2 Background

The proposed CAD process in our previous work [ZBB$^+$06] consists of three steps: pre-detection of polyp candidates, candidate selection and finally enhanced visualization. Polyp candidates were pre-detected using the approach developed by Yoshida et al. [YN01] based on the shape index and volumetric curvedness. These pre-detections included all true polyps as documented with the data sets used and a large number of false-positive detections. We made use of curvature streamlines as additional information to avoid false-positive detections without losing sensitivity.

The idea was based on a generalization of the polyp surface. We modeled a polyp as composed of the top part and the bottom part, namely the cap and the neck. Visualization of principal curvature direction fields around the polyp showed a circular pattern in the maximum curvature direction and a focus pattern in the minimum curvature direction, with consistently outward-pointing surface normals. To exploit such polyp characteristics, we distributed curvature streamlines in the neighborhood per polyp candidate. We developed techniques that trace surface-constrained streamlines for both explicit and implicit surface representations. In order to cover necessary surface shape information, curvature streamlines were distributed using a curvature-controlled spacing approach. Distance between neighboring streamlines is dependent on local surface curvatures. Geometric properties of curvature streamlines are good descriptors of local surface shape. Circular or closed streamlines that follow maximum curvature direction were inspected around the polyp neck area. Therefore such patterns could be used as indicators of colonic polyps. The winding angle and mean radius were calculated on curvature streamlines as features used in our polyp candidate selection process. The winding angle is defined as the cumulative change of direction along a streamline (Figure 5.1). Mean radius is a coarse measure of the polyp size. As the indicator of a polyp instance, a closed streamline has a winding angle of at least 2π. We performed an experimental study of these features on 5 patient data sets, including 50 true polyps and 281 false-positive detec-

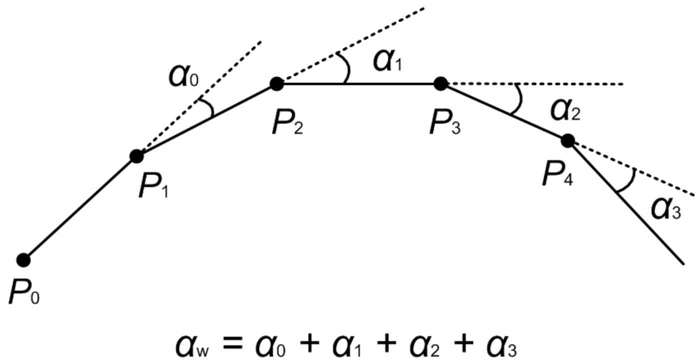

Figure 5.1: Winding angle is the cumulative change of direction of a streamline.

tions. The result showed a high correlation between curvature streamline features and true polyp detections. We used this correlation to separate true and false positive detections.

We performed further test with a larger number of data sets and found that this correlation sometimes could be significantly affected by noise and the characteristics of our curvature streamline generation scheme. Due to the thresholding for streamline spacing and inevitable data noise, many short streamline fragments were generated. Importantly, expected circular or closed streamlines could be fragmented. This streamline fragmentation made the winding angle feature less robust particularly for larger polyps. Often short streamline segments were distributed around the polyp neck area, and none of them had a winding angle of at least 2π. In this case, the enclosed polyp could not be characterized by the winding angle feature because of these short streamline fragments. Long streamlines are preferable for obtaining high values of winding angle. Therefore the streamline spacing technique should promote the generation of long streamlines.

In addition, our streamline seeding strategy was inefficient due to its greedy nature, in which a pair of seed points was placed on both sides of the streamline for each integration step. This fact increased the computational complexity of our method and slowed down the system.

An improvement of our curvature streamline based CAD system is required to achieve a low number of false positives, but without losing sensitivity. In the next section, we present two major improvements to increase the efficiency of our streamline computation and make our streamline features more robust.

5.3 Methods

5.3.1 Adaptive Curvature Streamline Seeding

The greedy streamline seeding strategy [JL97] used in our previous work generated a large number of seed points (Figure 5.2(a)). For each integration step of streamline tracing, a pair

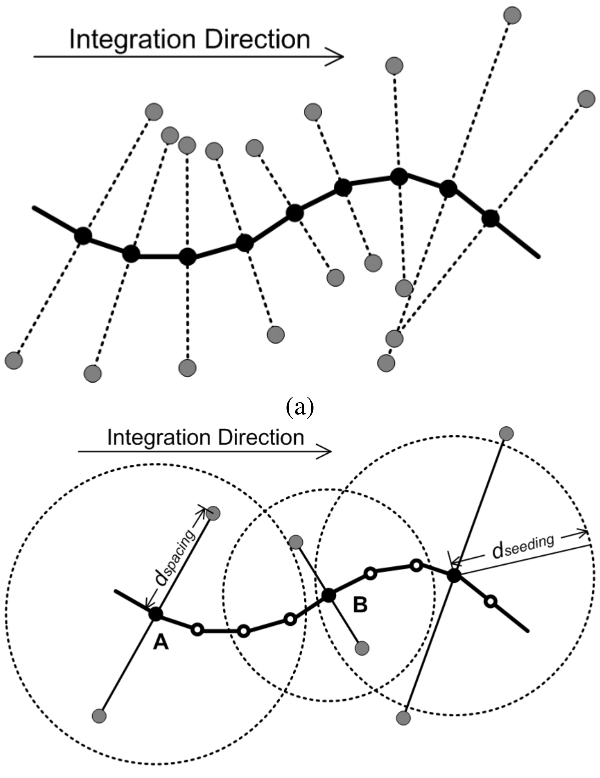

Figure 5.2: Curvature streamline seeding: (a) Greedy streamline seeding generated potential seed points for each streamline integration step, many redundant seed points were not actually used for streamline generation; (b) Adaptive streamline seeding improves the efficiency of streamline computation, the density of seed points is controlled by local surface geometry. Gray dots indicate seed points, black dots are integration steps where seeds are placed, and hollow white dots are integration steps where seeds are not placed.

of potential new seed points was placed perpendicular to the local streamline segment on both sides. All these seed points were put into a seed queue for starting new streamlines. After a new streamline was generated, seed points too close to existing streamlines were removed from the queue. Thus many potential seeds were calculated but not used for streamline tracing and it was always needed to validate these redundant seeds and remove them if necessary. These seeds were also very close to each other. Only a small number of them were actually used as starting points for tracing new streamlines. This significantly increased the computational complexity of our streamline generation.

In order to increase the efficiency of our streamline seeding strategy, the number of redundant seed points calculated on the fly can be reduced. In our streamline spacing, local surface curvature magnitudes are used to estimate the optimal distance between two neighboring streamlines. We adopt this idea to improve the streamline seeding. The density of potential seed points is adapted to the local surface shape, i.e. controlled by the local curvature values. Seed points are only calculated if they have a high probability to be actually used for tracing new streamlines.

This surface-adaptive streamline seeding is explained in Figure 5.2(b). When tracing a streamline, integration steps are selected to place seed pairs. After a pair of seeds is placed at an integration step A, we calculate a seeding distance using:

$$d_{seeding} = \sqrt{\varepsilon_s \left(\frac{2}{|k|} + \varepsilon_s \right)} \tag{5.1}$$

where ε_s is a user-specified error boundary to constrain the local surface approximation and $|k|$ is the controlling curvature value that corresponds to the curvature direction that the streamline follows. This equation is similar to the one that we used in our previous work [ZBB$^+$06] for the calculation of optimal streamline spacing distance. The only difference is that we are now using the same principal curvature that the streamline follows. With this seeding distance, we continue to integrate the streamline until we arrive at integration step B that is far enough, i.e. the Euclidean distance between integration A and B is no less than $d_{seeding}$. Then we place another pair of seeds and continue. We set a maximum seeding distance to ensure that necessary seed points can always be calculated. Although not all adaptively calculated seed points are actually used for streamline generation, the number of redundant seeds is significantly reduced.

5.3.2 Curvature Streamline Defragmentation

Our work employs flow visualization techniques, more specifically streamlines in vector fields, for polyp surface characterization. The streamline generation in our work is based on the algorithm for generating evenly-spaced streamlines proposed by Jobard and Lefer [JL97]. A problem introduced is the stringent thresholding for streamline spacing distance. This can result in many short streamlines, which are less meaningful for characteristic features. To promote the computation of many long streamlines, Jobard and Lefer suggested to reduce their fixed threshold by half for spacing.

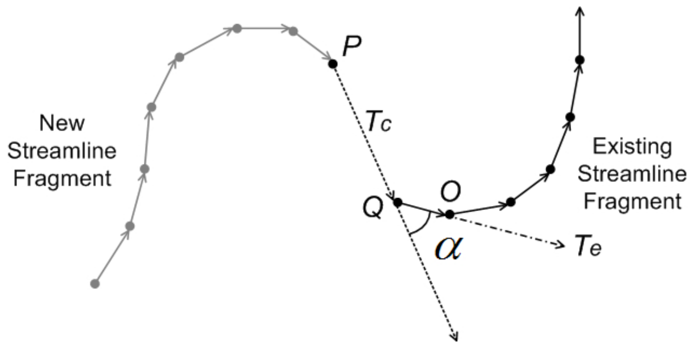

Figure 5.3: Connection of a newly integrated streamline with an existing streamline at the end points. The new streamline is shown in gray, the existing streamline is shown in black. Dotted line indicates a tentative connection, dash-dotted line indicates the direction at the end of the existing streamline.

We adapted the streamline spacing threshold to local surface curvatures and followed Jobard and Lefer's suggestion. However our observation showed that curvature streamlines were often terminated when they could have continued. This fact made our curvature streamline features less robust for polyp candidate selection. To avoid this, we develop a streamline defragmentation approach and obtain sufficiently long streamlines.

Our streamline defragmentation is based on the correlation between two streamlines. Streamline correlation is a similarity measure that quantifies the probability that two streamline segments belong to the same streamline. An application of streamline similarity is streamline clustering. Many streamline clustering methods have been presented in the literature, particularly for fiber tracks in diffusion tensor imaging (DTI) [MVvW05]. Brun et al. [BPKW03] defined a DTI fiber similarity based on the Euclidean distance between end points of fibers. Corouge et al. [CGG04] computed point pairs of two streamlines and used them to define fiber distance.

Our streamline defragmentation approach consists of two stages. In the first stage, we trace streamlines that are as long as possible so that they capture more surface information. In the second stage, neighboring fragments with endpoints that are very close are connected, only if the direction of the connecting line segment is similar to the respective directions of the two streamline fragments at their connecting endpoints. Each connection combines two streamline fragments into a longer streamline fragment.

In our previous work, streamline spacing was dependent on local surface curvature. In order to generate longer streamlines, spacing is now also dependent on the correlation between streamline directions at their endpoints. We use a correlation-based streamline spacing distance to determine when and where a streamline stops. We compute the correlation between a newly integrated streamline point P and an existing streamline end point Q by (Figure 5.3):

$$\begin{cases} R = T_c \cdot T_e = \cos\alpha, \\ if\ \ R < 0\ \ then\ \ R = 0. \end{cases} \tag{5.2}$$

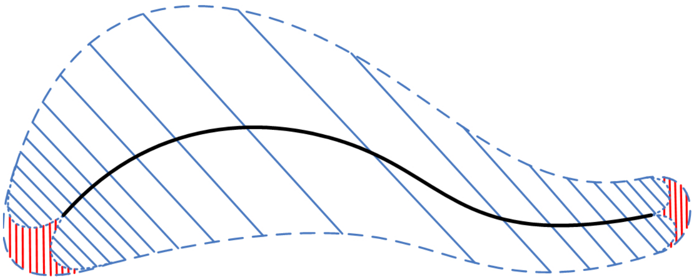

Figure 5.4: Correlation-based streamline spacing: For a streamline indicated by the central black line, the area filled with diagonal lines is the correlation-based spacing region. The area filled with vertical lines demonstrates the difference from purely curvature-controlled spacing.

with:

$$\begin{cases} T_c = \frac{\overrightarrow{PQ}}{\|\overrightarrow{PQ}\|}, \\ T_e = \frac{\overrightarrow{QO}}{\|\overrightarrow{QO}\|}. \end{cases} \tag{5.3}$$

where O is the previous streamline point of Q. For the correlation between P and an existing streamline point that is not an end point, R is always equal to 0. Then we compute the local spacing distance between two streamlines by:

$$d_{spacing} = l_s\sqrt{1-R^2} \tag{5.4}$$

where l_s is the curvature-controlled streamline spacing distance defined in our previous work [ZBB+06].

Figure 5.4 shows the spacing region of a streamline. New streamline integration stops at the region border. If a new streamline integration step is approaching the end of an existing streamline and has a high correlation with it locally, they can be very close at their end points. For streamline fragments that are arbitrarily close at their end points, we need to examine both the tentative connection direction and the two streamline propagating directions at corresponding end points. We define a measure:

$$\eta = \sqrt{\frac{(T_n \cdot T_c)^2 + (T_c \cdot T_e)^2}{2}} \tag{5.5}$$

to quantify the probability that two streamline fragments belong to one single streamline (Figure 5.5). T_n and T_e are local directions of the two streamline fragments and T_c is the tentative connection direction. All vectors are of unit length. We define a tolerance for this quantity by a suitable threshold and connect streamline fragments that fulfil the criteria.

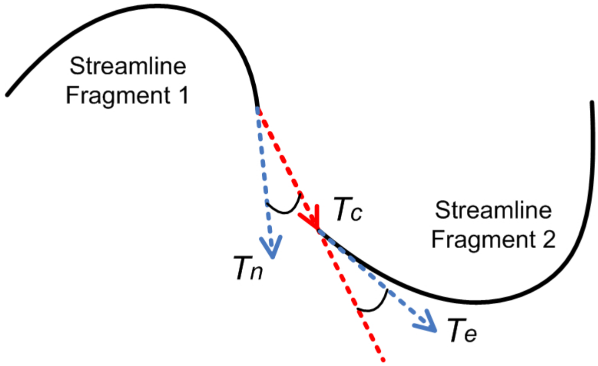

Figure 5.5: When two streamline fragments are very close and locally propagate almost in the same direction, we assume that they belong to one single streamline and connect them.

5.4 Experimental Results

We have evaluated the effects of streamline defragmentation on our polyp detection strategy. We first compare the new surface-adaptive streamline seeding with the previous greedy strategy and show how the efficiency of curvature streamline computation is improved. We then demonstrate that the discriminating power of our curvature streamline features for characterizing true polyp detections is significantly strengthened by the streamline defragmentation. We also illustrate how our streamline defragmentation enhances the visualization of polyp surface shape.

5.4.1 Streamline Computation Efficiency

As in earlier work, streamline generation and feature calculation are integrated in a complete polyp detection protocol. Polyp candidates are pre-detected using an existing detection scheme [YN01]. Many false-positive detections are included and all true-positive detections are annotated by radiologists. Colonic surfaces are represented as implicit iso-surfaces embedded in 3D volume data and rendered using volume ray casting technique. Surface-constrained curvature streamlines are directly traced in the 3D volume and distributed over a small neighborhood surrounding the polyp candidate. Linear interpolation and first-order integration were used in streamline tracing.

We compared our improved streamline computation with our previous work. The streamline computation also included implicit iso-surface curvature estimation. Our workstation had dual 3.20GHz Intel Xeon CPUs with 3GB memory. The average computation times for both seeding strategies are shown in table. 5.1. The result indicates that our surface-adaptive streamline seeding is more than twice as fast as the greedy seeding approach. A far smaller number of redundant seed points were generated while maintaining a good adaptation to the local surface shape.

Table 5.1: Comparison of streamline seeding strategies: using surface-adaptive seeding, curvature streamline computation is accelerated to be twice as fast.

Per candidate area	Greedy Seeding	Surface-adaptive Seeding
Average number of streamlines	66.2	63.1
Average number of seeds	2056.8	631.6
Average number of streamline points	2352.3	2216.6
Average computation time (sec.)	15.233	5.786

5.4.2 Discriminating Power of Curvature Streamline Features

In previous work [ZBB+06] we presented an assessment of our curvature streamline features to discriminate between true- and false-positive polyp detections, based on 5 patient data sets. 50 sites were true polyps and 281 candidates were false-positive detections. These candidates were pre-detected based on the volumetric shape index. Curvature streamlines were applied to all 331 detections. A scatter plot of the streamline winding angle and mean radius features showed a high correlation with true polyp detections.

In further testing, we included another 13 patients. Each patient had 2 CT scans, performed using a Philips Mx8000 multislice scanner. The average voxel size of the 3D volume image is $0.75mm \times 0.75mm \times 1.60mm$. Some of these data sets have a higher noise level. 4598 polyp candidates were pre-detected in the preprocessing stage. An experienced radiologist classified all candidate areas as either true- or false-positive detections. 168 sites were annotated as true polyp detections, found in all 13 patients. Some of them were large ($10-19mm$) polyps and in some cases even classified as masses ($20mm$ and above). We calculated curvature streamline features, i.e. the winding angle and mean radius, on all these candidates. A scatter plot (Figure 5.6(a)) based on the previous work shows that the discriminating power of curvature streamline features can be significantly reduced due to data noise and the size of the polyps. For large polyps, our previous winding angle feature became much less meaningful. An important reason for this was the streamline fragmentation.

We applied our curvature streamline defragmentation approach to improve the discriminatory power of curvature streamline features. The average streamline length was increased by 25%. Figure 5.6(b) shows the scatter plot of our improved winding angle and mean radius features on all polyp candidates in the 26 patient data sets. The result indicates that the discriminating power of the curvature streamline features is significantly strengthened by streamline defragmentation, especially for large true polyp detections.

The visualization of the shaded colon wall is also improved by longer curvature streamlines. We compared our correlation-based long streamline approach with our previous work in Figure 5.7. In these images, it appears that longer streamlines better emphasize polyp surface features. We expect that this will facilitate visual inspection and expert detection. In

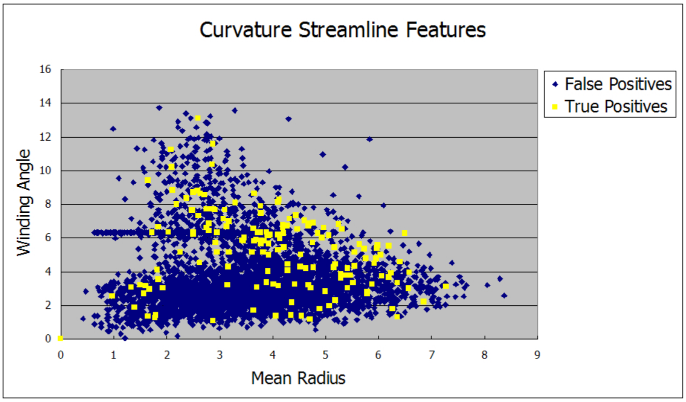

(a)

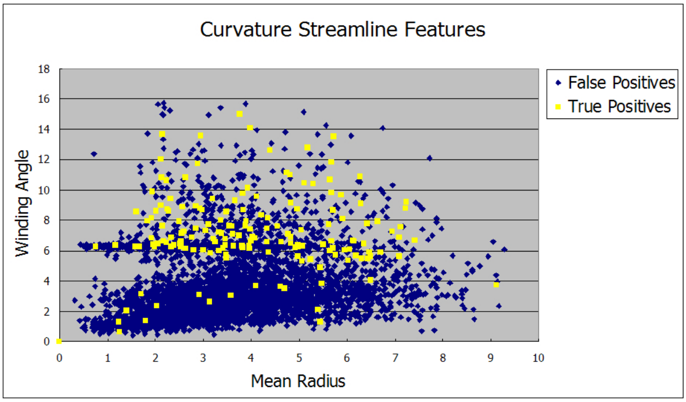

(b)

Figure 5.6: Scatter plot of curvature streamline features for polyp candidates: (a) features calculated on curvature streamlines without using streamline defragmentation; (b) features calculated on defragmentized curvature streamlines. By streamline defragmentation, the discriminating power of curvature streamline features for classifying true polyp detections is increased.

Figure 5.7: Comparison of previous streamline generation (left images) and improved approach using streamline defragmentation (right images): we often inspect streamline fragments using our previous tracing algorithm. If this case happens around a polyp surface, then we will not detect closed streamlines using winding angle feature. Our streamline defragmentation is a helpful addition to solve this problem.

future work, this hypothesis will be experimentally evaluated.

5.5 Conclusions and Future Work

Our curvature streamline based polyp detection scheme explored the characteristics of colonic polyps embedded in principal surface curvature direction fields. Streamlines of curvature were used to visualize these two vector fields and extract specific features. A crucial problem was that streamline generation significantly influences the discriminating power of our curvature streamline features to classify true polyp detections. In this paper, we presented two major improvements to increase the efficiency and robustness of our previous work. We adapted our streamline seeding to local surface shape and reduced the computational complexity of streamline generation. The process was accelerated generating a significantly smaller number of seed points. Our streamline defragmentation approach yielded longer curvature streamlines that better characterize the colonic surface shape. We applied our curvature streamline technique on more data sets, of which some have a higher noise level. The result shows that our features calculated on longer curvature streamlines correlate more strongly with true polyp detections.

In addition, the robustness of our improved streamline features will be further validated in later research. We will also work on deriving other useful features from curvature streamlines as helpful additions for our polyp candidate classification.

CHAPTER 6

Colonic Surface Partitioning Based on Curvature Line Clustering for Polyp Detection in CT Colonography

This chapter is based on our paper for the first Eurographics Workshop on Visual Computing for Biomedicine 2008 (VCBM'08) [ZvRB+08].

Abstract

Automatic polyp detection is a helpful addition to laborious visual inspection in CT colonography. Traditional detection methods are based on calculating image features at discrete positions on the colon wall. However large scale surface shapes are not captured. This paper presents a novel approach to aggregate surface shape information for automatic polyp detection. The iso-surface of the colon wall can be partitioned into geometrically homogeneous regions based on clustering of curvature lines, using a spectral clustering algorithm and a symmetric line similarity measure. Each partition corresponds with the surface area that is covered by a single cluster. For each of the clusters, a number of features are calculated, based on the volumetric shape index and the surface curvedness, to select the surface partition corresponding to the cap of a polyp. We have applied our clustering approach to nine annotated patient datasets. Results show that the surface partition-based features are highly correlated with true polyp detections and can thus be used to reduce the number of false-positive detections.

6.1 Introduction

CT colonography is a minimal-invasive technique that enables effective screening of the large intestine [vGVS+02, Bar05, KPT+07]. The main task is to identify adenomatous colonic polyps, which are well-known precursors of colon cancer. Typically, colonic polyps are visible as protrusions on the interior colonic surface. In virtual CT colonography, the iso-surface of the colon wall is first extracted as a triangle mesh, or as an implicit iso-surface using volume ray casting techniques. Unfortunately, a complete visual inspection of the colon wall is rather time consuming and important areas are inevitably missed. To maintain high effectiveness and efficiency, computer-aided diagnosis (CAD) has been proposed as a helpful addition to the CT colonography pipeline.

The majority of existing CAD schemes [YN01, SYP+05] for automatic polyp detection are based on calculating image features, e.g. surface principal curvatures, at discrete points on the colon wall. These image features are then filtered using hysteresis thresholding to identify suspected regions that belong to colonic polyps. Polyp candidates are detected by fuzzy clustering of these connected components. Such approaches mainly focus on point-wise surface shape characteristics. Large scale shapes of the colonic surface are not captured. Point-sampling features are in general more sensitive to CT data noise and surface irregularities. Aggregation of shape information within a certain area is necessary to enhance the robustness of polyp surface characterization.

Instead of calculating point-sampling features on the colon wall, we first partition the colonic surface into regions that exhibit consistent behaviour with respect to surface geometry. We perform this partitioning by clustering surface-constrained curvature lines. Curvature lines are curves everywhere tangent to one of the two principal curvature direction vector fields on the surface. Geometric features are then computed within each surface partition, over the clustered curvature lines, and used to classify these surface partitions into various predefined types. These features are also used to identify surface partitions that contain polyps.

We integrated our colonic surface partitioning and aggregated surface shape feature calculation with an existing CAD pipeline. Polyp candidates are pre-detected using an existing automatic polyp detection scheme [vWvRV+06], which yields all true polyp detections for the data set we used, as confirmed by an experienced radiologist, and also a large number of false detections. We make use of techniques from [ZBB+06] to generate surface-constrained curvature lines in the area around each detected candidate position. Then each candidate area is partitioned into geometrically homogeneous regions by clustering curvature lines. New features are derived as aggregation of surface shape information within each surface partition. These features are integrated at curvature line points of each cluster that covers a surface partition. Our experimental study showed that these features can be used to discriminate between clusters that contain polyps and clusters that do not.

Our contribution is two-fold:

- We present surface-constrained curvature line clustering algorithm as a new method for surface partitioning in polyp detection. This idea can also be applied in other problems where larger scale surface shapes have to be captured and analyzed.

- We show that features calculated over surface partitions could be used to discriminate effectively between polyps and non-polyps.

The remainder of the paper is structured as follows. Related research is briefly reviewed in Section 6.2. Section 6.3 explores the relation between curvature line clustering and colonic surface partitioning. In Section 6.4, our curvature line clustering method is described. We discuss how to compute geometric features within each surface partition in Section 6.5. An experimental study to analyze the discriminative power of these features is given in Section 6.6. We draw conclusions in Section 6.7, as well as outline our future work.

6.2 Related Work

Many existing polyp detection schemes make use of surface shape features derived from scalar principal curvatures, which are important concepts in differential geometry. It was shown that the per patient sensitivity of computer-aided polyp detection in an asymptomatic screening population is comparable to that of optical colonoscopy for polyps of 8 mm or larger and is generalizable to new CT colonography data in [SYP$^+$05]. Yoshida et al. [YN01] developed a method that started by computing volumetric shape index and curvedness to characterize polyps, folds and colonic walls at each voxel in the extracted colon. Afterwards, polyp candidates were obtained using fuzzy clustering to connected components filtered based on these geometric features. Huang et al. [HSH05] introduced a two-stage curvature estimation approach based on cubic spline fitting on triangulated surface meshes for automatic polyp detection.

There are also methods not or indirectly based on scalar surface curvatures. Hong et al. [HQK06] presented an automatic polyp detection pipeline that integrated texture and shape analysis with volume rendering and conformal colon flattening. Van Wijk et al. [vWvRV$^+$06] proposed a shape and size invariant approach in which a “protrusion”measure was used to find polyp candidates. In [ZBB$^+$06], the potential of surface principal curvature direction fields for automatic polyp detection was explored. Techniques were developed for computing surface-constrained curvature lines on the colon wall. Features strongly correlated with true positive polyp detections are derived from the geometry of curvature lines and used to reduce the number of false positive detections in a complete polyp detection protocol.

Techniques have been developed for surface partitioning. Based on Morse-Smale complex, Natarajan et al. [NWB$^+$06] proposed a method using topological analysis of a scalar function defined on the surface. Partition-based techniques are also widely-used in flow visualization. A survey article on this topic was recently published by Salzbrunn et al. [SJWS08]. Chen et al. [CML$^+$07] provided a technique for vector field modification.

Many line clustering methods can be found in the literature. In flow visualization, Chen et al. [CCK07] presented a streamline similarity distance metric that considered not only Euclidean distance but also shape and directions. A well-known application is the clustering of fibers to obtain bundles in diffusion tensor imaging (DTI) [MVvW05]. An important issue of clustering fibers (or streamlines) is to define a good similarity (or distance) metric between fibers. Brun et al. [BKP+04] mapped fibers to a Euclidean feature space and used a Gaussian kernel for pairwise fiber comparison. They proposed a clustering method in which a normalized cut criterion was used to partition a weighted undirected graph derived from their fiber similarity measure. Corouge et al. [CGG04] computed closest point pairs to define distance between fibers. Based on this distance measure, they propagated cluster labels from fiber to neighboring fibers. Klein et al. [KBL+07] calculated an affinity matrix based on the use of a reconstructed 3D grid to represent fiber similarity. The number of clusters were automatically determined by performing a linear eigenvalue regression of this affinity matrix. Brain white matter fibers were clustered using a spectral clustering method based on multiple eigenvectors.

6.3 Colonic Surface Partitioning

Point-sampling features are not capable to characterize large scale surface shapes, which are necessary to identify polyps. It is important for automatic polyp detection schemes to aggregate surface shape information within a certain region to avoid localization. This requires a partitioning of the colonic surface before feature calculation.

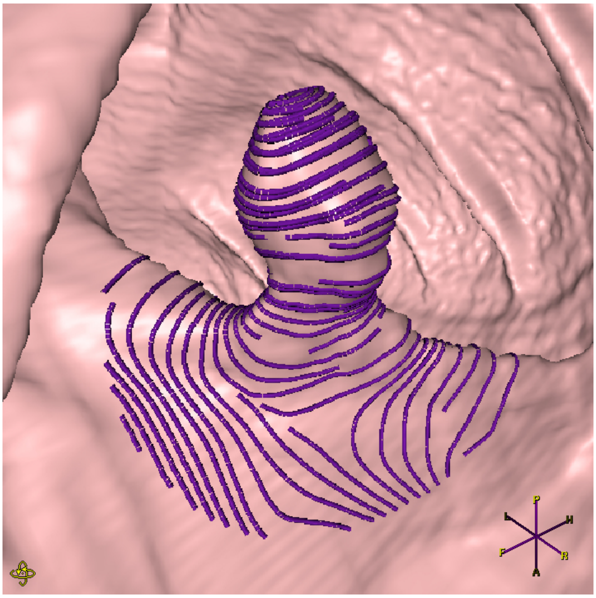

Figure 6.1: Maximum curvature lines on a polyp surface.

By applying curvature lines [ZBB+06], colonic surface shape is well outlined (Figure 6.1). We calculate principal curvature values and directions on implicit iso-surfaces using the method developed by van Vliet et al. [vVYV98]. This method is based on the eigen analysis of Hessian matrix, of which entries are second order partial derivatives. Gaussian convolution is used to compute these 3D image derivatives. We choose $\sigma = 2.0$ for the Gaussian kernel with regard to iso-surface smoothing and computational efficiency. Curvature lines are traced directly in 3D volume and constrained on the colonic iso-surface using an iso-projection approach. The seeding and spacing distance is determined by principal curvature values. In rare cases, there are umbilics on the colonic iso-surface. Curvature line integration stops at these isotropic points.

We use principal curvature direction vectors to cluster coherent surface shapes for surface partitioning. For arbitrarily close positions on the surface, they have coherent shapes when their principal curvature directions are sufficiently parallel. Otherwise, even their shape types are analogical, their shapes are not coherent and belong to different structures. By definition, curvature lines are curves that everywhere follow one principal curvature direction field. It is intuitive that parallel curvature lines link coherent shapes over a surface area and demonstrate meaningful structures. Such a structure presents homogeneous geometry since its embedded shapes are coherent. This leads to the idea that the colonic surface can be partitioned by grouping parallel curvature lines.

In our surface partitioning approach, each partition corresponds with the surface area covered by a single group of parallel curvature lines. Thus the surface partitioning problem is converted into a curvature line clustering problem.

6.4 Clustering Curvature Lines

This section decribes our curvature line clustering method for colonic surface partitioning, using a new curvature line similarity measure and a multiple-eigenvector spectral clustering algorithm.

6.4.1 Symmetric Curvature Line Similarity Metric

A number of clustering algorithms exist, for example agglomerative hierarchical clustering and spectral clustering. By using different similarity metrics between clusters, variations are devised for the same clustering method. In our work, a similarity measure based on parallelism between curvature lines is desired. The Euclidean distance should of course also contribute to the similarity.

We define a symmetric line-to-line similarity measure in our application, based on the work by Chen et al. [CCK07]. As a symmetric measure, the similarity between two curvature lines is unchanged no matter it is calculated from one curvature line to the other or the other way around. In our definitions, the similarity between two curvature lines is always calculated from the shorter line to the longer line.

For a point p on a curvature line l_i, a window W of size $m+1$ centered at p is computed. On both sides of point p, $\frac{m}{2}$ neighboring points of p on l_i are included in W. W is a portion of l_i. On the other curvature line l_j, we find the point q, closest to p in an Euclidean sense.

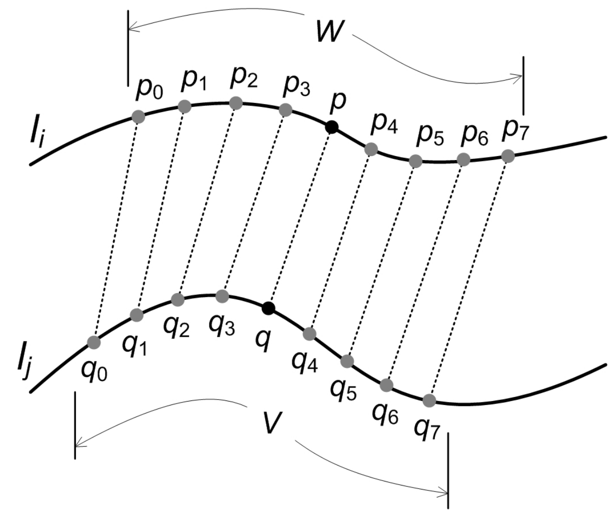

Figure 6.2: Similarity measure between curvature lines l_i and l_j: point pairs are formed by corresponding window w and v. Solid black dots indicate window centers and grey dots indicate point pairs. This similarity is direction-independent.

Another window V of size $m+1$ is centered at q on l_j. Thus we yield $p_0, p_1, \cdots, p_{m-1}$ in window W about p and $q_0, q_1, \cdots, q_{m-1}$ in window V about q. A correspondence between these two windows W and V is defined such that p_i and q_i $(i = 0, 1, \cdots, m-1)$ form one point pair. There are now $m+1$ point pairs including the center point pair $\{p, q\}$. The similarity distance d_{sim} from point p to curvature line l_j is computed as:

$$d_{sim} = \|p-q\| + \alpha \frac{\sum_{i=0}^{m-1}(\|p_i - q_i\| - \|p-q\|)}{m} \tag{6.1}$$

This computation is described in Figure 6.2. d_{sim} is computed from every point on curvature line l_i to curvature line l_j. Then the average value of d_{sim} is taken as the overall similarity distance d_{ij} from l_i to l_j. Since we only consider the parallelism and Euclidean distance between curvature lines, note that this similarity distance is direction-independent, as described in Figure 6.2. This is different than the similarity distance defined by Chen et al. [CCK07].

Larger similarity distance d_{ij} indicates less similarity between curvature lines l_i and l_j. This distance is transformed to a similarity measure using:

$$S_{ij} = \exp(-d_{ij}) \tag{6.2}$$

This similarity measure can be affected by the Euclidean distance between curvature lines and their parallelism. A larger Euclidean distance increases the term $\|p-q\|$ in Eq.6.1. This leads to a lower similarity measure. A larger deviation of point pair distances within the window from the center point pair distance indicates less parallelism between two curvature lines.

This increases the second term in Eq.6.1 and results in a smaller similarity. The coefficient α is a scale factor that can be used to strengthen the effect of parallelism. The window size m also influences this similarity measure. A zero window size will result in a similarity metric purely based on the Euclidean distance. In our experience, $\alpha = 2.0$ and $WindowSize = 20$ yielded the best result as suggested by Chen et al. [CCK07].

6.4.2 Spectral Clustering Algorithm

We applied our new similarity metric described in Section 6.4.1 in a spectral clustering algorithm [KBL$^+$07] to cluster curvature lines. There are also alternative hierarchical clustering methods [CHH$^+$03]. A disadvantage of hierarchical clustering is that the number of clusters is application dependent and sometimes difficult to determine.

The algorithm proposed by Klein et al. [KBL$^+$07] uses a linear eigenvalue regression technique to compute a reasonable number of clusters. It takes an affinity matrix as input. Based on our new curvature line similarity metric, the affinity matrix M is computed as:

$$\begin{pmatrix} S_{0,0} & S_{0,1} & \cdots & \cdots & S_{0,N-1} \\ S_{1,0} & \ddots & & & \vdots \\ \vdots & & S_{i,j} & & \vdots \\ \vdots & & & \ddots & \vdots \\ S_{N-1,0} & \cdots & \cdots & \cdots & S_{N-1,N-1} \end{pmatrix} \tag{6.3}$$

where N is the total number of curvature lines generated on the colon wall at the candidate position and in its vicinity. The entry $S_{i,j}$ $(i, j \in \{0, 1, \cdots, N-1\})$ of the affinity matrix is the similarity measure defined by Eq. 6.2 between curvature lines l_i and l_j. Since by definition $S_{i,j} = S_{j,i}$, this affinity matrix is symmetric. It has N eigenvalues and eigenvectors.

The affinity matrix M is normalized by:

$$S_{i,j} = \frac{S_{i,j}}{S_{max}} \tag{6.4}$$

where S_{max} is the maximum value of entries in matrix M, except diagonal items. These diagonal items are set to 1. Eigenvalues of the normalized matrix $\hat{M}$ are indexed and plotted against their indices in descending order. At each index, these eigenvalues are splitted. The resulting two halves are fitted with two linear functions. The index at which the smallest fitting error occurs corresponds with the number of clusters. This number K enables the identification of inner clusters within coarse structures.

The K largest eigenvectors of $\hat{M}$ are selected and assembled as columns in a $N \times K$ matrix X. Rows of X are considered as K-dimensional vectors. Each of these vectors corresponds with a curvature line with the same index. A hierarchical clustering method [MVvW05] is performed on these N K-dimensional vectors to create K clusters. The indices of rows of X in each resulting cluster correspond to the indices of curvature lines that belong to the same

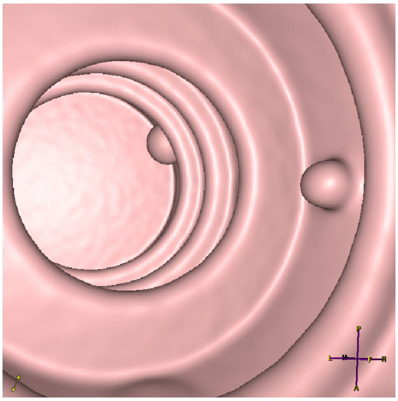

(a)

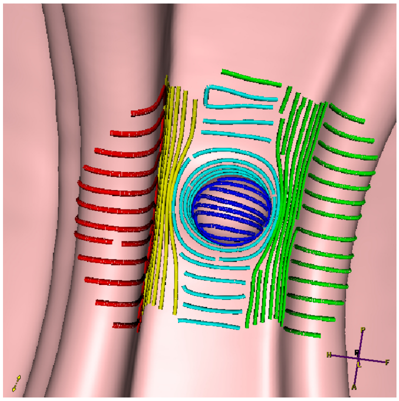

(b)

Figure 6.3: Clustering curvature lines: (a) A synthetic colonic surface; (b) Curvature line clusters on a fabricated polyp, different colors represent different clusters.

cluster. In our experiments, using the complete linkage in the hierarchical clustering provided the best result.

There are two advantages of this spectral clustering algorithm. First, a reasonable number of clusters is automatically determined, considering the inter-cluster connectivity. Second, using multiple eigenvectors for clustering leads to more accurate and robust results [AKY99]. Figure 6.3 shows the result of our curvature line clustering algorithm on a synthetic 3D volume data. The simulated colonic surface is rendered as an implicit iso-surface using volume ray casting. Curvature lines that follow maximum curvature direction are traced. Parallel curvature lines are clustered into several groups, each of which corresponds with a surface partition. This clustering algorithm can also be used in other applications, e.g. clustering white matter fibers to find bundles in DTI of the human brain.

6.5 Geometric Features for Surface Shape Analysis

In this section, we describe how geometric features are calculated to characterize the large scale shape of each surface partition. These features are used to identify the surface partition that captures a colonic polyp.

To describe the overall shape of a surface area, a traditional way is to calculate the average or mean values of geometric features in most existing automatic polyp detection approaches. Unfortunately, important surface shape information could be neglected in such a way. Therefore we need to aggregate surface shape information as much as possible within the surface partition for shape analysis.

Volumetric shape index and curvedness of iso-surfaces are two well-known features used for automatic polyp detection. They were firstly introduced by Yoshida et al. [YN01] to

CAD schemes in CT colonography. These two features are derived from surface principal curvatures:

$$SI = \frac{1}{2} - \frac{1}{\pi} \arctan \frac{k_{min} + k_{max}}{k_{min} - k_{max}} \tag{6.5}$$

and

$$CV = \sqrt{\frac{k_{min}^2 + k_{max}^2}{2}} \tag{6.6}$$

where k_{min} is the minimum curvature value and k_{max} is the maximum curvature value. However, SI and CV were mostly used as point-sampling measures for shape analysis and large scale shapes were difficult to be described in existing approaches. We define a new feature based on the aggregation of SI and CV at curvature line points corresponding to a surface partition to characterize its overall shape.

6.5.1 Feature Definition

Curvature line points of a cluster are treated as sampling points of the corresponding surface partition. To identify the overall shape of a surface partition, surface shape information is aggregated through these sampling points. SI and CV are calculated and aggregated within each surface partition.

The most important feature is the shape index SI. A unique value of SI describes a distinct surface shape [YN01]. The value of SI varies in the closed interval $[0.0, 1.0]$. Five predefined shape types are represented by their characteristic shape index values (Table 6.1):

Table 6.1: Five predefined shape types and their corresponding shape index values.

Shape type	Shape index value
Cup	0.0
Rut	0.25
Saddle	0.5
Ridge	0.75
Cap	1.0

These values divide the shape index value range into four subintervals. Values that fall into one of these subintervals represent transitional shapes from one predefined shape type to another. Such a shape transition is continuous over the whole domain of SI.

The iso-surface curvedness CV is a complementary feature to the shape index SI. The shape index only measures the shape type of a surface. The curvedness can represent how significant the surface shape is. The value of CV varies in the interval $[0.0, +\infty)$, where a small value implies a more flat surface and a large value implies a sharp edge or peak. Using the mean value of SI and CV as an aggregation for surface analysis has a significant drawback. For example, if a surface partition has most of its sampling points where SI values fall into the

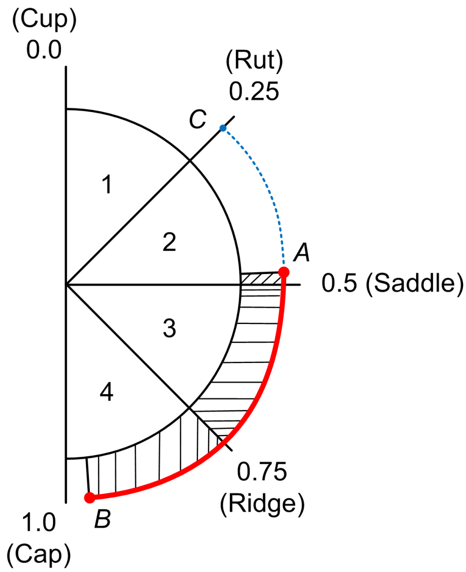

Figure 6.4: Using *SI* subintervals to characterize the overall shape of a surface partition: a surface partition has its *SI* value range *a* (red line) overlapped with 2nd, 3rd and 4th *SI* subintervals. In this case, the surface partition has overall cap-like shapes.

intervals $[0.0, 0.25]$ and $[0.75, 1.0]$, the mean value of its *SI* is close to 0.5. Thus the dominant shape of this surface partition is represented as the saddle, which is obviously incorrect.

We define new features, which account not only for values of *SI* and *CV* but also for the shape types at sampling points over the surface partition. This definition is demonstrated in Figure 6.4. Values of *SI* over a surface partition are mapped to the four subintervals of the *SI* value domain. Assuming a geometrically homogeneous surface partition has analogical shapes over it in general, we intend to use shape subintervals, in which shapes described by the majority of sampling points are included, to characterize the overall shape of a surface partition. Values of *SI* and *CV* are calculated through curvature line points of the single cluster that corresponds with a surface partition. The value ranges a and b of these discrete *SI* and *CV* values can be determined. Then we compute four overlaps of range a with the four subintervals of *SI* (Figure 6.4):

$$F_i = \frac{n_i}{\overline{N}} \times 100\%, (i = 0, 1, 2, 3) \tag{6.7}$$

where n_i is the number of curvature line points that have their *SI* values included in the ith *SI* subinterval. $\overline{N}$ is the total number of curvature line points that belong to the cluster corresponding to the surface partition. If there is no overlap of a with a *SI* subinterval, then a negative value is calculated as:

$$F_i = -\frac{||C-A||}{||A-B||} \times 100\% \tag{6.8}$$

where A and B are the two values at the border of range a and C is the closest value of the non-overlapped *SI* subinterval to a. In the case shown in Figure 6.4, C and A are the closest domain border values. The overlap of range b with a proper value domain is also computed for the iso-surface curvedess of the surface partition using similar functions. This proper *CV* value domain is determined as suggested by Yoshida et al. [YN01]. Reasonably curved surface partitions are significant for shape analysis in our automatic polyp detection scheme, whereas approximately flat regions are much less meaningful. For finding surface significant overall shapes, the *CV* value domain is $[0.08, +\infty)$. We compute a percentage F_{CV} of the number of points with their *CV* values of at least 0.08 against the total number of points to characterize the general curvedness of a surface partition. Now we have a 5-dimensional vector feature $F = \{F_0, F_1, F_2, F_3, F_{CV}\}$ for each surface partition. It can be used to identify the surface partition that captures a polyp surface.

6.5.2 Shape of Colonic Polyps

The vector feature defined in Section 6.5.1 has four *SI* components and one *CV* component. If a *SI* component of this vector has a larger value than other *SI* components, the overall shape of the corresponding surface partition is described by that shape subinterval. As shown in Figure 6.4, the *SI* range a of an example surface partition has larger overlaps with the 3rd and 4th *SI* subintervals, while just a very small overlap with the 2nd *SI* subinterval and no overlap at all with the 1st *SI* subinterval. Its feature vector F has a negative 1st component and a small and positive 2nd component. Its 3rd and 4th components have larger positive values. This indicates that the overall shapes are ridge and cap-like.

In most current CAD schemes, colonic polyps are usually modeled as approximately spherical or ellipsoidal protrusions. A polyp surface consists of the head and the neck. As shown in Figure 6.5, the polyp head is a cap-like surface while the polyp neck is an anticlastic (or saddle) surface. Since irregularities are included on most significant polyps, sometimes not all points on a polyp head present a cap shape. Ridge-like or even saddle-like shapes could also be presented on the polyp head. The polyp neck presents saddle-like shapes in general. Therefore, overall shapes on a polyp surface have significant overlaps with the 3rd and 4th *SI* subintervals. As discussed by Yoshida et al. [YN01], the vector feature F for a surface partition that captures a polyp surface also has a significant overlap of its *CV* range b with the interval of $[0.08, +\infty)$.

Summarizing these issues, we hypothesize that overall shapes of a polyp are mainly included in the 3rd and 4th *SI* subintervals, i.e. these overall shapes correspond to *SI* values in $[0.5, 0.75]$ and $[0.75, 1.0]$. Importantly, the *SI* component F_3 has a larger value to represent the polyp head. Otherwise, the corresponding surface partition does not capture the polyp cap. We calculate $\{F_0, F_1, F_2, F_3, F_{CV}\}$ for each surface partition of a pre-detected polyp candidate. If the sum of its 3rd and 4th *SI* components (F_2, F_3) is larger than the value of F_0 or

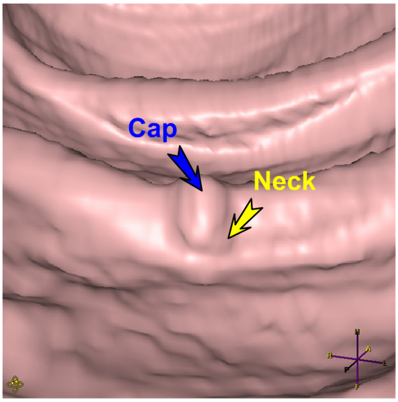

(a)

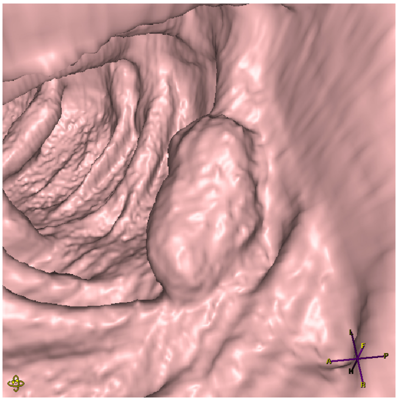

(b)

Figure 6.5: (a) A polyp surface consists of a cap and a neck. (b) Irregular shapes of a large polyp.

F_1, and F_3 is significant by itself, such a surface partition is considered to correspond with a polyp surface. On the other hand, its *CV* component should be able to indicate that it is a sufficiently curved surface partition. For each polyp candidate, we pick one of its surface partitions that most likely captures a polyp surface. The vector feature F of this partition is used to represent corresponding polyp candidate. We use this feature to discriminate between true polyps and false detections.

6.6 Results

This section documents the results of an experimental study in which our surface partition-based features were tested on nine real patient data sets.

6.6.1 Materials and CAD approach

Our patients underwent CT colonography before optical colonoscopy, which is considered as the golden standard. Each patient has two CT scans in prone and supine directions. The average resolution of these CT data is $512 \times 512 \times 267$ and the average voxel size is $0.77\text{mm} \times 0.77\text{mm} \times 1.60\text{mm}$.

Our automatic polyp detection system consists of three fully automatic steps. First an existing approach [vWvRV$^+$06] was used to pre-detect polyp candidates. These candidates included all true polyps and a large number of false detections. In second step, we took pre-detected candidate positions as the input and applied our approach to calculate surface partition-based features for the vicinity of each candidate. The third step is supervised pattern recognition, by which these features were processed and the number of false detections was reduced.

6.6.2 Colonic Surface Partitioning

Curvature lines are directly traced in 3D volume data and rendered as polylines [ZBB$^+$06]. In our study, curvature lines that follow the maximum principal curvature direction were used for colonic surface partitioning. The average time cost for curvature line computation per candidate area (centered at the pre-detected position with a radius of 15mm) is 16.871 seconds. For curvature line clustering, the average time cost per candidate area (on average 221 lines and $7-9$ clusters) is 1.082 seconds. We show our colonic surface partitioning results at some true polyp detection areas in our CAD pipeline (Figure 6.6). Visual inspection of our results shows that the curvature line clustering method provides a reasonable pre-segmentation of the polyp candidate area. Most importantly, as shown in images on the lower row of Figure 6.6 a surface partition that corresponds well with a true polyp surface can be obtained. This indicates that our overall shape features calculated in such a surface partition can be used to discriminate between true and false detections.

6.6.3 Discriminating Candidate Detections

The polyp candidate pre-detection step based on the method of van Wijk et al. [vWvRV$^+$06] returned 4036 candidates in total 18 scans. Protrusions are calculated on the surface throughout the entire colon. Candidate detections are found by hysteresis thresholding of protrusions as suggested in [vWvRV$^+$06]. Medical diagnosis confirmed that these polyp candidates included all polyps of the 9 patients. 30 polyps (larger than or equal to 6mm) were annotated using an expert opinion of an experienced radiologist. A polyp was counted as a true positive if it was classified as a polyp in at least one of the two scans. There were 4006 false-positive detections, which needed to be significantly reduced.

In order to estimate the discriminating power of the five-dimensional vector feature, we first performed basic statistic analysis on all pre-detected polyp candidates. In univariate logistic regression analyses, each of the five components were separately found to be significantly related to the polypness of clusters ($p = 0.000, 0.000, 0.001, 0.000$ and 0.011). However, in a multivariate logistic regression analysis, only F_3 was found to be independently associated with the polypness of clusters (p=0.000). In other words, each of the other features does not significantly improve the prediction of polypness over that attainable with F_3 by itself. This analysis does show that F_3 could be used to discriminate between clusters over polyps and non-polyps.

The features F_3 and F_{CV} were used in our pattern recognition step to classify polyps out of false-positive candidates. Only candidates with a mean internal intensity of around that of tissue were retained. This excluded all candidates that were detected as a result of the partial volume effect and due to artifacts of CT. A nine-fold cross-validation was used to compute the system's performance. A logistic classifier [Web02] was trained on the training data set consisting of 16 scans from 8 patients, and was used to classify the two scans of the remaining patient to obtain the classification results. The results for all patients were summed up to get an estimate of the performance of the CAD system.

The system achieved 95% sensitivity for polyps while presenting on average less than 11

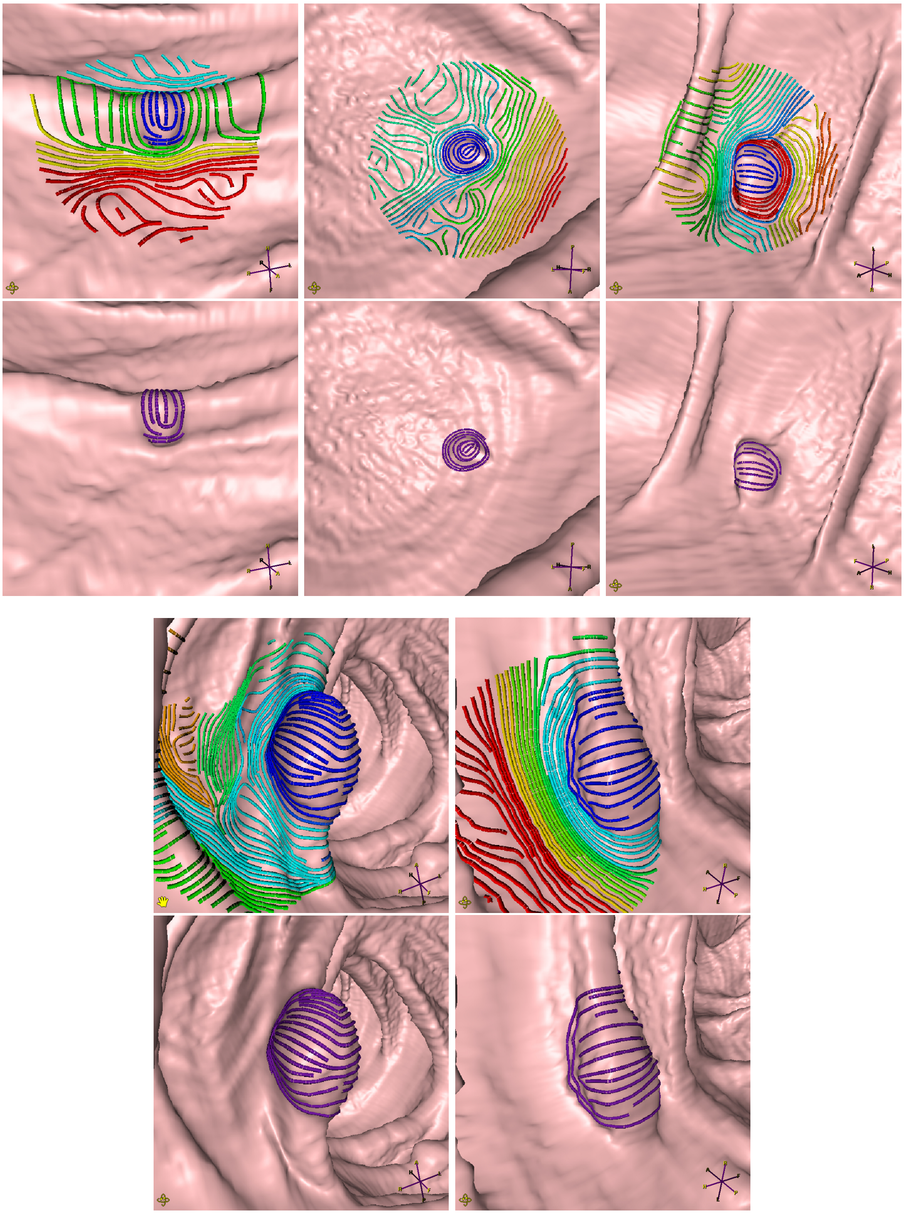

Figure 6.6: Five pairs of images for curvature line clustering based polyp candidate area partitioning and the line clusters that capture polyps. Images in the upper row: Colonic surface partitioning based on clustering curvature lines. Each surface partition corresponds with the surface area covered by a single cluster. Different colors indicate different curvature line clusters. Images in the lower row: The curvature line cluster that corresponds with a colonic polyp.

false positives per scan and 80% sensitivity with on average 7 false positives per scan. This means that more than 95% of the false-positive detections, i.e. 3808 false positives, were discarded while retaining high sensitivity that 28 true positives were correctly detected. To conclude, this analysis shows that the features derived from the surface partitions correlate quite well with the polyp annotations.

6.7 Conclusions and Future Work

In this paper, we presented surface-constrained curvature line clustering as a new method for surface partitioning in polyp detection. These surface regions are able to capture polyp characteristics. They could also be used to capture and analyze other larger scale surface shapes. We proposed a new direction-independent, line-to-line and symmetric similarity metric between curvature lines. This similarity metric was applied in a spectral clustering algorithm, in which a reasonable number of clusters is automatically determined. Results showed that polyp surfaces can be captured by corresponding surface partitions. A 5-dimensional feature based on the volumetric shape index and iso-surface curvedness was proposed to describe overall surface partition shapes. Statistical analysis showed that one of the five components could be used to discriminate between clusters over polyps and non-polyps. We demonstrated that our new proposed features can be used in a polyp detection system. Visual inspection of the clustered curvature lines showed a strong correlation with expected polyp areas.

We plan to investigate the possibility of using our colonic surface partitioning approach for polyp segmentation. Optimizing our scheme will be an important avenue for future work. Our approach will be further tested with a larger number of clinical data sets and other clustering algorithms will be explored, as well as more partition-based discriminative features for polyp detection.

CHAPTER 7

Evaluation of Automatic Polyp Detection Integrating Curvature Line Based Visualization Techniques

This chapter is partly based on our paper for the IEEE International Symposium on Biomedical Imaging: From Nano to Macro, 2009 (ISBI'09) [vRZB+09]. The paper presented a joint work on the evaluation of a prototype CAD system. Our curvature line based techniques were integrated into a complete automatic polyp detection pipeline. This chapter mainly documents my contribution to the paper, as well as new results we obtained during further testing on additional data sets. In order to have a full context of the work by the author, contributions by our collaborators are also briefly explained.

7.1 Introduction

Previous chapters introduced a new technique from data visualization that can be applied for automatic polyp detection in CT colonography. This technique used geometric features of iso-surface curvature lines to facilitate the reduction of false positives obtained in a pre-detection of polyp candidates. The detection performance was demonstrated via experimental studies on a relatively small number of datasets, containing a large number of polyp instances.

This chapter presents a further evaluation of how surface curvature line features contribute to improve CAD performance in CT colonography. Our evaluation made use of many more real patient CT data sets than that of previous chapters, to achieve a better generalization of CAD performance. A complete CAD system that integrates our curvature line generation and feature calculation is introduced. Our new technique from data visualization is incorporated to increase the specificity of an existing polyp detection scheme [vWvRV+06] without regressively affecting sensitivity. Surface and volume characteristics with additional shape information described by our curvature lines are applied to the detection and classification of polyp candidates. Evaluation results demonstrate that surface curvature lines can provide distinctive shape features for the reduction of false positive detections. A simple pattern recognition approach based on these features indicated that the CAD performance can be improved to be less than 1.6 false positives per scan at 92% sensitivity per polyp.

With regard to the automatic polyp detection pipeline, my main contribution to the work presented in [vRZB$^+$09] is supplying geometric features of curvature lines for the false positive reduction step. Polyp candidates including all true polyps were pre-detected by the approach presented in [vWvRV$^+$06]. Protrusion-based features and curvature line features were selected and used in the supervised pattern recognition step for the CAD performance evaluation. The FROC analysis was conducted by our collaborators.

Apart from the work presented in [vRZB$^+$09], an additional resource of CT data sets obtained using a different scanning protocol is employed in the evaluation. In section 7.2, properties of the two data collections used in the evaluation are compared. Section 7.3 gives an overview of our prototype polyp detection system. Evaluation results are presented in Section 7.4. We discuss our evaluation results and draw our conclusions in Section 7.5.

7.2 Materials

Two collections of patient CT scans were used for the evaluation. Each collection has its unique image and pathological properties, e.g. the voxel size, image noise level and the number of polyp instances. In such a way, not only the discriminating power of curvature line features for polyp candidate classification was validated, but also the correlation between the experimental result and the CT data set properties.

The evaluation presented in [vRZB$^+$09] used 28 patients from a larger study [vGNF$^+$04], the AMC-ZON data. Further testing was conducted on additional data sets of 138 patients from the MADISON CT scan repository. All testing data sets were obtained by scanning patients in both prone and supine positions. Every patient was subject to an extensive laxative regime to clean colorectal residues and no fecal tagging agent was administered. The reference standard for the evaluation is optical colonoscopy. All true polyps were indicated by expert radiologists as positions in the 3D volume data and confirmed with optical colonoscopy. A polyp was counted as a true positive detection if it was found in at least one of the two CT scans per patient. Image and pathological properties of these two collections of CT data sets are documented in Table 7.1.

7.3 Automatic Polyp Detection System

The automatic polyp detection process in our evaluation consists of three basic steps: (1) Pre-detection of polyp candidates, (2) Feature calculation for false positive reduction, (3) Polyp candidate classification using supervised pattern recognition. All polyp candidates are

Table 7.1: Image and pathological properties of AMC-ZON data and MADISON data.

Repository	AMC-ZON data	MADISON data
Number of Patients	28	138
Number of Datasets	56	276
Image Properties		
Slice Resolution	512×512	512×512
Slice Distance	$1.60mm$	$1.00mm$
Grey Value	12 or 16 bits	16 bits
Pathological Properties		
Number of Polyp Annotations	65	302
Number of Polyps $\geqslant 6mm$	40	174

detected using the protrusion-based detection algorithm [vWvRV$^+$06]. Surface protrusion measurement, volume intensity and curvature line geometric features are then calculated per candidate area. Finally, these features are used in a supervised pattern recognition step to classify polyp candidates into false positives and true polyps.

7.3.1 Protrusion-Based Polyp Detection

Due to the shape of the cap (see Figure 4.2), a polyp can be characterized by the fact that the smallest principal curvature is larger than zero. Such a polypoid shape can be flattened applying a surface evolution technique. At a certain point of this evolution, the surface is deformed so that the complete polyp is removed. The amount of surface displacement for this deformation is defined as the “protrusion”, which can be used as a criterion to locate possible polyps on the colon wall.

Van Wijk et al. [vWvRV$^+$06] proposed two distinct, iterative schemes for the detection of colonic polyps using the protrusion measure. The explicit method was applied to flatten triangle mesh surfaces and the implicit method directly deformed iso-surfaces embedded in 3D volume data. In both approaches, the surface flattening process is conducted using an abstracted surface evolution function:

$$X^{t+1} = X^t + dt \cdot f(-\kappa_2) \tag{7.1}$$

where $f(-\kappa_2)$ is a force function that is designed to operate on an object which has a positive smallest principal curvature. dt means a time step for the repeat. The method deforms the surface until the smallest principal curvature is smaller or equal to zero everywhere or some convergence criterion is satisfied. The total amount of resulting surface displacement is then taken as a protrusion measure. For triangle mesh surfaces, the force function is applied to mesh vertices, which are iteratively repositioned until the surface is flattened. On implicit iso-surfaces, the force function modifies the intensity of voxels in such a way that the protruding intensities are smoothed into the background. The protrusion measure is computed at each mesh vertex as either the displacement of the vertex in millimeters, or the number of voxels whose intensities are smoothed for the iso-surface flattening. Polyp candidates are generated by applying a threshold on the displacement field.

All true polyps can be detected using the protrusion-based method. Resulting pre-detections included a large number of false positives. It was found that in practice, the false detections of both explicit and implicit methods are uncorrelated. Complementary protrusion analysis was conducted for false positive reduction, in which additional features are derived from explicit and implicit protrusion-based methods.

7.3.2 Curvature Line Based Visualization Technique

The protrusion-based method is used for the pre-detection of polyp candidates and features derived from protrusion measure are applied to the candidate classification. However so far surface shape information of the objects remains limited. Our curvature line techniques presented in previous chapters of this thesis can provide important additional discriminating shape features for the polyp candidate classification. In our evaluation, we incorporated shape information by our technique with protrusion-based features to see how curvature line features improve the false positive reduction phase of the polyp detection. The winding angle feature of surface constrained curvature lines was used to help improve the performance of our prototype CAD system.

7.4 Experiments and Results

All polyp candidates detected by the protrusion-based technique [vWvRV$^+$06] are used as input for additional feature calculation and then supervised pattern recognition is applied for false positive reduction. This section explains how additional features are used and documents details of our evaluation methods and results. At the end of this section, the improvement of the curvature line winding angle feature is discussed.

7.4.1 Additional Features for False Positive Reduction

For classification of pre-detected polyp candidates, three additional features were derived from the explicit and implicit protrusion-based methods. The explicit method involves two features. The first feature ϕ_T measures the percentage of the candidate with a displacement larger than a certain threshold T in millimeters. To favor candidates with steep edges and compact forms, we set $T = 0.6mm$. The mean intensity of the candidate was used as the second feature. It was calculated as a total weighted sum of all voxels included in a segmentation mask, which consists of the area included between the original and the displaced iso-surface.

The third feature was calculated using the implicit method. Polyp candidates were predetected on the triangle mesh of the colon wall. Volumetric properties were later analyzed using underlying data of the colon wall, and in the vicinity of each candidate area. To do this, the candidate area on the mesh emanating from the candidate position was mapped to a binary image. This binary image was dilated ten times to define the region-of-interest (ROI) on the colon wall in 3D volume for the implicit method. Then, the original volume was smoothed iteratively using the evolution function (7.1) to all voxels inside the ROI. A corresponding segmentation for the implicit method was derived from the smoothed volume by thresholding the intensity difference at a value of 100 Hounsfield units (HU). Each candidate from the implicit method was therefore linked to a corresponding candidate on the mesh.

Figure 7.1 shows two scatter plots of the protrusion-based features: maximum displacement of the mesh (in millimeters), maximum intensity difference (in HU) and ϕ_T. The maximum mesh displacement and the maximum intensity difference correlate well for true polyps. The indicated feature space boundaries (dash-dotted lines) were used as the two thresholds in the polyp candidate generation. The two features: ϕ_T and mean intensity of each candidate area were further used in the supervised pattern recognition step to separate true polyps from false positive detections.

For all detections on the mesh, a center line through the center of gravity and the center of curvature of the segmentation mask is computed [DvWV$^+$05]. The intersection of this line and the mesh defines the initial seed point for the streamline analysis. For each detection curvature streamlines are generated within a spherical ROI with 16 mm radius around the initial seed point. The winding angle is calculated on these streamlines as the cumulative signed change of direction along the streamline. At each sample point, the differential curvature is derived relative to the surface normal at that point. In other words, when a streamline forms a loop, its absolute winding angle is 2π or more (for polyp characterization the sign of the winding angle is not important). Importantly, an absolute winding angle of more than 2π is not necessarily more "polyp-like" than a winding angle equal to 2π. Therefore, we clip this feature to a maximum of 2π, i.e. $\psi_c = min(|\psi|, 2\pi)$. This hypothesis is confirmed by the later FROC analysis in section 7.4.3.

Figure 7.2 shows scatter plots of (a) the absolute winding angle $|\psi|$ and (b) the clipped winding angle ψ_c vs. ϕ_T (derived from the mesh displacement field). Observe that almost all polyps have a winding angle close to or larger than 2π, whereas many false detections have lower winding angles. In other words, the winding angle might indeed help to distinguish between polyps and false detections.

7.4.2 Evaluation Methods

The four above mentioned additional features, ϕ_T and the mean intensity (from the explicit protrusion-based method), maximum intensity difference (from the implicit protrusion-based method), and the winding angle ($|\psi_c|$) of curvature lines were used in a supervised pattern recognition step for the classification of pre-detected polyp candidates. We evaluated the improvement of the overall CAD performance by means of a FROC analysis. The FROC curves are computed by a ten times repeated ten-fold cross-validation, which measures the practical performance of our classification model. In all cases, a logistic classifier was used and detections on the rectal tube were discarded.

Initially, the CAD system made use of the two protrusion-based features: ϕ_T and the mean intensity. Then the maximum intensity difference feature was added by applying the implicit protrusion-based technique. Finally the clipped winding angle feature ψ_c was included in

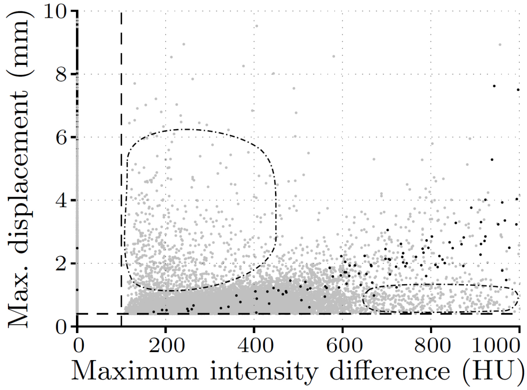

(a)

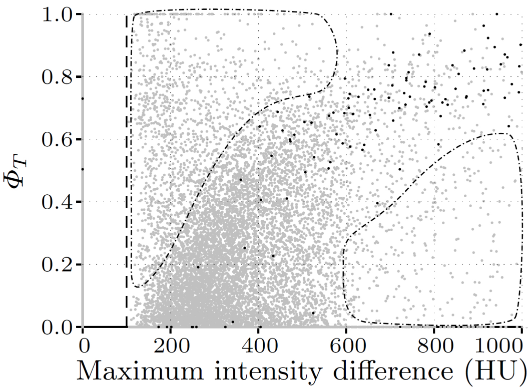

(b)

Figure 7.1: Scatter plots of a larger data sets (86 patients): (a) the maximum mesh displacement of a candidate, and (b) ϕ_T against the maximum intensity difference derived from the implicit method. Black dots indicate true polyps and grey dots indicate false positives. Dash doted lines are boundaries of the feature space.

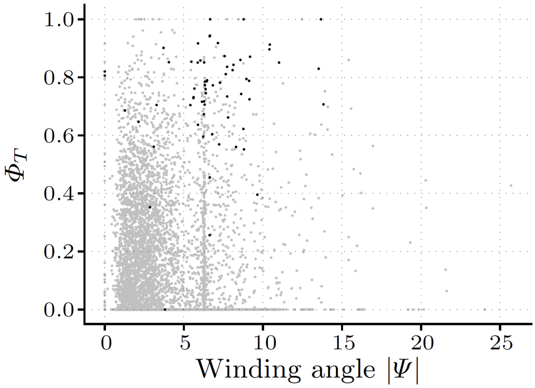

(a)

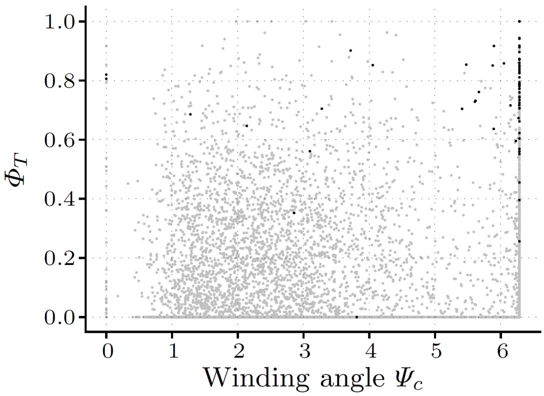

(b)

Figure 7.2: Scatter plots of ϕ_T against (a) $|\psi|$ and (b) ψ_c. Black dots indicate true polyps and grey dots indicate false positives.

both previous configurations. All these four scenarios were performed and the results are presented in the next section.

7.4.3 Evaluation Results

For each of the two CT data set collections, four FROC curves were computed to describe the performance of the CAD system, as elaborated in the previous section. First, the FROC curves for the AMC-ZON data collection are shown in Figure 7.3. The result indicates obvious improvements by using the curvature line based surface shape analysis approach. The specificity of the protrusion-based polyp detection scheme was significantly increased without any loss of sensitivity. Also, the curvature line winding angle feature clipped to 2π does improve the CAD performance, compared to the non-clipped winding angle feature.

We concluded that 92% of the polyps were correctly detected in 28 AMC-ZON data sets. When all four features were employed, less than 1.6 false positive detections were made per CT scan. The error bars denote two times the standard deviation in the number of false positives over all scans at 85% sensitivity. Actually, the standard deviation of these FROC curves is over seven times smaller due to averaging over all scans.

Besides the test using AMC-ZON data, we made a further evaluation using a different data resource, the MADISON CT data repository. We randomly selected 138 patients and would like to see how our curvature line winding angle feature can improve the polyp detection on various CT data sets. FROC curves shown in figure 7.4 demonstrates that our curvature line technique indeed improves the reduction of false positive detections. The winding angle feature of curvature lines provides surface shape information that improves classification of polyps and non-polyps.

7.5 Discussion and Conclusions

7.5.1 Discussion

Our curvature line based winding angle feature makes the following contributions to the improvement of the protrusion-based automatic polyp detection scheme:

- Our new feature provides additional geometric surface shape information for the characterization of colonic polyps. As stated by the authors [vWvRV$^+$06], the protrusion-based feature is invariant to the surface shape and polyp size. This means surface shape information is not included in the protrusion measure. A combination of surface protrusion and our curvature line geometry can therefore better describe the polyp surface. By applying our curvature line technique, helpful shape information is added to the CAD pipeline and the performance of protrusion-based scheme is improved.

- Our curvature line geometric feature describes shapes of large scale surface areas. It is more robust against image noise and polyp shape variation, and has more discriminating power than point-based surface shape features for automatic polyp detection.

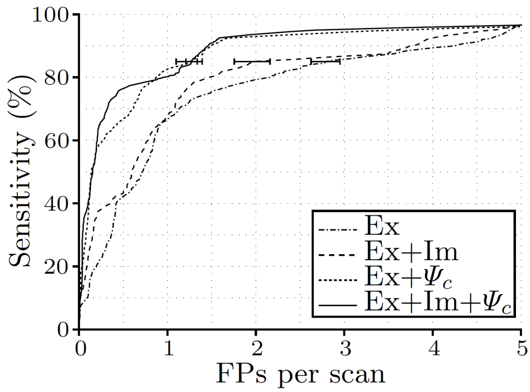

(a)

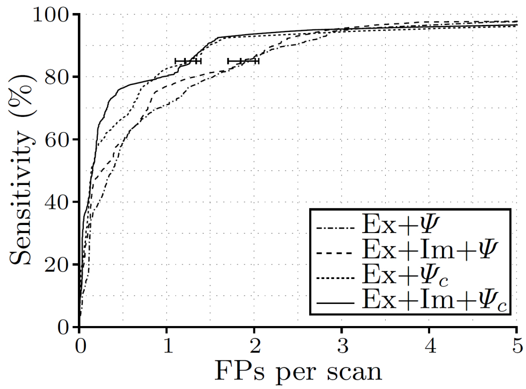

(b)

Figure 7.3: FROC curves for the polyp detection system on AMC-ZON data. Four features were used: ϕ_T and the mean intensity from the explicit protrusion-based method (Ex), maximum intensity difference from the implicit protrusion-based method (Im), clipped and non-clipped winding angle feature (ψ_c/ψ) by curvature line based shape analysis.

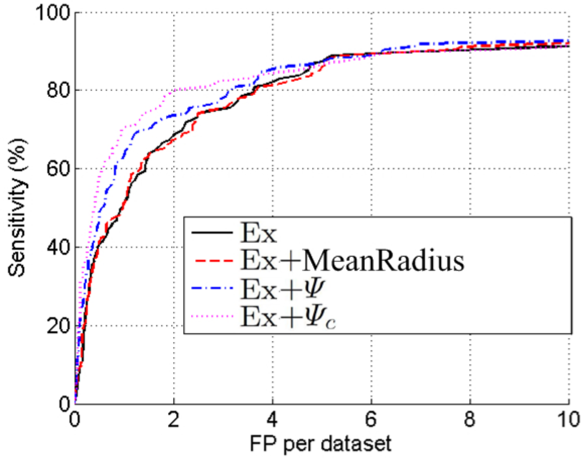

Figure 7.4: FROC curves for the polyp detection system on MADISON data. The four above mentioned features: ϕ_T, mean intensity, clipped and non-clipped winding angle, as well as mean radius (Section 4.5.2) were used in the supervised pattern recognition process.

- Protrusion-based technique does not use the polyp neck area, which can also be used to identify colonic polyps. Our curvature line feature can provide complementary surface information of such a polyp characteristic. This useful shape feature improves the performance of our prototype CAD system.

However, there is a limitation of our current curvature line based technique. Our curvature line feature is only applied for the false-positive reduction step, but not suitable for the whole CAD pipeline (including polyp candidate pre-detection step). This is mainly because of the expensive computation of curvature line generation. Curvature lines are currently generated per candidate area when these polyp candidates are pre-detected. However for the whole colonic surface, the generation cost of curvature lines is too high. Therefore, the contribution of our technique for the entire CAD system is dependent on the performance of the polyp candidate pre-detection step, i.e. the protrusion-based technique. The sensitivity basically has already been determined by the pre-detection algorithm and cannot be improved any more. On the other hand, the specificity can be significantly improved if the false-positive rate is high. This is demonstrated by our evaluation results. However, much less can be done if the specificity is already high enough in the polyp candidates pre-detected.

7.5.2 Conclusions

In this chapter, we documented our evaluation of the new curvature line based technique for automatic polyp detection in CT colonography. We combined our curvature line feature, the winding angle, with protrusion-based features for discriminating between polyps and false positive detections, in the additional feature computation and supervised pattern recognition phases of the CAD pipeline. Our technique added a useful colonic surface shape-descriptor to identify polyps. It was shown that the feature based on the mesh displacement field, the mean intensity, the maximum intensity difference and the curvature line winding angle are comparable in CAD performance. We analyzed various CT data sets, 56 scans from 28 patients in the AMC-ZON data collection and 276 scans from 138 patients in the MADISON data collection. It was found that the curvature line winding angle feature can significantly improve the specificity of the polyp detection result by incorporating it into the candidate classification process. Our prototype CAD system detected over 92% of the polyps with an average of less than 1.6 false positives per scan.

CHAPTER 8

Conclusions and Future Work

This thesis documents our research towards the improvement of automatic polyp detection in CT colonography by integrating techniques from scientific visualization. The focused theme is applying curvature line based visualization techniques to surface and volume geometry processing for polyp surface shape characterization. In this chapter, we summarize our results and contributions, discuss some thoughts and findings, and provide our views on research directions for the future.

8.1 Conclusions

Automatic polyp detection is a helpful addition to visual inspection using CT colonography. It facilitates the laborious procedure of diagnosing colon cancer by radiologists. A common CAD approach includes polyp feature computation, polyp candidate pre-detection and reduction of the false-positive rate (the number of false-positive pre-detections). As a prerequisite, polyp feature computation plays an important role in subsequent steps and greatly influences the performance of the entire CAD system. Most of the existing automatic polyp detection schemes make use of surface geometric and volumetric features. However, many proposed polyp features do not provide sufficient information for polyp shape characterization. There are at least two reasons for this:(1) features are dependent on the pre-defined polyp shape model whereas polyp shapes vary greatly in practice, (2) point-based features are incapable of characterizing shapes of large scale areas (such as polyps) and are sensitive to image noise. Therefore, a large number of false-positive polyp candidates is generated by the CAD procedure. This is the research problem that is addressed by the work presented in this thesis.

In chapter 2, background knowledge of CT colonography and particularly automatic polyp detection techniques was reviewed. General techniques in CT colonography, e.g. visualization of the colonic surface, navigation and interaction approaches and digital colon cleansing, were first discussed. Then the body of literature on CAD was outlined. Our discussion focused mainly on polyp feature computation due to its importance to the entire pipeline. Subsequently, current research of other CAD steps, such as supervised pattern recognition and polyp segmentation and measurement, were also presented.

Chapter 3 gave an overview of visualization techniques related to our automatic polyp detection technique. We first discussed existing methods for the estimation of 3D surface principal curvatures and important applications of using these curvature measurements. These algorithms were based on different geometric methods. Some made use of surface fitting strategies and approximated the discrete surface representation with a parametric surface function. Some directly computed principal curvatures using methods adapted to discrete differential geometry. The accuracy and robustness of these approaches were also discussed. It was concluded that a balanced directional sampling with a sufficiently large sampling scale could overcome bad iso-surface quality and result in more robust and accurate curvature estimation results. We then discussed important vector field visualization techniques related to our research. Surface curvature line generation was of interest in this regard. It has important applications in non-photorealistic rendering and surface remeshing. How well lines of curvature generated on a surface correlate with the global or local shapes is significantly controlled by the streamline distribution, i.e. the streamline seeding and spacing strategies. Streamline seeding and spacing are used for vector field visualization. Therefore, a suitable streamline distribution approach is also crucial to our automatic polyp detection scheme.

The remaining chapters of the thesis presented three techniques that make use of curvature line based visualization techniques for polyp detection and visualization.

In chapter 4, we presented a method that used lines of curvature to visualize the two vector fields of surface principal curvature directions. Geometric features of curvature lines were used for surface and volume geometry processing and to characterize colonic polyp shapes. The work included the following aspects:

1. Robust estimation methods were applied on real CT images for the iso-surface curvature computation, including curvature values and directions.
2. We developed methods that compute surface constrained lines of curvature on both explicit triangle mesh surfaces and implicit iso-surfaces embedded in 3D volume data. Curvature lines were distributed over the 3D surface by applying curvature controlled streamline seeding and spacing strategies.
3. We proposed to identify colonic polyps by detecting polyp neck areas, which are typically closed-ring and anticlastic surfaces. We considered approximately closed curvature lines a good polyp indicator and used the winding angles of these streamlines as a feature for polyp candidate classification.

In Chapter 5, we presented two techniques for the improvement of curvature line generation:

1. To improve the computation efficiency, curvature values were used to control the streamline seeding and spacing strategies. Redundant seeding points were removed during the computation.
2. To improve the streamline quality, we developed a streamline defragmentation approach that computed sufficiently long curvature lines.

Chapter 6 described a novel colonic surface partitioning algorithm based on the clustering of curvature lines. We showed that colonic surface partitions can be used to aggregate point-wise shape features within large scale surface areas for automatic polyp detection.

Chapter 7 documented the results of our evaluation. Our curvature line based techniques were integrated into a prototype automatic polyp detection system. Curvature line features were incorporated with other useful polyp features proposed in the literature for the reduction of false positive pre-detections. The results indicated that our curvature line features could be used to improve the specificity of existing automatic polyp detection approaches without losing the sensitivity.

This above mentioned work makes contributions to the field of computer-aided diagnosis of colonic polyps using CT colonography. Our new curvature line based techniques enabled 3D surface and volume geometry processing based on the analysis of surface principal curvature directions, which are two orthogonal surface vector fields. The curvature line features have a significant discriminating power for the identification of true polyp detections. The performance of existing CAD schemes can be improved by using these new polyp features.

Three important research themes related to our project are discussed in the following three subsections.

8.1.1 Visualization-Based Surface and Volume Geometry Processing

3D surface geometry processing is the core topic of our research on automatic polyp detection. Surface curvature is widely used in most existing surface geometry processing approaches. There are scalar curvature values, such as principal curvatures, and curvature directions, which represent two orthogonal vector fields along the surface. Both scalar and vector quantities are based on the local surface geometry. Surface shape features can be intuitively identified by visualizing these scalar and vector fields on a 3D surface. Based on such a visualization, the correlation between computed surface features and specific surface shapes is examined. The research work documented in this thesis actually started with a visual inspection for finding what is correlated with the polyp-like shape.

Furthermore, techniques developed in scientific visualization can be used for feature computation and eventual shape characterization. There are common ideas between surface processing and pure visualization problems. Surface shapes can be visually presented by applying visualization techniques. The main problem is to visualize a surface feature field that is correlated with specific surface shapes. For instance, such a field can be curvature scalar values or direction vectors. Feature extraction techniques from scientific visualization were used in our research for finding characteristics of surface curvature direction fields. Such characteristics correlated well with polyp-like shapes. Therefore the surface processing problem of finding polyp-like shape is converted to a visualization problem of visualizing and extracting curvature direction field features.

In the application of automatic polyp detection in CT colonography, the techniques presented in Chapters 4, 5 and 6 provide a new way of surface shape characterization, which is visualization-based. Our surface geometry processing approach takes the surface principal curvature direction fields for feature identification, instead of scalar curvatures. This is a novel application of surface geometry processing research. We evaluated the correlation of polyp-like surface shape and circular pattern of the vector curvature fields. This correlation was first reviewed via visualizing surface curvature lines in the neighborhood of polyps on the colon wall and then used to identify colonic polyps.

8.1.2 Identifying Modeled Shapes

In order to find the correct correlation of specific surface shape (e.g. polyp-like shape) and computed features, a proper model of the shape must be built first. It should be known what behavior of these features is unique for the shape and this should be regularized to allow for some variations. A improper shape model can result in incorrect identification. In our experience, a proper shape model should cover all representative forms of a shape. Only the variation of degree is tolerated, but not the variation of type. Otherwise, we lose sensitivity. On the other hand, a proper model should only apply to the shape itself, not other shapes. This means the model is unique for the identified shape and cannot be used to identify other shapes. Otherwise, we lose specificity.

In our automatic polyp detection approach, the polyp surface is modeled to consist of two parts, the polyp cap and the polyp neck. We found that the polyp neck area is usually a smooth anticlastic surface, which is unique to colonic polyps on the colon wall. In our experience, all polyps have such neck areas. Our evaluation presented in Chapter 7 shows that our polyp model is adequate for the polyp surface shape characterization.

8.1.3 Effectiveness, Efficiency and Robustness

Three other important themes run through our research: efficiency, effectiveness and robustness. We have applied these as criteria in the evaluation of our results and also in guiding possible improvement.

In the application of automatic polyp detection in CT colonography, effectiveness is the most important factor that explains how good our polyp detection technique is. It measures how much the polyp detection sensitivity and specificity can be improved by our techniques. Another criterion is efficiency, which measures computational expense. It also indicates the feasibility of a polyp detection technique in clinical environment. The third factor is robustness. Robustness shows the variation of the result accuracy if real-world effects are inevitable. For example, CT image noise has strong impact on polyp detection accuracy.

To achieve a high performance of automatic polyp detection, these three aspects may have severe conflicts. In our experience, a higher effectiveness usually demands more accurate feature computation. This may require more expensive computations and therefore reduce the efficiency. However, a faster computation may be rather simplified and can not guarantee its robustness. A good example is the principal curvature estimation approach discussed in Section 4.4.1. The enlarged k-ring geodesic neighborhood used for the sampling of curvature estimation at a surface point leads to more complicated computations but more robust results against surface noise and artifacts. Our approach needs more expensive computations, although it provides more effective polyp detection results. The priority adjustment of these three criteria is dependent on the practical application. For the polyp detection problem, the effectiveness and robustness of the technique are more important. For other applications, the choice of their priorities can be different.

8.2 Future Work

The most important contribution of the research work presented in this thesis is applying visualization techniques to CAD schemes in CT colonography. This differentiates our approach from existing automatic polyp detection methods. There are still potential research directions that can be addressed for further improvement.

8.2.1 Improving Lines of Curvature Generation

A significant drawback of our approach is that the current streamline generation is computationally expensive. The curvature estimation, streamline integration and streamline distribution consume much computation time. This makes our approach difficult for the pre-detection of polyp candidates, and only suitable for the false-positive reduction step. This limits the effectiveness of our technique in terms of overall CAD performance (sensitivity and specificity). The reason is that features of lines of curvature are only applied after polyp candidates have been found. In this case, the sensitivity can not be improved, even if the result can be very good when pre-detection specificity is already low.

Therefore, in order to make our approach suitable for the entire CAD pipeline and not too much dependent on other steps and techniques, the computation of curvature lines and their features has to be greatly accelerated. There are at least two directions for possible improvements:

- Faster and more robust surface curvature estimation.
- Accelerated curvature line integration, seeding and spacing.

One important concern is that the acceleration method should not sacrifice the accuracy of curvature estimation, the appearance of curvature lines and subsequent polyp detection specificity.

8.2.2 Searching for More Characteristic Polyp Features

A longer term research direction is to search for more discriminating polyp features. A more in-depth study of polyp shapes should be carried out. In order to have more discriminating features for polyp detection, a more universal polyp model that can handle polyps of variant shapes and sizes needs to be built. Such a model should be able to manage a diversity of practical polyp shapes.

It has been suggested that features that describe information at a large scale are preferable and more discriminating for polyp detection. These features are capable of overcoming the effects of CT image noise and variability of the polyp shape. This is worthy of more research effort in the future.

Surface shape features do not help to identify flat lesions, which are malignant growths invading into the colon wall. This kind of polyps appears to be really flat in CT colonography and have already attracted research interests in recent years. Particular image features not exclusively based on surface shape are sought for the detection of flat lesions. The use of iso-surface curvature lines of multiple depths in the colon wall is promising for future research. These curvature lines may provide more useful features for the detection of not only normal polyps but also flat lesions.

8.2.3 Polyp Surface Segmentation

In chapter 6, we presented initial experiments in using curvature line clustering for colonic surface partitioning. The main purpose of this work is to explore the possibility of aggregating point-based features in large scale surface areas for polyp detection. The partitioning result also suggests a pre-segmentation of the polyp candidate.

There are some limits of using curvature line clustering for polyp surface partitioning. First, the clustering does not always provide desired and stable results. For example, for a perfect polyp cap, round and protruding, there are sometimes multiple streamline clusters on it instead of only one. Second, we still have to investigate how accurately that a streamline cluster fits a geometrically homogeneous surface partition.

8.2.4 Enhanced Visualization of the Colon Wall

An important benefit of our curvature line based technique is that the colonic surface visualization can be significantly enhanced by displaying curvature lines on the colon wall. The conventional shaded rendering of the colon wall sometimes limits the perceptibility of colon wall features. Rendering curvature lines may help the observer to better understand the local or global surface shapes.

Techniques from non-photorealistic rendering (NPR) can be applied for the rendering of curvature lines on the colonic surface. For example, developing a stylized curvature line rendering approach is a potential direction of our future research. Curvature lines can be represented using stylized line primitives with additional visual attributes, including color, line width and texture. Suitable stylistic shading techniques, e.g. pen-and-ink illustration, pencil sketching, watercolor or cartoon shading, can be implemented to enhance the visualization of colon wall in CT colonography.

The effectiveness has to be evaluated in practical applications and confirmed by radiologists. A comparison between conventional shaded rendering and rendering with curvature lines should be performed. In context of modern graphics and visualization techniques, graphics hardware accelerated curvature line generation and rendering are of great interest.

Bibliography

[ABG+02] Burak Acar, Christopher F. Beaulieu, Salih B. Göktürk, Carlo Tomasi, David S. Paik, R. Brook Jeffrey, Jr. Judy Yee, and Sandy Napel, *Edge Displacement Field-Based Classification for Improved Detection of Polyps in CT Colonography*, IEEE Transactions on Medical Imaging **21** (2002), no. 12, 1461–1467.

[ACMS98] Fabio Allamandri, Paolo Cignoni, Claudio Montani, and Roberto Scopigno, *Adaptively Adjusting Marching Cubes Output to Fit a Trilinear Reconstruction Filter*, Proceedings of Eurographics Workshop on Scientific Visualization '98 Conference (Dirk Bartz, ed.), Springer Wien, 1998, pp. 25–34.

[ACSD+03] Pierre Alliez, David Cohen-Steiner, Olivier Devillers, Bruno Lévy, and Mathieu Desbrun, *Anisotropic Polygonal Remeshing*, ACM Transactions on Graphics (Proceedings of ACM SIGGRAPH 2003) **22** (2003), no. 3, 485–493.

[AG01] Samir Akkouche and Eric Galin, *Adaptive Implicit Surface Polygonization Using Marching Triangles*, Computer Graphics Forum **20** (2001), no. 2, 67–80.

[AKY99] Charles J. Alpert, Andrew B. Kahng, and So-Zen Yao, *Spectral partitioning with multiple eigenvectors*, Discrete Applied Mathematics (Special volume on VLSI) **90** (1999), no. 1-3, 3–26.

[ANP+01] Burak Acar, Sandy Napel, David Paik, Burak Göktürk, Carlo Tomasi, and Christopher F. Beaulieu, *Using Optical Flow Fields for Polyp Detection in Virtual Colonoscopy*, Proceedings of Medical Image Computing and Computer-Assisted Intervention (MICCAI'01), October 2001, pp. 637–644.

[AUGA05] Pierre Alliez, Giuliana Ucelli, Craig Gotsman, and Marco Attene, *Recent Advances in Remeshing of Surfaces*, Shape Analysis and Structuring (2005), 53–82.

[Bar05] Dirk Bartz, *Vrrtual Endoscopy in Research and Clinical Practice*, Computer Graphics Forum **24** (2005), no. 1, 111–126.

[BBJ+07] M. Bose, J. Bell, L. Jackson, P. Casey, J. Saunders, and O. Epstein, *Virtual vs. Optical Colonoscopy in Symptomatic Gastroenterology Out-patients : the Case for Virtual Imaging Followed by Trgeted Diagnostic or Therapeutic Colonoscopy*, Alimentary pharmacology & therapeutics **26** (2007), no. 5, 727–736.

[BCD+05] Luca Bogoni, Pascal Cathier, Murat Dundar, Anna Jerebko, Sarang Lakare, Jianming Liang, Senthil Periaswamy, Mark E. Baker, and Michael Macari, *Computer-Aided Detection (CAD) for CT colonography: A Tool to Address a Growing Need*, The British Journal of Radiology **78** (2005), no. Special Issue, S57–S62.

[BFH86] James M. Beck, Rida T. Farouki, and John K. Hinds, *Surface Analysis Methods*, IEEE Computer Graphics and Applications **6** (1986), no. 12, 18–36.

[BGKS07] Arye Blachar1, Moshe Graif, Ada Kessler, and Jacob Sosna, *State-of-The-Art CT colonography: Update on Technique and Performance*, Current Colorectal Cancer Reports **3** (2007), no. 1, 49–54.

[BJ88] Paul J. Besl and Ramesh C. Jain, *Segmentation Through Variable-Order Surface Fitting*, IEEE Transactions on Pattern Analysis and Machine Intelligence **10** (1988), no. 2, 167–192.

[BJK+99] Christopher F. Beaulieu, R. Brooke Jeffrey, Chandu Karadi, David S. Paik, and Sandy Napel, *Display Modes for CT Colonography: Part II. Blinded Comparison of Axial CT and Virtual Endoscopic and Panoramic Endoscopic Volume-Rendered Studies*, Radiology **212** (1999), no. 1, 203–212.

[BK07] Didier Bielen and Gabriel Kiss, *Computer-Aided Detection for CT Colonography: Update 2007*, Abdominal Imaging **32** (2007), no. 5, 571–581.

[BKG99] Anna Vilanova Bartrolí, Andreas König, and Eduard Gröller, *VirEn: A Virtual Endoscopy System*, Machine Graphics and Vision **8** (1999), no. 3, 469–487.

[BKP+04] Anders Brun, Hans Knutsson, Hae-Jeong Park, Martha E. Shenton, and Carl-Fredrik Westin, *Clustering Fiber Traces Using Normalized Cuts*, Proceedings of the International Conference on Medical Image Computing and Computer-Assisted Intervention (MICCAI'04), September 2004, Lecture Notes in Computer Science, pp. 368–375.

[BMR+99] Fausto Bernardini, Joshua Mittleman, Holly Rushmeier, Cláudio Silva, and Gabriel Taubin, *The Ball-Pivoting Algorithm for Surface Reconstruction*, IEEE Transaction on Visualization and Computer Graphics **5** (1999), no. 4, 349–359.

[BMS+01] Rahul Bhotika, Paulo R.S. Mendonça, Saad A. Sirohey, Wesley D. Turner, Ying lin Lee, Julie M. McCoy, Rebecca E.B. Brown, and James V. Miller, *A Learning Method for Automated Polyp Detection*, Proceedings of the International Conference on Medical Image Computing and Computer-Assisted Intervention (MICCAI'01), October 2001, pp. 85–93.

[Boe94] Edwin Boender, *Reliable Delaunay-Based Mesh Generation and Mesh Improvement*, Communications in Numerical Methods in Engineering **10** (1994), 773–783.

[BPKW03] Anders Brun, Hae-Jeong Park, Hans Knutsson, and Carl-Fredrik Westin, *Coloring of DT-MRI Fiber Traces Using Laplacian Eigenmaps*, Proceedings of EUROCAST 2003, Lecture Notes in Computer Science 2809, February 2003, pp. 564–572.

[BS99] Dirk Bartz and Martin Skalej, *VIVENDI – A Virtual Ventricle Endoscopy System for Virtual Medicine*, Data Visualization (Proceedings of Symposium on Visualization), 1999, pp. 155–166.

[BWK+01] Anna Vilanova Bartrolí, Rainer Wegenkittl, Andreas König, Eduard Gröller, and E. Sorantin, *Virtual Colon Flattening*, Proceedings of EG/IEEE TCVG Symposium on Visualization (VisSym'01), 2001, pp. 127–136.

[BWKG01] Anna Vilanova Bartrolí, Rainer Wegenkittl, Andreas König, and Eduard Gröller, *Nonlinear Virtual Colon Unfolding*, Proceedings of IEEE Visualization (VIS'01), October 2001, pp. 441–418.

[Car76] Manfredo Do Carmo, *Differential Geometry of Curves and Surfaces*, Prentice-Hall, Englewood Cliffs, NJ, 1976.

[CCF94] Brian Cabral, Nancy Cam, and Jim Foran, *Accelerated Volume Rendering and Tomographic Reconstruction Using Texture Mapping Hardware*, Proceedings of the Symposium on Volume Visualization, 1994, pp. 91–98.

[CCK07] Yuan Chen, Jonathan D. Cohen, and Julian H. Krolik, *Similarity-Guided Streamline Placement with Error Evaluation*, IEEE Transactions on Visualization and Computer Graphics **13** (2007), no. 6, 1448–1455.

[CGG04] Isabelle Corouge, Sylvain Gouttard, and Guido Gerig, *Towards a Shape Model of White Matter Fiber Bundles Using Diffusion Tensor MRI*, Proceedings of IEEE International Symposium on Biomedical Imaging, April 2004, pp. 344–347.

[CGMS00] Paolo Cignoni, Fabio Ganovelli, Claudio Montani, and Roberto Scopigno, *Reconstruction of Topologically Correct and Adaptive Trilinear Isosurfaces*, Computer & Graphics **24** (2000), no. 3, 399–418.

[CHH$^+$03] Christopher S. Co, Bjoern Heckel, Hans Hagen, Bernd Hamann, and Kenneth I. Joy, *Hierarchical Clustering for Unstructured Volumetric Scalar Fields*, Proceedings of IEEE Visualization (VIS'03), October 2003, pp. 325–332.

[CK97] Laurent D. Cohen and Ron Kimmel, *Global Minimum for Active Contour Models: A Minimal Path Approach*, International Journal of Computer Vision **24** (1997), no. 1, 57–78.

[CML$^+$07] Guoning Chen, Konstantin Mischaikow, Robert S. Laramee, Pawel Pilarczyk, and Eugene Zhang, *Vector Field Editing and Periodic Orbit Extraction Using Morse Decomposition*, IEEE Transactions on Visualization and Computer Graphics **13** (2007), no. 4, 769–785.

[CMM$^+$97] Paolo Cignoni, Paola Marino, Claudio Montani, Enrico Puppo, and Reberto Scopigno, *Speeding Up Isosurface Extraction Using Interval Trees*, IEEE Transactions on Visualization and Computer Graphics **3** (1997), no. 2, 158–170.

[CN93] Timothy J. Cullip and Ulrich Neumann, *Accelerating Volume Reconstruction With 3D Texture Hardware*, Technical Report TR93-027, University of North Carolina at Chapel Hill N.C. USA, 1993.

[cola] `http://www.gastro.org/patient-center/procedures/colonoscopy`.

[colb] `http://www.gastrointestinalatlas.com/English/Colon_and_Rectum`.

[colc] `http://commons.wikimedia.org/wiki/File:Colonoscope.jpg`.

[col09a] *Cancer Facts and Figures 2009*, Tech. report, May 2009, Atlanta.

[col09b] *What Are the Risk Factors for Colorectal Cancer?*, Tech. report, 2009, Last Medical Review: 18th May, 2009.

[CPZ07] Wujun Che, Jean-Claude Paul, and Xiaopeng Zhang, *Lines of Curvature and Umbilical Points for Implicit Surfaces*, Computer Aided Geometric Design **24** (2007), 395–409.

[Cro] William Crochot, `http://www.science-et-vie.net`.

[CS92] Xin Chen and Francis Schmitt, *Intrinsic Surface Properties from Surface Triangulation*, Proceedings of 2nd European Conference on Computer Vision (ECCV'92) (St. Margherita Ligure, Italy) (G. Sandini, ed.), May 1992, pp. 739–743.

[CS04] Shannon R. Campbell and Ronald M. Summers, *Analysis of Kernel Method for Surface Curvature Estimation*, International Congress Series, vol. 1268, 2004, pp. 999–1003.

[CTC$^+$05] Ann Chao, Michael J. Thun, Cari J. Connell, Marjorie L. McCullough, Eric J. Jacobs, W. Dana Flanders, Carmen Rodriguez, Rashmi Sinha, and Eugenia E. Calle, *Meat Consumption and Risk of Colorectal Cancer*, The Journal of the American Medicine Association **293** (2005), no. 2, 172–182.

[CWG06] Tarik A. Chowdhury, Paul F. Whelan, and Ovidiu Ghita, *The Use of 3D Surface Fitting for Robust Polyp Detection and Classification in CT Colonography*, Computerized Medical Imaging and Graphics **30** (2006), 427–436.

[Dac09] Abraham H. Dachman, *Comparison of Optical Colonoscopy and CT Colonography for Polyp Detection*, American Journal of Roentgenology **193** (2009), no. 5, 1289–1290.

[DBK$^+$09] Pinaki Dutta, Anil Bhansali, Naveen Kalra, Rakesh Kochhar, Shreekala Narayanan, Usha Dutta, Sanjay Bhadada, and Niranjan Khandelwal, *Comparative Evaluation of Optical Colonoscopy and Multidetector Computerized Tomographic Colonoscopy for Detection of Colonic Polyps in Acromegaly: A Preliminary Study*, the Endocrinologist **19** (2009), no. 6, 280–284.

[dBvMV+02] Paul Wessel de Bruin, P. M. van Meeteren, Frans M. Vos, Albert M. Vossepoel, and Frits H. Post, *Accurate and High Quality Triangle Models from 3D Grey Scale Images*, Proceedings of the International Conference on Medical Image Computing and Computer-Assisted Intervention (MICCAI'02), 2002, pp. 348–355.

[dBVP+00] Paul Wessel de Bruin, Frans M. Vos, Frits H. Post, Sarah F. Frisken-Gibson, and Albert M. Vossepoel, *Improving Triangle Mesh Quality with SurfaceNets*, Proceedings of the International Conference on Medical Image Computing and Computer-Assisted Intervention (MICCAI'00), 2000, pp. 804–813.

[DC00] Thomas Deschamps and Laurent D. Cohen, *Minimal Paths in 3D Images and Application to Virtual Endoscopy*, European Conference on Computer Vision (ECCV'00) (D. Vernon, ed.), 2000, pp. 543–557.

[DC01] ______, *Fast Extraction of Minimal Paths in 3D Images and Applications to Virtual Endoscopy*, Medical Image Analysis **5** (2001), no. 4, 281–299.

[DHKL01] Nira Dyn, Kai Hormann, Sun-Jeong Kim, and David Levin, *Optimizing 3D Triangulations Using Discrete Curvature Analysis*, Mathematical Methods for Curves and Surfaces: Oslo 2000 (2001), 135–146.

[Die93] Paul Dierckx, *Curve and surface fitting with splines*, Oxford University Press, Inc., New York, NY, USA, 1993.

[DKW+01] Frank Dachille, Kevin Kreeger, Mark Wax, Arie Kaufman, and Zhengrong Liang, *Interactive Navigation for PC-Based Virtual Colonoscopy*, Proceedings of SPIE Medical Imaging 2001 (Chin-Tu Chen and Anne V. Clough, eds.), vol. 4321, 2001.

[DMP93] D. Dutta, Ralph R. Martin, and M.J. Pratt, *Cyclides in Surface and Solid Modeling*, IEEE Transactions on Computer Graphics and Applications **13** (1993), no. 1, 53–59.

[DMSB99] Mathieu Desbrun, Mark Meyer, Peter Schröder, and Alan H. Barr, *Implicit Fairing of Irregular Meshes Using Diffusion and Curvature Flow*, Proceedings of ACM SIGGRAPH, August 1999, pp. 317–324.

[DS96] Alan Davies and Philip Samuels, *An introduction to computational geometry for curves and surfaces*, Oxford University Press, Inc., New York, NY, USA, 1996.

[DT97] Gregory Dudek and John K. Tsotsos, *Shape Representation and Recognition from Multiscale Curvature*, Computer Vision and Image Understanding **68** (1997), no. 2, 170–189.

[DvWV+05] Joost J. Dijkers, C. van Wijk, Frans M. Vos, J. Florie, Y.C. Nio, Henk W. Venema, Roel Truyen, and Lucas J. van Vliet, *Segmentation and Size Measurement of Polyps in CT Colonography*, Proceedings of the International Conference on Medical Image Computing and Computer-Assisted Intervention (MICCAI'05), 2005, pp. 712–719.

[Elb98] Gershon Elber, *Line Art Illustrations of Parametric and Implicit Forms*, IEEE Transactions on Visualization and Computer Graphics **4** (1998), no. 1, 71–81.

[Elb99] ______, *Interactive Line Art Rendering of Freeform Surfaces*, EUROGRAPHICS **19** (1999), no. 3.

[FF91] William H. Frey and David A. Field, *Mesh Relaxation: A New Technique for Improving Triangulations*, International journal for Numerical Methods in Engineering **31** (1991), 1121–1133.

[Fre01] Lori A. Freitag, *On Combining Laplacian and Optimization-Based Mesh Smoothing Techniques*, AMD Trends in Unstructured Mesh Generation (ASME) **220** (2001), 37–43.

[Fuk90] Keinosuke Fukunaga, *Introduction to Statistical Pattern Recognition*, 2nd ed., Academic Press Professional, Inc., San Diego, CA, USA, 1990.

[Gal00] Jean Gallier, *Geometric Methods and Applications For Computer Science and Engineer*, Springer-Verlag, London, UK, 2000.

[GBKG04a] Sören Grimm, Stefan Bruckner, Armin Kanitsar, and Eduard Gröller, *A Refined Data Addressing and Processing Scheme to Accelerate Volume Raycasting*, Computers & Graphics **28** (2004), no. 5, 719–729.

[GBKG04b] ______, *Memory Efficient Acceleration Structures and Techniques for CPU-based Volume Raycasting of Large Data*, Proceedings IEEE/SIGGRAPH Symposium on Volume Visualization and Graphics (C. Silva D. Silver, T. Ertl, ed.), October 2004, pp. 1–8.

[GIHL00] Ahna Girshick, Victoria Interrante, Steven Haker, and Todd Lemoine, *Line Direction Matters: an argument for the use of principal directions in 3D line drawings*, Proceedings of First International Symposium on Non-Photorealistic Rendering, 2000, pp. 43–52.

[GKS00] Meenakshisundaram Gopi, Shankar Krishnan, and Claudio T. Silva, *Surface Reconstruction Based on Lower Dimensional Localized Delaunay Triangulation*, Computer Graphics Forum (Eurographics) **19** (2000), no. 3, 467–478.

[GS03] Rao V. Garimella and Blair K. Swartz, *Curvature Estimation for Unstructured Triangulations of Surfaces*, Tech. Report LA-UR-03-8240, Los Alamos National Laboratory, November 2003.

[GTA$^+$01a] Salih Burak Göktürk, Carlo Tomasi, Burak Acar, Christopher F. Beaulieu, David S. Paik, R. Brooke Jeffrey, Judy Yee, and Sandy Napel, *A Statistical 3D Pattern Processing Method for Computer-Aided Detection of Polyps in CT Colonography*, IEEE Transactions on Medical Imaging **20** (2001), no. 12, 1251–1260.

[GTA$^+$01b] Salih Burak Göktürk, Carlo Tomasi, Burak Acar, David S. Paik, Christopher F. Beaulieu, and Sandy Napel, *A Learning Method for Automated Polyp Detection*, Proceedings of the International Conference on Medical Image Computing and Computer-Assisted Intervention (MICCAI'01), October 2001, pp. 85–93.

[GWGS02] Stefan Guthe, Michael Wand, Julius Gonser, and Wolfgang Straβer, *Interactive Rendering of Large Volume Data Sets*, Proceedings of IEEE Visualization (VIS'02), October 2002, pp. 53–60.

[Ham93] Bernd Hamann, *Curvature Approximation for Triangulated Surfaces*, Geometric Modelling (1993), 139–153.

[HATK00] Steven Haker, Sigurd Angenent, Allen Tannenbaum, and Ron Kikinis, *Nondistorting Flattening Maps and the 3D Visualization of Colon CT Images*, IEEE Transactions on Medical Imaging **19** (2000), no. 7, 665–670.

[HGQ$^+$06] Wei Hong, Xianfeng Gu, Feng Qiu, Miao Jin, and Arie Kaufman, *Conformal Virtual Colon Flattening*, Proceedings of ACM Symposium on Solid and Physical Modeling (SPM'06), 2006, pp. 85–94.

[HH99] Taosong He and Lichan Hong, *Reliable Navigation for Virtual Endoscopy*, Proceedings of IEEE Symposium on Nuclear Science, vol. 3, October 1999, pp. 1339–1343.

[HKW$^+$95] Lichan Hong, Arie Kaufman, Yi-Chih Wei, Ajay Viswambharan, Mark Wax, and Zhengrong Liang, *3D Virtual Colonoscopy*, Proceedings of IEEE Symposium on Biomedical Visualization (BioMedVis '95), October 1995, pp. 26–32.

[HMK$^+$97] Lichan Hong, Shigeru Muraki, Arie Kaufman, Dirk Bartz, and Taosong He, *Virtual Voyage: Interactive Navigation in the Human Colon*, Proceedings of ACM SIGGRAPH, 1997, pp. 27–34.

[HMSC00] Jian Huang, Klaus Mueller, Naeem Shareef, and Roger Crawfis, *FastSplats: Optimized Splatting on Rectilinear Grids*, Proceedings of IEEE Visualization (VIS'00), 2000, pp. 219–226.

[Hon08] Wei Hong, *Image-Based Path Planning for Automatic Virtual Colonoscopy Navigation*, Proceedings of SPIE Medical Imaging 2008 (Xiaoping Hu and Anne V. Clough, eds.), vol. 6916, 2008.

[Hou73] Godfrey N. Hounsfield, *Computerized Transverse Axial Scanning (Tomography). Part 1: Description of System*, British Journal of Radiology **46** (1973), 1016–1022.

[HPW05] Klaus Hildebrandt, Konrad Polthier, and Max Wardetzky, *Smooth Feature Lines on Surface Meshes*, Proceedings of the 3rd Eurographics Symposium on Geometry Processing (SGP'05) (Mathieu Desbrun and Helmut Pottmann, eds.), July 2005, pp. 85–90.

[HQK06] Wei Hong, Feng Qiu, and Arie Kaufman, *A Pipeline for Computer Aided Polyp Detection*, IEEE Transactions on Visualization and Computer Graphics **12** (2006), no. 5, 861–868.

[HSH05] Adam Huang, Ronald M. Summers, and Amy K. Hara, *Surface Curvature Estimation for Automatic Colonic Polyp Detection*, Medical Image 2005: Physiology, Function and Structure from Medical Images, Proceedings of SPIE, vol. 5746, 2005, pp. 393–402.

[HZ00] A. Hertzmann and D. Zorin, *Illustrating Smooth Surfaces*, Proceedings of ACM SIGGRAPH, 2000, pp. 517–526.

[IFP95] Victoria Interrante, Henry Fuchs, and Stephen Pizer, *Enhancing Transparent Skin Surfaces with Ridge and Valley Lines*, Proceedings of IEEE Visualization (VIS'95), 1995, pp. 52–59.

[IFP96] ———, *Illustrating Transparent Surfaces with Curvature-Directed Strokes*, Proceedings of IEEE Visualization (VIS'96), 1996.

[Int97] Victoria Interrante, *Illustrating Surface Shape in Volume Data via Principal Direction-Driven 3D Line Integral Convolution*, Proceedings of ACM SIGGRAPH, 1997, pp. 109–116.

[JL97] Bruno Jobard and Wilfrid Lefer, *Creating Evenly-Spaced Streamlines of Arbitrary Density*, Proceedings of the Eurographics Workshop on Visualization in Scientific Computing, 1997, pp. 45–55.

[JMFS03] Anna K. Jerebko, James D. Malley, Marek Franaszek, and Ronald M. Summers, *Multiple Neural Network Classification Scheme for Detection of Colonic Polyps in CT Colonography Data Sets*, Academic Radiology **10** (2003), no. 2, 154–160.

[JMFS05] ———, *Support Vector Machines Committee Classification Method for Computer-Aided Polyp Detection in CT Colonography* , Academic Radiology **12** (2005), no. 4, 479–486.

[JMT02] Ming Jiang, Raghu Machiraju, and David Thompson, *Geometric Verification of Swirling Features in Flow Fields*, Proceedings of IEEE Visualization (VIS'02), October 2002, pp. 307–314.

[JSM+03] Anna K. Jerebko, Ronald M. Summers, James D. Malley, Marek Franaszek, and C. Daniel Johnson, *Computer-Assisted Detection of Colonic Polyps with CT Colonography Using Neural Networks and Binary Classification Trees*, Medical Physics **30** (2003), no. 1, 52–60.

[JTFS03] Anna K. Jerebko, Sheldon Teerlink, Marek Franaszek, and Ronald M. Summers, *Polyp Segmentation Method for CT Colonography Computer-Aided Detection*, Proceedings of SPIE Medical Imaging 2003 (Anne V. Clough and Amir A. Amini, eds.), vol. 5031, 2003, pp. 359–369.

[KAP+07] Ender Konukoglu, Burak Acar, David S. Paik, Christopher F. Beaulieu, Jarrett Rosenberg, and Sandy Napel, *Polyp Enhancing Level Set Evolution of Colon Wall: Method and Pilot Study*, IEEE Transactions on Medical Imaging **26** (2007), no. 12, 1649–1656.

[KBL+07] Jan Klein, Philip Bittihn, Peter Ledochowitsch, Horst K. Hahn, Olaf Konrad, Jan Rexilius, and Heinz-Otto Peitgen, *Grid-Based Spectral Fiber Clustering*, Proceedings of SPIE Medical Imaging 2007, February 2007, pp. 65140V–1–65140V–10.

[KCT+02] Gabriel Kiss, Johan Van Cleynenbreugel, Maarten Thomeer, Paul Suetens, and Guy Marchal, *Computer-Aided Diagnosis in Virtual Colonography via Combination of Surface Normal and Sphere Fitting Methods*, European Radiology **12** (2002), no. 1, 77–81.

[KKL02] Sun-Jeong Kim, Chang-Hun Kim, and David Levin, *Surface Simplification Using a Discrete Curvature Norm*, Computer & Graphics **26** (2002), no. 5, 657–663.

[KLL+07] Se Hyung Kim, Jeong Min Lee, Joon-Goo Lee, Jong Hyo Kim, Philippe A. Lefere, Joon Koo Han, and Byung Ihn Choi, *Computer-Aided Detection of Colonic Polyps at CT Colonography Using a Hessian Matrix-Based Algorithm: Preliminary Study*, American Journal of Roentgenology **189** (2007), 41–51.

[KLM98] Pavel Krsek, Gabor Lukács, and Ralph R. Martin, *Algorithms for Computing Curvatures from Range Data*, Proceedings of the 8th Conference on Mathematics of Surfaces, Information Geometers (A. Ball et al., ed.), August 1998, pp. 1–16.

[Kni00] Gunter Knittel, *The UltraVis System*, Proceedings of the IEEE Symposium on Volume Visualization, 2000, pp. 71–79.

[KPH97] Pavel Krsek, Tomáš Pajdla, and Václav Hlaváč, *Estimation of Differential Parameters on Triangulated Surface*, Proceedings of the Czech Pattern Recognition Workshop '97, February 1997, pp. 151–155.

[KPT+07] David H. Kim, Perry J. Pickhardt, Andrew J. Taylor, Winifred K. Leung, Thomas C. Winter, J. Louis Hinshaw, Deepak V. Gopal, Mark Reichelderfer, Richard H. Hsu, and Patrick R. Pfau, *CT Colonography versus Colonoscopy for the Detection of Advanced Neoplasia*, New England Journal of Medicine **357** (2007), no. 14, 1403–1412.

[KS01] Tasso Karkanis and A. James Stewart, *Curvature-Dependent Triangulation of Implicit Surfaces*, IEEE Computer Graphics and Applications **21** (2001), no. 2, 60–69.

[KT96] Alan D. Kalvin and Russell H. Taylor, *Surfaces: Polygonal Mesh Simplification with Bounded Error*, IEEE Computer Graphics and Applications **16** (1996), no. 3, 64–77.

[KvCD+05] Gabriel Kiss, Johan van Cleynenbreugel, Stylianos Drisis, Didier Bielen, Guy Marchal, and Paul Suetens, *Computer Aided Detection for Low-Dose CT Colonography*, Proceedings of the International Conference on Medical Image Computing and Computer-Assisted Intervention (MICCAI'05), 2005, pp. 859–867.

[KvCMS04] Gabriel Kiss, Johan van Cleynenbreugel, Guy Marchal, and Paul Suetens, *Computer Aided Detection in CT Colonography via Spin Images*, Proceedings of the International Conference on Medical Image Computing and Computer-Assisted Intervention (MICCAI'04), September 2004, pp. 804–812.

[KvCSM03] Gabriel Kiss, Johan van Cleynenbreugel, Paul Suetens, and Guy Marchal, *Computer Aided Diagnosis for CT Colonography via Slope Density Functions*, Proceedings of the International Conference on Medical Image Computing and Computer-Assisted Intervention (MICCAI'03), November 2003, pp. 746–753.

[KW03] Jens Krüger and Rüdiger Westermann, *Acceleration Techniques for GPU-Based Volume Rendering*, Proceedings of IEEE Visualization (VIS'03), October 2003, pp. 287–292.

[KWTM03] Gordon Kindlmann, Ross Whitaker, Tolga Tasdizen, and Torsten Möller, *Curvature-Based Transfer Function for Direction Volume Rendering: Methods and Applications*, Proceedings of IEEE Visualization (VIS'03), October 2003, pp. 513–520.

[LC87] William E. Lorensen and Harvey E. Cline, *Marching Cubes: A High Resolution 3D Surface Construction Algorithm*, ACM SIGGRAPH Computer Graphics **21** (1987), no. 4, 163–169.

[LCL+03] Sarang Lakare, Dongqing Chen, Lihong Li, Arie Kaufman, Mark Max, and Zhengrong Liang, *Robust Colon Residue Detection Using Vector Quantization Based Classification for Virtual Colonoscopy*, Proceedings of SPIE Medical Imaging 2003 (Anne V. Clough Amir A. Amini, ed.), vol. 5031, 2003.

[LDB05] Guillaume Lavoué, Florent Dupont, and Atilla Baskurt, *A New CAD Mesh Segmentation Method, Based on Curvature Tensor Analysis*, Computer-Aided Design **37** (2005), no. 10, 975–987.

[LdlC03] Henry T. Lynch and Albert de la Chapelle, *Hereditary Colorectal Cancer*, The New England Journal of Medicine **348** (2003), no. 10, 919–932.

[Lev88] Marc Levoy, *Display of Surfaces from Volume Data*, IEEE Computer Graphics and Applications **8** (1988), no. 3, 29–37.

[LFB98] David H. Laidlaw, Kurt W. Fleischer, and Alan H. Barr, *Partial-Volume Bayesian Classification of Material Mixtures in MR Volume Data Using Voxel Histogram*, IEEE Transactions on Medical Imaging **17** (1998), no. 1, 74–86.

[LFP+06] Jiang Li, Marek Franaszek, Nicholas Petrick, Jianhua Yao, Adam Huang, and Ronald M. Summers, *Wavelet Method for CT Colonography Computer-Aided Polyp Detection*, Proceedings of IEEE International Symposium on Biomedical Imaging, April 2006, pp. 1316–1319.

[LHD+04] Robert S. Laramee, Helwig Hauser, Helmut Doleisch, Benjamin Vrolijk, Frits H. Post, and Daniel Weiskopf, *The State of the Art in Flow Visualization: Dense and Texture-Based Techniques*, Computer Graphics Forum **23** (2004), no. 2, 203–221.

[LKS06] Jeongjin Lee, Moon Koo Kang, and Yeong Gil Shin, *A Visibility-Based Automatic Path Generation Method for Virtual Colonoscopy*, Computer Graphics International, June 2006, pp. 452–459.

[LL94] Philippe Lacroute and Marc Levoy, *Fast Volume Rendering Using a Shear-Warp Factorization of the Viewing Transformation*, Proceedings of ACM SIGGRAPH, July 1994, pp. 451–458.

[LMG06] Zhanping Liu, Robert J. Moorhead, and Joe Groner, *An Advanced Evenly-Spaced Streamline Placement Algorithm*, IEEE Transactions on Visualization and Computer Graphics **12** (2006), no. 5, 965–972.

[LP82] C. Lin and M. J. Perry, *Shape Description Using Surface Triangulation*, Proceedings of the IEEE Workshop on Computer Vision: Representation and Control, 1982, pp. 38–43.

[LS07] Liya Li and Han-Wei Shen, *Image-Based Streamline Generation and Rendering*, IEEE Transactions on Visualization and Computer Graphics **13** (2007), no. 3, 630–640.

[LSJ96] Yarden Livnat, Han-Wei Shen, and Christopher R. Johnson, *A Near Optimal Isosurface Extraction Algorithm Using the Span Space*, IEEE Transactions on Visualization and Computer Graphics **2** (1996), no. 1, 73–84.

[LWSK00] Sarang Lakare, Ming Wan, Mie Sato, and Arie Kaufman, *3D Digital Cleansing Using Segmentation Rays*, Proceedings of IEEE Visualization (VIS'00), October 2000, pp. 37–44.

[MAD05] Abdelkrim Mebarki, Pierre Alliez, and Olivier Devillers, *Farthest Point Seeding for Efficient Placement of Streamlines*, Proceedings of IEEE Visualization (VIS'05), October 2005, pp. 479–486.

[Mar83] Ralph R. Martin, *Principal Patches: A New Class of Surface Patch Based on Differential Geometry*, Proceedings of 4th Annual European Association for Computer Graphics Conference and Exhibition, Zagreb, Yugoslavia (North-Holland, Amsterdam) (P.J.W. Ten Hagen, ed.), 1983, pp. 47–55.

[Mar98] ______, *Estimation of Principal Curvatures from Range Data*, International Journal of Shape Modeling **4** (1998), no. 3&4, 99–109.

[MAS91] Olivier Monga, Nicholas Ayache, and Peter Sander, *From Voxel to Curvature*, Proceedings of IEEE Computer Society Conference on Computer Vision and Pattern Recognition (CVPR'91), June 1991, pp. 644–649.

[MBF92] Olivier Monga, Serge Benayoun, and Olivier D. Faugeras, *From Partial Derivatives of 3D Density Images to Ridge Lines*, Proceedings of IEEE Computer Society Conference on Computer Vision and Pattern Recognition (CVPR'02), June 1992, pp. 354–359.

[MDSB02] Mark Meyer, Mathieu Desbrun, Peter Schröder, and Alan H. Barr, *Discrete Differential-Geometry Operators for Triangulated 2-Manifolds*, Proceedings of Visualization and Mathematics (VisMath'02), 2002.

[MHS99] Michael Meiβner, Ulrich Hoffmann, and Wolfgang Straβer, *Enabling Classification and Shading for 3D Texture Mapping Based Volume Rendering*, Proceedings of IEEE Visualization (VIS'99), October 1999, pp. 207–214.

[MiHiT+96] Kensaku Mori, Jun ichi Hasegawa, Jun ichiro Toriwaki, Hirofumi Anno, and Kazuhiro Katada, *A Fast Rendering Method Using the Tree Structure of Objects in Virtualized Bronchus Endoscope System*, Proceedings of the 4th International Conference on Visualization in Biomedical Computing, 1996, Lecture Notes In Computer Science; Vol. 1131, pp. 33–42.

[MJC02] Benjamin Mora, Jean Pierre Jessel, and René Caubet, *A New Object-Order Ray-Casting Algorithm*, Proceedings of IEEE Visualization (VIS'02), 2002, pp. 107–113.

[MKY02] Farzin Mokhtarian, Nasser Khalili, and Peter Yuen, *Estimation of Error in Curvature Computation on Multi-Scale Free-Form Surfaces*, International Journal of Computer Vision **48** (2002), no. 2, 131–149.

[MMC99] Klaus Mueller, Torsten Möller, and Roger Crawfis, *Splatting Without The Blur*, Proceedings of IEEE Visualization (VIS'99), 1999, pp. 363–370.

[MSHC99] Klaus Mueller, Naeem Shareef, Jian Huang, and Roger Crawfis, *High-Quality Splatting on Rectilinear Grids with Efficient Culling of Occluded Voxels*, IEEE Transactions on Visualization and Computer Graphics **5** (1999), no. 2, 116–134.

[MSR07] Evgeni Magid, Octavian Soldea, and Ehud Rivlin, *A Comparison of Gaussian and Mean Curvature Estimation Methods on Triangular Meshes of Range Image Data*, Computer Vision and Image Understanding **107** (2007), no. 3, 139–159.

[MSS94] Claudio Montani, Riccardo Scateni, and Roberto Scopigno, *Discretized Marching Cubes*, Proceedings of IEEE Visualization (VIS'94) (R.D. Bergeron and A.E. Kaufman, eds.), 1994, pp. 281–287.

[MSS00] ______, *Decreasing Isosurface Complexity via Discrete Fitting*, Computer-Aided Geometric Design **17** (2000), no. 3, 207–232.

[MTHG03] Oliver Mattausch, Thomas Theußl, Helwig Hauser, and Eduard Gröller, *Strategies for Interactive Exploration of 3D Flow Using Evenly-Spaced Illuminated Streamlines*, Proceedings of the 19th Spring Conference on Computer Graphics (SCCG'03) (Budmerice, Slovakia), April 2003, pp. 213–222.

[Mun87] F.C. Munchmeyer, *On Surface Imperfections*, Proceedings on Mathematics of Surfaces II (Oxford) (Ralph R. Martin, ed.), Oxford University Press, 1987, pp. 459–474.

[MVvW05] Bart Moberts, Anna Vilanova, and Jarke J. van Wijk, *Evaluation of Fiber Clustering Methods for Diffusion Tensor Imaging*, Proceedings of IEEE Visualization (VIS'05), October 2005, pp. 65–72.

[MW99] Alan P. Mangan and Ross T. Whitaker, *Partitioning 3D Surface Meshes Using Watershed Segmentation*, IEEE Transactions on Visualization and Computer Graphics **5** (1999), no. 4, 308–321.

[MWP96] T. Maekawa, F.E. Wolter, and N.M. Patrikalakis, *Umbilics and Lines of Curvature for Shape Interrogation*, Computer Aided Geometric Design **13** (1996), 133–161.

[NH91] Gregory M. Nielson and Bernd Hamann, *The Asymptotic Decider: Resolving the Ambiguity in Marching Cubes*, Proceedings of IEEE Visualization (VIS'91), 1991, pp. 83–91.

[NHKG01] Delphine Nain, Steven Haker, Ron Kikinis, and W. Eric L. Grimson, *An Interactive Virtual Endoscopy Tool*, Proceedings of Interactive Medical Image Visualization and Analysis workshop (IMIVA) at MICCAI (Utrecht, The Netherlands), September 2001.

[Nie03] Gregory M. Nielson, *On Marching Cubes*, IEEE Transactions on Visualization and Computer Graphics **9** (2003), no. 3, 283–297.

[NSW02] Zoltán Nagy, Jens Schneider, and Rüdiger Westermann, *Interactive Volume Illustration*, Proceedings of Vision, Modeling and Visualization Workshop (VMV), 2002.

[NWB+06] Vijay Natarajan, Yusu Wang, Peer-Timo Bremer, Valerio Pascucci, and Bernd Hamann, *Segmenting Molecular Surfaces*, Computer Aided Geometric Design **23** (2006), no. 6, 495–509, Special issue: Applications of geometric modeling in the life sciences.

[NY02] Janne Näppi and Hiroyuki Yoshida, *Automated Detection of Polyps with CT Colonography: Evaluation of Volumetric Features for Reduction of False-Positive Findings*, Academic Radiology **9** (2002), no. 4, 386–397.

[NY03] ———, *Feature-guided Analysis for Reduction of False Positives in CAD of Polyps for Computed Tomographic Colonography*, Medical Physics **30** (2003), no. 7, 1592–1601.

[OBS04] Yutaka Ohtake, Alexander Belyaev, and Hans-Peter Seidel, *Ridge-Valley Lines on Meshes via Implicit Surface Fitting*, ACM Transactions on Graphics **23** (2004), no. 3, 609–612.

[O'N97] Barrett O'Neill, *Elementary Differential Geometry*, second ed., Academic Press, Orlando, FL, 1997.

[Org09] World Health Organization, *Cancer*, Fact Sheet 297, February 2009.

[PBR+04] David S. Paik, Christopher F. Beaulieu, Geoffrey D. Rubin, Burak Acar, R. Brooke Jeffrey, Jr. Judy Yee, Joyoni Dey, and Sandy Napel, *Surface Normal Overlap: A Computer-Aided Detection Algorithm with Application to Colonic Polyps and Lung Nodules in Helical CT*, IEEE Transactions on Medical Imaging **23** (2004), no. 6, 661–675.

[PC03] Perry J. Pickhardt and Jong-Ho Richard Choi, *Electronic Cleansing and Stool Tagging in CT Colonography: Advantages and Pitfalls with Primary Three-Dimensional Evaluation*, American Journal of Roentgenology **181** (2003), no. 3, 799–805.

[PCH+03] Perry J. Pickhardt, J. Richard Choi, Inku Hwang, James A. Butler, Michael L. Puckett, Hans A. Hildebrandt, Roy K. Wong, Pamela A. Nugent, Pauline A. Mysliwiec, and William R. Schindler, *Computed tomographic virtual colonoscopy to screen for colorectal neoplasia in asymptomatic adults*, The New England Journal of Medicine (NEJM) **349** (2003), no. 23, 2191–2200.

[PFTV92] William H. Press, Brian P. Flannery, Saul A. Teukolsky, and William T. Vetterling, *Numerical Recipes in C: The Art of Scientific Computing*, 2nd ed., Cambridge University Press, New York, NY, USA, 1992.

[Pic] Perry J. Pickhardt, University of Wisconsin Medical School.

[Pic04] ———, *CT Colonography (Virtual Colonoscopy) for Primary Colorectal Screening: Challenges Facing Clinical Implementation*, Abdominal Imaging **30** (2004), no. 1, 1–4.

[PKS+01] David L. Page, Andreas F. Koschan, Yiyong Sun, Joonki Paik, and Mongi A. Abidi, *Robust Crease Detection and Curvature Estimation of Piecewise Smooth Surfaces from Triangle Mesh Approximations Using Normal Voting*, Proceedings of IEEE Computer Society Conference on Computer Vision and Pattern Recognition (CVPR'01), December 2001, pp. 162–167.

[PM02] Nicholas M. Patrikalakis and Takashi Maekawa, *Shape Interrogation for Computer Aided Design and Manufacturing*, first ed., Springer, 2002.

[Por97] Luis Manuel Portela, *Identification and Characterization of Vortices in the Turbulent Boundary Layer*, Ph.D. thesis, Stanford University, 1997.

[PSBG93] John D. Potter, Martha L. Slattery, Roberd M. Bostick, and Susan M. Gapstur, *Colon Cancer: a Review of the Epidemiology*, Epidemiologic Reviews **15** (1993), no. 2, 499–545.

[PSK+02] David L. Page, Yiyong Sun, Andreas F. Koschan, Joonki Paik, and Mongi A. Abidi, *Normal Vector Voting: Crease Detection and Curvature Estimation on Large, Noisy Meshes*, Graphical Models **64** (2002), no. 3/4, 199–229.

[PTK+06] Perry J. Pickhardt, Andrew J. Taylor, David H. Kim, Mark Reichelderfer, Deepak V. Gopal, and Patrick R. Pfau, *Screening for Colorectal Neoplasia with CT Colonography: Initial Experience from the 1st Year of Coverage by Third-Party Payers*, Radiology **241** (2006), no. 2, 417–425.

[PVH+03] Frits H. Post, Benjamin Vrolijk, Helwig Hauser, Robert S. Laramee, and Helmut Doleisch, *The State of the Art in Flow Visualization: Feature Extraction and Tracking*, Computer Graphics Forum **22** (2003), no. 4, 775–792.

[RBA+96] Geoffrey D. Rubin, Christopher F. Beaulieu, Vincent Argiro, Helmut Ringl, Alexander M. Norbash, John F. Feller, Michael D. Dake, R. Brooke Jeffrey, and Sandy Napel, *Perspective Volume Rendering of CT and MRI Images: Applications for Endoscopic Imaging*, Radiology **199** (1996), no. 2, 321–330.

[RGW+03] Stefan Roettger, Stefan Guthe, Daniel Weiskopf, Thomas Ertl, and Wolfgang Strasser, *Smart Hardware-Accelerated Volume Rendering*, Proceedings of EG/IEEE TCVG Symposium on Visualization (VisSym'03), 2003, pp. 231–238.

[RK00] Christian Rössl and Leif Kobbelt, *Line-Art Rendering of 3D Models*, Proceedings of Pacific Graphics, 2000, pp. 87–96.

[RTvVV04] Bernd Rieger, Frederik J. Timmermans, Lucas J. van Vliet, and Piet W. Verbeek, *On Curvature Estimation of ISO surfaces in 3D Gray-Value Images and the Computation of Shape Descriptors*, IEEE Transactions on Pattern Analysis and Machine Intelligence **26** (2004), no. 8, 1088–1094.

[SBP+00] Ronald M. Summers, Christopher F. Beaulieu, Lynne M. Pusanik, James D. Malley, R. Brooke Jeffrey, Daniel I. Glazer, and Sandy Nappel, *Automated Polyp Detector for CT Colonography: Feasibility Study*, Radiology **216** (2000), no. 1, 284–290.

[SdVV+08] Iwo W.O. Serlie, Ayso H. de Vries, Frans M. Vos, Yung Nio, Roel Truyen, Jaap Stoker, and Lucas J. van Vliet, *Lesion Conspicuity and Efficiency of CT Colonography with Electronic Cleansing Based on a Three-Material Transition Model*, American Journal of Roentgenology **191** (2008), no. 11, 1493–1502.

[Set99] James A. Sethian, *Level Set Methods: Evolving Interfaces in Computational Geometry, Fluid Mechanics, Computer Vision and Materials Sciences*, Cambridge University Press, 1999.

[SF03] Georgios Stylianou and Gerald Farin, *Crest Lines Extraction from 3D Triangulated Meshes*, Hierarchical and Geometrical Methods in Scientific Visualization (Gerald Farin, Bernd Hamann, and Hans Hagen, eds.), Springer Verlag, 2003, pp. 269–281.

[SF04] ______, *Crest Lines for Surface Segmentation and Flattening*, IEEE Transactions on Visualization and Computer Graphics **10** (2004), no. 5, 536–544.

[SFYC96] Raj Shekhar, Elias Fayyad, Roni Yagel, and J. Fredrick Cornhill, *Octree-Based Decimation of Marching Cubes Surfaces*, Proceedings of IEEE Visualization (VIS'96), 1996, pp. 335–342.

[Sha04] Ariel Shamir, *A Formulation of Boundary Mesh Segmentation*, Proceedings of 2nd International Symposium on 3D Data Processing, Visualization and Transmission (3DPVT'04), September 2004, pp. 82–89.

[SHH+07] Michael Schlemmer, Ingrid Hotz, Bernd Hamann, Florian Morr, and Hans Hagen, *Priority Streamlines: A Context-Based Visualization of Flow Fields*, Proceedings of Eurographics/IEEE-VGTC Symposium on Visualization (EuroVis'07) (Ken Museth and Torsten Möller, and Anders Ynnerman, ed.), May 2007, pp. 227–234.

[SHLJ96] Han-Wei Shen, Charles D. Hansen, Yarden Livnat, and Christopher R. Johnson, *Isosurfacing in Span Space Using Utmost Efficiency*, Proceedings of IEEE Visualization (VIS'96), 1996, pp. 287–294.

[SJP+01] Ronald M. Summers, C. Daniel Johnson, Lynne M. Pusanik, James D. Malley, Ashraf M. Youssef, and Judd E. Reed, *Automated Polyp Detection at CT Colonography: Feasibility Assessment in a Human Population*, Radiology **219** (2001), no. 1, 51–59.

[SJWS08] Tobias Salzbrunn, Heike Jänicke, Thomas Wischgoll, and Gerik Scheuermann, *The State of the Art in Flow Visualization: Partition-Based Techniques*, Proceedings of Simulation and Visualization (SimVis'08) (Helwig Hauser, Steffen Strassburger, and Holger Theisel, eds.), February 2008, pp. 75–92.

[SMS+03a] Tatiana Surazhsky, Evgeny Magid, Octavian Soldea, Gershon Elber, and Ehud Rivlin, *A Comparison of Gaussian and Mean Curvature Estimation Methods on Triangular Meshes*, Proceedings of the IEEE International Conference on Robotics and Automation (ICRA'03), vol. 1, September 2003, pp. 1021–1026.

[SMS+03b] ______, *A Comparison of Gaussian and Mean Curvatures Estimation Methods on Triangular Meshes*, Proceedings of IEEE International Conference on Robotics and Automation, vol. 1, September 2003, pp. 1021–1026.

[SP99] Ari Sadarjoen and Frits H. Post, *Geometric Methods for Vortex Extraction*, Data Visualization, proceedings of VisSym 99, May 1999, pp. 53–62.

[SSFS06] John Schreiner, Carlos E. Scheidegger, Shachar Fleishman, and Cláudio T. Silva, *Direct (Re)meshing for Efficient Surface Processing*, Computer Graphics Forum (Proceedings of Eurographics 2006) **25** (2006), no. 3, 527–536.

[SSM+98] Ronald M. Summers, W. Scott Selbie, James D. Malley, Lynne M. Pusanik, Andrew J. Dwyer, Nikos A. Courcoutsakis, David J. Shaw, David E. Kleiner, Michael C. Sneller, Carol A. Langford, Steven M. Holland, and James H. Shelhamer, *Polypoid Lesions of Airways: Early Experience with Computer-Assisted Detection by Using Virtual Bronchoscopy and Surface Curvature*, Radiology **208** (1998), no. 2, 331–337.

[sSS06] John schreiner, Carlos E. Scheidegger, and Cláudio T. Silva, *High-Quality Extraction of Isosurfaces from Regular and Irregular Grids*, IEEE Transactions on Visualization and Computer Graphics **12** (2006), no. 5, 1205–1212.

[STF+03] Iwo W.O. Serlie, Roel Truyen, Jasper Florie, Frits H. Post, Lucas J. van Vliet, and Frans M. Vos, *Computed Cleansing for Virtual Colonoscopy Using a Three-Material Transition Model*, Proceedings of the International Conference on Medical Image Computing and Computer-Assisted Intervention (MICCAI'03), November 2003, pp. 175–183.

[SVvG+01] Iwo W.O. Serlie, Frans M. Vos, Rogier E. van Gelder, Jaap Stoker, Roel Truyen, Frans A. Gerritsen, C. Yung Nio, and Frits H. Post, *Improved Visualization in Virtual Colonoscopy Using Image-Based Rendering*, Proceedings of EG/IEEE TCVG Symposium on Visualization (VisSym'01), 2001, pp. 137–146.

[SW92] Ernest M. Stokely and Shang You Wu, *Surface Parameterization and Curvature Measurement of Arbitrary 3D-Objects: Five Practical Methods*, IEEE Transactions on Pattern Analysis and Machine Intelligence **14** (1992), no. 8, 833–840.

[SYP+05] Ronald M. Summers, Jianhua Yao, Perry J. Pickhardt, Marek Franaszek, Ingmar Bitter, Daniel Brickman, Vamsi Krishna, and J. Richard Choi, *Computed Tomographic Virtual Colonoscopy Computer-Aided Polyp Detection in a Screening Population*, Gastroenterology **129** (2005), no. 6, 1832–1844.

[SZL92] William J. Schroeder, Jonathan A. Zarge, and William E. Lorensen, *Decimation of Triangle Meshes*, Proceedings of the 19th annual conference on Computer graphics and interactive techniques, 1992, pp. 65–70.

[TA] Alan B.R. Thomson and Dennis J. Ahnen, *Intestinal Polypoid Adenomas*, Tech. report, URL: http://emedicine.medscape.com/article/179284-overview.

[Tau95a] Gabriel Taubin, *A Signal Processing Approach to Fair Surface Design*, Proceedings of ACM SIGGRAPH, August 1995, pp. 351–358.

[Tau95b] ______, *Estimating the Tensor of Curvature of a Surface From a Polyhedral Approximation*, Proceedings of the 5th International Conference on Computer Vision, 1995, pp. 902–907.

[TB96] Greg Turk and David Banks, *Image-Guided Streamline Placement*, Proceedings of the 23rd Annual Conference on Computer Graphics and Interactive Techniques (SIGGRAPH'96), August 1996, pp. 453–460.

[TDC01] Roel Truyen, Thomas Deschamps, and Laurent D. Cohen, *Clinical Evaluation of an Automatic Path Tracker for Virtual Colonoscopy*, Proceedings of the International Conference on Medical Image Computing and Computer-Assisted Intervention (MICCAI'01), October 2001, pp. 169–176.

[TG95a] Jean-Philippe Thirion and Alexis Gourdon, *Computing the Differential Characteristics of Isointensity Surfaces*, Computer Vision and Image Understanding **61** (1995), no. 2, 190–202.

[TG95b] Jean Philippe Thirion and Alexis Gourdon, *Computing the differential characteristics of isointensity surfaces*, Computer Vision and Image Understanding **61** (1995), no. 2, 190–202.

[TT05] Wai-Shun Tong and Chi-Keung Tang, *Robust Estimation of Adaptive Tensors of Curvature by Tensor Voting*, IEEE Transactions on Pattern Analysis and Machine Intelligence **27** (2005), no. 3.

[Tur92] Greg Turk, *Re-Tiling Polygonal Surfaces*, Computer Graphics (Proceedings of ACM SIGGRAPH'92) **26** (1992), no. 2, 55–64.

[Vap95] Vladimir N. Vapnik, *The Nature of Statistical Learning Theory*, Springer-Verlag New York, Inc., New York, NY, USA, 1995.

[vdWvVVvG01] Joost van de Weijer, Lucas J. van Vliet, Piet W. Verbeek, and Michael van Ginkel, *Curvature Estimation in Oriented Patterns Using Curvilinear Models Applied to Gradient Vector Fields*, IEEE Transactions on Pattern Analysis and Machine Intelligence **23** (2001), no. 9, 1035–1042.

[vGNF+04] Rogier E. van Gelder, C. Yung Nio, Jasper Florie, Joep F. Bartelsman, Pleun Snel, Steven W. de Jager, Sander J. van Deventer, Johan S. Laméris, Patrick M. M. Bossuyt, and Jaap Stoker, *Computed Tomographic Colonography Compared with Colonoscopy in Patients at Increased Risk for Colorectal Cancer*, Gastroenterology **127** (2004), no. 1, 41–48.

[vGVS+02] Rogier E. van Gelder, Henk W. Venema, Iwo W. O. Serlie, C. Yung Nio, Rogier M. Determann, Corinne A. Tipker, Frans M. Vos, Afina S. Glas, Joep F. W. Bartelsman, Patrick M. M. Bossuyt, Johan S. Laméris, and Jaap Stoker, *CT Colonography at Different Radiation Dose Levels: Feasibility of Dose Reduction*, Radiology **224** (2002), no. 1, 25–33.

[vGW94] Allen van Gelder and Jane Wilhelms, *Topological Considerations in Isosurface Generation*, ACM Transactions of Graphics **13** (1994), no. 4, 337–375.

[VKP00] Vivek Verma, David Kao, and Alex Pang, *A Flow-Guided Streamline Seeding Strategy*, Proceedings of IEEE Visualization (VIS'00), 2000, pp. 163–170.

[vRZB+09] Vincent F. van Ravesteijn, Lingxiao Zhao, Charl P. Botha, Frits H. Post, Frans M. Vos, and Lucas J. van Vliet, *Combining Mesh, Volume, and Streamline Representations for Polyp Detection in CT Colonography*, Proceedings of IEEE International Symposium on Medical Imaging: From Nano to Macro, June 2009, pp. 907–910.

[VSA+97] David J. Vining, David R. Stelts, David K. Ahn, Paul F. Hemler, Yaorong Ge, Gordon W. Hunt, Christopher Siege, Daniel B. McCorquodale, Mark E. Sarojak, and Gilbert R. Ferretti, *FreeFlight: A Virtual Endoscopy System*, Proceedings of the First Joint Conference on Computer Vision, Virtual Reality and Robotics in Medicine and Medial Robotics and Computer-Assisted Surgery, vol. 1205, 1997, pp. 413–416.

[VvGS+03] Frans M. Vos, Rogier E. van Gelder, Iwo W.O. Serlie, Jasper Florie, C. Yung Nio, Afina S. Glas, Frits H. Post, Roel Truyen, Frans A. Gerritsen, and Jaap Stoker, *Three-Dimensional Display Modes for CT Colonography: Conventional 3D Virtual Colonoscopy Versus Unfolded Cube Projection*, Radiology **228** (2003), no. 3, 878–885.

[vVV93] Lucas J. van Vliet and Piet W. Verbeek, *Curvature and Bending Energy in Digitized 2D and 3D Images*, Proceedings of 8th Scandinavian Conference on Image Analysis (SCIA'93), May 1993, Tromso, Norway, pp. 1403–1410.

[vVYV98] Lucas J. van Vliet, Ian Theodore Young, and Piet W. Verbeek, *Recursive Gaussian Derivative Filters*, Proceedings of the 14th International Conference of Pattern Recognition (ICPR'98), August 1998, pp. 509–514.

[vWTvG+04] Cees van Wijk, Roel Truyen, Rogier E. van Gelder, Lucas J. van Vliet, and Frans M. Vos, *On Normalized Convolution to Measure Curvature Features for Automatic Polyp Detection*, Proceedings of the International Conference on Medical Image Computing and Computer-Assisted Intervention (MICCAI'04), September 2004, pp. 200–208.

[vWvRV+06] Cees van Wijk, Vincent F. van Ravesteijn, Frans M. Vos, Roel Truyen, Ayso H. de Vries, Jaap Stoker, and Lucas J. van Vliet, *Detection of Protrusions in Curved Folded Surfaces Applied to Automated Polyp Detection in CT Colonoscopy*, Proceedings of the International Conference on Medical Image Computing and Computer-Assisted Intervention (MICCAI'06), 2006, pp. 471–478.

[WB01] Kouki Watanabe and Alexander G. Belyaev, *Detection of Salient Curvature Features on Polygonal Surfaces*, Computer Graphics Forum (Eurographics) **20** (2001), no. 3, 385–392.

[WDSB00] Zoë J. Wood, Mathieu Desbrun, Peter Schröder, and David Breen, *Semi-Regular Mesh Extraction from Volumes*, Proceedings of IEEE Visualization (VIS'00), 2000, pp. 275–282.

[WE98] Rüdiger Westermann and Thomas Ertl, *Efficiently Using Graphics Hardware in Volume Rendering Applications*, Computer Graphics (Proceedings of ACM SIGGRAPH'98) **32** (1998), no. 4, 169–177.

[Web02] Andrew R. Webb, *Statistical Pattern Recognition*, second ed., John Wiley and Sons Ltd., 2002.

[Wes91] Lee A. Westover, *SPLATTING: A Parallel, Feed-Forward Volume Rendering Algorithm*, Ph.d. dissertation, Department of Computer Science, University of North Carolina at Chapel Hill, 1991.

[WLK+02] Ming Wan, Zhengrong Liang, Qi Ke, Lichan Hong, Ingmar Bitter, and Arie Kaufman, *Automatic Centerline Extraction for Virtual Colonoscopy*, IEEE Transactions on Medical Imaging **21** (2002), no. 12, 1450–1460.

[WLL05a] Zigang Wang, Bin Li, and Zhengrong Liang, *Feature-Based Texture Display for Detection of Polyps On Flattened Colon Volume*, Proceedings of the 27th Annual Conference on Engineering in Medicine and Biology, September 2005, pp. 3359–3362.

[WLL+05b] Zigang Wang, Zhengrong Liang, Lihong Li, Xiang Li, Bin Li, Joseph Anderson, and Donald Harrington, *Reduction of False Positives by Internal Features for Polyp Detection in CT-Based Virtual Colonoscopy*, Medical Physics **32** (2005), no. 12, 3602–3616.

[WLL+06] Zigang Wang, Zhengrong Liang, Xiang Li, Lihong Li, Bin Li, Daria Eremina, and Hongbing Lu, *An Improved Electronic Colon Cleansing Method for Detection of Colonic Polyps by Virtual Colonoscopy*, IEEE Transactions on Biomedical Engineering **53** (2006), no. 8, 1635–1646.

[WMBV98] Ge Wang, Elizabeth G. McFarland, Bruce P. Brown, and Michael W. Vannier, *GI Tract Unraveling with Curved Cross-Sections*, IEEE Transactions on Medical Imaging **17** (1998), no. 2, 318–322.

[WS01] Rüdiger Westermann and Bernd Sevenich, *Accelerated Volume Ray-Casting Using Texture Mapping*, Proceedings of IEEE Visualization (VIS'01), October 2001, pp. 271–278.

[WV95] Ge Wang and Michael W. Vannier, *GI Tract Unraveling by Spiral CT*, Proceedings of SPIE Medical Imaging 1995 (Chin-Tu Chen and Anne V. Clough, eds.), vol. 2434, 1995, pp. 307–315.

[WvG92] Jane Wilhelms and Allen van Gelder, *Octrees for Faster Isosurface Generation*, ACM Transactions of Graphics **11** (1992), no. 3, 201–227.

[XPB06] Guoliang Xu, Qing Pan, and Chandrajit L. Bajaj, *Discrete Surface Modeling Using Partial Differential Equations* , Computer Aided Geometric Design **23** (2006), no. 2, 125–145.

[YBS05] Shin Yoshizawa, Alexander Belyaev, and Hans-Peter Seidel, *Fast and Robust Detection of Crest Lines on Meshes*, Proceedings of ACM Symposium on Solid and Physical Modeling (SPM'05) (MIT, Cambridge, MA, USA), June 2005, pp. 227–232.

[YCL02] II Dong Yun, Kyowoong Choo, and Sang Uk Lee, *Mesh Simplification Using the Edge Attributes*, EURASIP Journal on Applied Signal Processing **2002** (2002), no. 1, 1102–1115.

[YKP05] Xiangong Ye, David Kao, and Alex Pang, *Strategy for Seeding 3D Streamlines*, Proceedings of IEEE Visualization (VIS'05), October 2005, pp. 471–478.

[YMFS04] Jianhua Yao, Meghan Miller, Marek Franaszek, and Ronald M. Summers, *Colonic Polyp Segmentation in CT Colonography-Based on Fuzzy Clustering and Deformable Models*, IEEE Transactions on Medical Imaging **23** (2004), no. 11, 1344–1352.

[YMM+02] Hiroyuki Yoshida, Yoshitaka Masutani, Peter MacEneaney, David T. Rubin, and Abraham H. Dachman, *Computerized Detection of Colonic Polyps at CT Colonography on the Basis of Volumetric Features: Pilot Study*, Radiology **222** (2002), no. 2, 327–336.

[YN01] Hiroyuki Yoshida and Janne Näppi, *Three-Dimensional Computer-Aided Diagnosis Scheme for Detection of Colonic Polyps*, IEEE Transactions on Medical Imaging **20** (2001), no. 12, 1261–1274.

[YNM+02] Hiroyuki Yoshida, Janne Näppi, Peter MacEneaney, David T. Rubin, and Abraham H. Dachman, *Computer-Aided Diagnosis Scheme for Detection of Polyps at CT Colonography*, Radiographics **22** (2002), 963–979.

[ZBB+06] Lingxiao Zhao, Charl P. Botha, Javier O. Bescos, Roel Truyen, Frans M. Vos, and Frits H. Post, *Lines of Curvature for Polyp Detection in Virtual Colonoscopy*, IEEE Transactions on Visualization and Computer Graphics **12** (2006), no. 5, 885–892.

[ZBT+08] Lingxiao Zhao, Charl P. Botha, Roel Truyen, Frans M. Vos, and Frits H. Post, *Efficient Seeding and Defragmentation of Curvature Streamlines for Colonic Polyp Detection*, Proceedings of SPIE Medical Imaging 2008 (Xiaoping Hu and Anne V. Clough, eds.), vol. 6916, 2008.

[ZPFH03] Michael E. Zalis, James Perumpillichira, Chiara Del Frate, and Peter F. Hahn, *CT Colonography: Digital Subtraction Bowel Cleansing with Mucosal Reconstruction Initial Observations*, Radiology **226** (2003), no. 3, 911–917.

[ZvRB+08] Lingxiao Zhao, Vincent F. van Ravesteijn, Charl P. Botha, Roel Truyen, Frans M. Vos, and Frits H. Post, *Surface Curvature Line Clustering for Polyp Detection in CT Colonography*, Proceedings of the first Eurographics Workshop on Visual Computing for Biomedicine 2008 (EG VCBM'08) (Charl P. Botha, Gordon Kindlmann, Wiro Niessen, and Bernhard Preim, eds.), October 2008, pp. 53–60.

List of Figures

List of Tables

Summary

Curvature lines for lesion detection and visualization in CT colonography

Colon cancer is one of the leading causes of cancer deaths in the world. Colonic polyps are an important precursor of colon cancer. Early detection and removal of colonic polyps can effectively prevent colon cancer. For the diagnosis of colonic polyps, CT colonography (virtual colonoscopy) is an advanced less-invasive screening technique which causes much less discomfort to the patient than traditional optical colonoscopy. However even using CT colonography, the visual detection of polyps can be complicated and time-consuming for the entire colonic surface. Computer-aided diagnosis has been suggested and become a major research topic for CT colonography. Many published approaches for automatic polyp detection made use of features derived from surface curvature. These features are usually too localized to fully describe characteristics of polyps. This can result in a large number of false-positive detections.

In this thesis, we present an automatic polyp detection approach that integrates knowledge from flow visualization techniques. Our primary goal was to compute additional characteristic polyp features that improve the CAD performance of existing polyp detection approaches by eliminating found false-positive polyp candidates.

We found that surface principal curvature directions presented discriminating patterns on surface areas that belong to colonic polyps. These could be visualized using lines of curvatures. This led us to the hypothesis that geometric features of lines of curvature could be used for automatic polyp detection. A robust algorithm that takes both balanced directional sampling and enlarged sampling area into account was used for curvature estimation. We developed novel approaches for generating lines of curvature on the colon wall. Our techniques can be applied to explicit triangle mesh surfaces and implicit iso-surfaces embedded in a 3D CT volume. In order to provide sufficient shape information, lines of curvature were distributed using curvature-adaptive streamline seeding and spacing strategies. Two features of lines of curvature: winding angle and mean radius, were used to differentiate between true polyp detections and false positives. The visualization of the colon wall was also enhanced by visualizing lines of curvature.

We present two major improvements of our lines of curvature generation in this thesis. First, a more efficient streamline seeding strategy was developed. The placement of streamline seeds were adapted to the local surface curvature. This significantly removed redundant seeds and accelerated the generation of lines of curvature, while still resulting in a comparable streamline distribution. Second, we observed that the correlation between curvature line features and true polyps was influenced by the quality of curvature lines generated. Our curvature line tracing algorithm was improved by using a streamline defragmentation approach. Sufficiently long lines of curvature that better describe polyp shapes were generated.

We also present a novel approach that was used to partition the colonic surface into geometrically homogeneous regions based on clustering of lines of curvature. This method applied a spectral clustering algorithm and a symmetric line similarity measure. The parallelism between lines of curvature was taken into account since we found that a collection of parallel curvature lines covered a surface area that has a similar geometry everywhere. Such a partitioning of the colon wall provided a possibility to aggregate shape information over the polyp surface for automatic polyp detection.

Our curvature line based polyp detection technique was evaluated by integrating it into a complete CAD system. Features of lines of curvature were used in the polyp candidate classification step for the reduction of the number of false-positive pre-detections. Two different data resources were chosen and a large number of CT data sets from real patients were used. The result showed that our new curvature line features are strongly correlated with true polyp detections and can be used to improve the performance of existing CAD systems.

This research was conducted at the Delft University of Technology, in corporation with Philips Healthcare Netherlands, who also partially sponsored the project.

Samenvatting

Curvatuurlijnen voor detectie en visualisatie van darmpoliepen in CT colonografie

Colonkanker is één van de belangrijkste oorzaken van sterfgevallen door kanker in de wereld. Dikke darmpoliepen zijn een belangrijke voorloper van colonkanker. Door vroegtijdige detectie en verwijdering van deze poliepen kan colonkanker effectief worden voorkomen. CT colonografie (virtuele colonoscopie) is een geavanceerde, minder invasieve onderzoekstechniek die de patiënt veel minder ongemak geeft dan optische colonografie. De visuele detectie van poliepen is echter ook bij virtuele colonoscopie complex en tijdrovend bij inspectie van het hele darmoppervlak. Met computerondersteunde diagnose (CAD) kunnen we deze problemen oplossen, en daarom werd dit een belangrijk onderzoeksthema in de CT colonografie. De meeste gepubliceerde automatische poliep detectie algoritmen maken gebruik van kenmerken gebaseerd op de kromming (curvatuur) van de colon-wand. Deze kenmerken zijn meestal te lokaal om de eigenschappen van poliepen volledig te beschrijven. Dit kan resulteren in een groot aantal valse detecties.

In dit proefschrift presenteren we een aanpak voor de automatische detectie van poliepen die mede gebaseerd is op technieken uit de stromings-visualisatie. Het primaire doel was om nieuwe karakteristieke kenmerken te berekenen die de prestaties van bestaande detectie technieken kunnen verbeteren door het verminderen van het aantal valse detecties.

We ontdekten dat met de hoofdrichtingen van curvatuur kenmerkende patronen voor darmpoliepen kunnen worden bepaald. Deze patronen kunnen worden gevisualiseerd met behulp van curvatuurlijnen. Dit deed ons vermoeden dat de geometrische eigenschappen van deze curvatuurlijnen kunnen worden gebruikt om automatische polyp detectie te verbeteren. We ontwikkelden een robuust algoritme voor de berekening van de curvatuur, dat gebaseerd is op een evenwichtige bemonstering in alle richtingen en een groter bemonsteringsgebied. Vervolgens ontwikkelden we nieuwe methoden om curvatuurlijnen te genereren op de darmwand. De methoden zijn zowel toepasbaar op expliciete oppervlaktemodellen met driehoekjes als op impliciete iso-oppervlakken in een 3D CT dataset. Voorts hebben we gewerkt aan een curvatuur-afhankelijke verdeling van curvatuurlijnen over het oppervlak. We gebruikten twee geometrische eigenschappen van de curvatuur lijnen, namelijk de winding angle en de mean radius, om onderscheid te maken tussen echte en valse poliep detecties. De visualisatie van de darmwand werd ook verbeterd door het afbeelden van de curvatuurlijnen.

We hebben onze techniek voor de berekening van curvatuurlijnen op twee manieren verder verbeterd. Eerst hebben we een efficiëntere methode ontwikkeld voor het plaatsen van startpunten voor de curvatuurlijnen, door de plaatsing afhankelijk te maken van de lokale curvatuur van het oppervlak. Deze aanpassing leidde tot een veel kleiner aantal overbodige startpunten en daarmee tot een snellere berekening, terwijl de kwaliteit niet significant werd beïnvloed. Een tweede verbetering werd bereikt door de observatie dat de correlatie tussen de eigenschappen van curvatuurlijnen en ware poliepen werd beïnvloed door de lengte van de curvatuurlijnen. Het curvatuurlijn generatie-algoritme kan nu kortere curvatuur lijnen automatisch aan elkaar verbinden (defragmentatie). De aldus berekende langere curvatuurlijnen leidden tot een betere beschrijving van de poliep vormen.

Door de curvatuur lijnen te clusteren, konden we de darmwand in de buurt van poliepen opdelen in geometrisch homogene regio's. Onze techniek maakt gebruik van een spectraal clustering algoritme en een symmetrische lijn similariteits maat, die gebaseerd is op de mate van evenwijdigheid van de curvatuur lijnen. Een dergelijke partitionering kan worden gebruikt om vorm informatie te aggregeren en daardoor detectie algoritmen verder te verbeteren.

Onze detectie techniek werd geëvalueerd door het in een automatisch poliepdetectiesysteem te integreren. Kenmerken van de curvatuurlijnen werden gebruikt in het classificatie stadium om het aantal valse pre-detecties te verminderen. Op basis van 332 datasets van 166 patiënten, lieten onze resultaten zien dat de winding angle eigenschap sterk correleert met ware poliep detecties, waardoor deze gebruikt kan worden om de prestaties van bestaande automatische detectie-systemen te verbeteren.

Dit onderzoek werd uitgevoerd bij de Technische Universiteit Delft, in samenwerking met Philips Healthcare Nederland, die het project financieel ondersteunde.

Curriculum Vitae

Lingxiao Zhao was born on July 25, 1977 in Zhengzhou, Henan province, China. He finished his secondary school education in 1996 at the No.1 High School administrated directly by Zhengzhou Railway Bureau. With his good performance at school and significant awards in China National High School Student Competitions for Mathematics and Physics, Lingxiao was recommended for admission to be an undergraduate student without exams.

In September of 1996, Lingxiao started pursuing his Bachelor's degree in Computer Science and Technology at Beijing University of Aeronautics and Astronautics. After his graduation from the university, he worked as a computer software engineer for two years at the Center of Aviation Safety Technology, Civil Aviation Administration of China.

He came to the Netherlands in the summer of 2002 and started studies on his Master's degree in Technical Informatics at TU Delft. After one year of courses and another year working in the Data Visualization group, he finished his Master thesis entitled, "Curvature Estimation for Automatic Polyp Detection in Virtual Colonoscopy". During this period, Lingxiao developed a strong interest in Computer Graphics and Medical Visualization. After September of 2004, he continued his research on automatic polyp detection in CT colonography as a PhD student, in cooperation with Philips Healthcare. Since January of 2009 when he finished his work at TU Delft, he has been working as a software engineer at Quintiq Applications B.V. in 's-Hertogenbosch.

Acknowledgements

The research work presented in this thesis was a collaboration between the Data Visualization group of the Computer Graphics and CAD/CAM section of Delft University of Technology and Philips Healthcare Netherlands, who was the major sponsor of this research. It formed part of the Virtual Colonoscopy project conducted at Philips Healthcare. The work in this thesis was performed at the Data Visualization group of TU Delft between the year 2004 and 2009. It was also an extension of my Master thesis entitled “Curvature Estimation for Automatic Polyp Detection in Virtual Colonoscopy”.

The research goal was to compute discriminating surface shape features that characterize polyp shapes for automatic polyp detection in CT colonography. The key idea of our research was employing streamline techniques used in vector field visualization for surface and volume geometry processing. Based on the result of my Master thesis project, it was found that surface principal curvature direction fields presented characteristic patterns that could help to identify polyp-like structures in CT image data. This led to the hypothesis that principal curvature lines on the 3D surface could be used for polyp detection in CT colonography. During our research, we further studied this hypothesis through implementation and evaluation.. The results of our work were twofold. From the visualization perspective, curvature lines were used to improve the traditional visualization of shaded colonic surfaces. From the polyp detection perspective, the winding angle feature of curvature lines was used to improve the performance of existing polyp detection approaches.

It was very exciting for me to work on this project. During the project and the writing of this thesis, I have been enlightened and helped by many fantastic people. At this moment, I have the pleasure to send my heartfelt thanks to all of them. Without their contributions, I would not have made such a great achievement in my life.

First of all, I would like to thank Charl Botha, my co-promotor and one of my direct supervisors, also good friend. His advices in my practical work were extremely important and irreplaceable. His knowledge of computer graphics and visualization and software programming always inspired me. I would also remember the “beer police” time of us for ever. His organization of these social events made my life at TU Delft very enjoyable. Thanks to Frits Post for being my another direct supervisor. His guidance always pointed me to the correct research direction and revealed how to proceed with the next step. His patience and encouragement greatly helped me when I had problems in my research work. I was also deeply influenced by his studious manner of research not only in my PhD life but also for my future. My special thanks to Prof. Erik Jansen for being my promotor, for his valuable feedback on my thesis and for his great support in my preparation for the thesis defense.

I would like to thank the group of people at Philips Healthcare that I worked with. Special thanks to Frans Gerritsen and Roel Truyen for offering me the opportunity of doing a PhD project sponsored by Philips. My regular meetings with them were very instructive and informative to me. Their comments and advices were very helpful to make my every progress. I would like to thank Iwo Serlie for making his own digital image processing libraries available. Thanks to him and Kees Visser for answering my technical questions. I had also nice discussions with Simona Grigorescu about flat lesion natures. Thanks to all other people present at the regular Philips meetings, in particular Henri Bouma, Petr Sereda and Anna Vilanova.

During my work, I had close contact and collaborations with people from the Quantitative Imaging group of the Imaging Science and Technology department of TU Delft. Herewith, I would like to thank all of them. Especially, thanks to Frans Vos for his supervision. His knowledge in radiology and medical applications was a great support and his feedbacks on my work was valuable references to me. I would like to thank Prof. Lucas van Vliet for his advices and kind help. Thanks to Kees van Wijk. As my good friend and close colleague working for the same project and in the same research field, he gave me a lot of suggestions for making the job done. We had a fantastic collaboration and I learned a lot from him. I would like to thank Vincent van Ravesteijn for performing the evaluation of my work results.

I would like to thank the rest of my colleagues in the Computer Graphics and CAD/CAM group of TU Delft. Special thanks to Jorik Blaas and Stef Busking for being my office mates and going through the PhD life with me. Thanks to Gerwin de Haan, Peter Krekel, Eric Griffith and Peter Kok for sharing our PhD life together in the Visualization field. Thanks to Wim Bronsvoort, Rafael Bidarra, Peter van Nieuwenhuizen, Rick van der Meiden, Ruud de Jong, Bart Vastenhouw and all other group members. I would also like to thank all MSc students who ever worked with me in our group for their contributions to the development of our group, in particular, Ruixin Wang, Yang Yang, Shi Pu and Erik Pols.

I thank all my Chinese friends who have shared the life with me here in the Netherlands and far away from home. Our friendships are precious fortunes in my life forever. Special thanks to Binbin Bai, Nan Liu, Rui Li, Bin Xi, Liang Xia, Yi Ding, Bei Li, Xiang Han. And thanks to all Delft Chinese student basketball team members. Our weekly basketball trainings and yearly competitions enriched my time outside the work.

Finally, I would like to thank my parents for their constant love, faith and support, which I always received wherever I was, whenever I needed it and whatever I chose to do. Most importantly, I would like to thank you, Ying, my beloved wife. We have lived together in the

Netherlands and experienced every memorial moment here. You witnessed every step of my PhD project. Your encouragement and steadfast trust were very important to me. Without your love, this world would not be so wonderful and all these things would not have been possible.

Lingxiao Zhao
Houten, August 2010

Stellingen

behorende bij het proefschrift

Curvature Lines for Lesion Detection and Visualization in CT Colonography

1. Richtingsaggregatie van krommingslijnen is een betere basis voor karakterisering van een vorm dan de aggregatie van scalaire krommingsmaten. (Dit proefschrift)
2. Bij vormanalyse van een oppervlak op basis van de principale krommingsrichtingen kunnen we gebruik maken van feature extractie technieken in wetenschappelijke visualisatie. (Dit proefschrift)
3. Om ons begrip van vormen te ondersteunen is directe visualisatie van geometrische eigenschappen van een oppervlak superieur aan directe rendering en shading van het oppervlak.
4. Vlakke laesies kunnen niet betrouwbaar gedetecteerd worden met de huidige CAD-technieken en CT-colonografie.
5. Clinici zullen altijd een computer-diagnose willen bevestigen met visuele inspectie.
6. De toepassing van visualisatie technieken in de geneeskunde demonstreert hoe de integratie van twee schijnbaar ongelijksoortige gebieden kan leiden tot waardevolle resultaten.
7. In het hedendaagse onderzoek zijn communicatieve vaardigheden minstens zo belangrijk geworden als wetenschappelijke vaardigheden.
8. Computational science vereist minstens zoveel goede programmering als goede wetenschap.
9. Er zijn mooie gedichten en goede computerprogramma's in elke taal.
10. Bepalen wat je wilt in het leven is belangrijker dan het bereiken daarvan.

Deze stellingen worden verdedigbaar geacht en zijn als zodanig goedgekeurd door de promotor prof. dr. ir. F.W. Jansen.

Propositions

accompanying the thesis

Curvature Lines for Lesion Detection and Visualization in CT Colonography

1. The directional aggregation of curvature lines is a better basis for shape characterization than the aggregation of scalar curvature measures. (This thesis)
2. Surface shape analysis based on principal curvature direction fields can benefit from feature extraction techniques in scientific visualization. (This thesis)
3. Direct visualization of surface geometric properties is superior to direct surface rendering and shading in facilitating our understanding of shapes.
4. Flat lesions cannot be reliably detected with current CAD techniques or CT colonography.
5. Clinicians will always want to confirm a diagnosis by visual inspection.
6. The application of visualization techniques in medicine demonstrates how the integration of two apparently disparate fields can lead to valuable results.
7. In modern research, communication skills have become at least as important as scientific skills.
8. Computational science requires at least as much good programming as it does good science.
9. There are beautiful poems and excellent programs in every language.
10. Determining what you want in life is more important than achieving it.

These propositions are considered defendable and are approved by the promotor prof. dr. ir. F.W. Jansen.

INVITATION

to the public defense
of my PhD thesis

CURVATURE LINES FOR LESION DETECTION AND VISUALIZATION IN CT COLONOGRAPHY

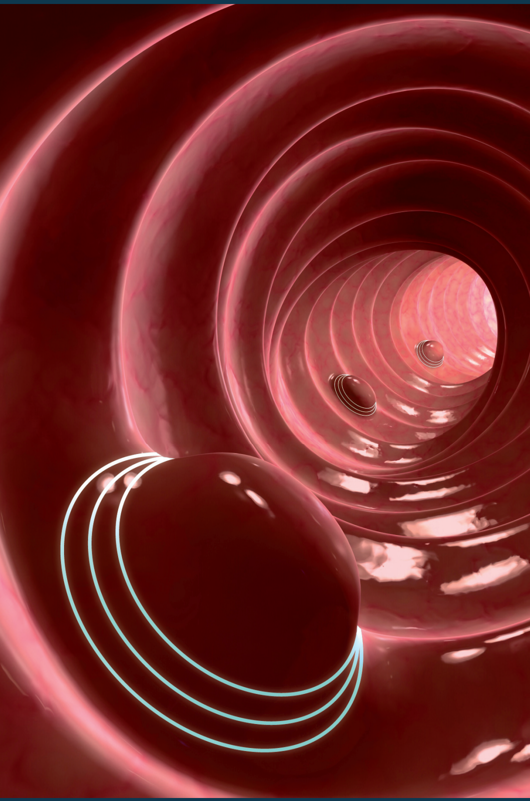

Wednesday 9 March 2011,
presentation 9:30, defense 10:00,
reception followed.
Senaatszaal Aula TU Delft
Mekelweg 5, Delft

Lingxiao Zhao